INFORMATION TO USERS

This manuscript has been reproduced from the microfilm master. UMI films the text directly from the original or copy submitted. Thus, some thesis and dissertation copies are in typewriter face, while others may be from any type of computer printer.

The quality of this reproduction is dependent upon the quality of the copy submitted. Broken or indistinct print, colored or poor quality illustrations and photographs, print bleedthrough, substandard margins, and improper alignment can adversely affect reproduction.

In the unlikely event that the author did not send UMI a complete manuscript and there are missing pages, these will be noted. Also, if unauthorized copyright material had to be removed, a note will indicate the deletion.

Oversize materials (e.g., maps, drawings, charts) are reproduced by sectioning the original, beginning at the upper left-hand corner and continuing from left to right in equal sections with small overlaps.

Photographs included in the original manuscript have been reproduced xerographically in this copy. Higher quality 6" x 9" black and white photographic prints are available for any photographs or illustrations appearing in this copy for an additional charge. Contact UMI directly to order.

ProQuest Information and Learning
300 North Zeeb Road, Ann Arbor, MI 48106-1346 USA
800-521-0600

Scattering From Periodic Array of Parallel Strips

Hao Liu

A Dissertation
in
The Department
of
Electrical and Computer Engineering

Presented in Partial Fulfillment of the Requirements
for the Degree of Doctor of Philosophy at
Concordia University
Montreal, Quebec, Canada

April 2001

Abstract

The field distribution between strips in a periodic array of parallel strips was modeled. The electric field integral equation (EFIE) together with method of moments was employed to solve the problem. The incident plane wave was assumed to be transverse magnetic (TM) and transverse electric (TE). The effect of the incident angle on the field between strips was investigated. For comparison, an array of the same configuration but containing a finite number of parallel strips was also modeled using the EFIE and solved via the method of moments. Good agreement between the results from the periodic array and the finite array was found even when the number of strips is small. It is also found that the presence of the ground plane does not have much effect on the field distribution, but only raises the field strength level when the observer is located below the top of the parallel strips. The results are of interest for cellular mobile radio community in predicting the range depedence of a signal from a base station antenna, when propagating in built up residential area.

Contents

List of Figures

List of Tables

ACKNOWLEDGMENT

The author wishes to thank his graduate advisor Professor Robert Paknys for providing guidance, excellent suggestions, critical review of this dissertation draft, and continuous financial support for the projects.

The author also wishes to thank Professor Jean-Jacques Laurin, Professor Sushil K. Misra, Professor Christopher W. Trueman and Professor Leslie M. Landsberger for their participation in the examination committee and providing invaluable information both on the dissertation draft as well as theoretical aspects.

Chapter 1

Introduction

In mobile radio communication, it is desired to predict the radio wave propagation characteristics in built-up areas. In most cities, outside the downtown area, the building height decreases gradually from 4-6 stories near the core to 1-2 stories far away. Most of these buildings are residential houses of nearly uniform height over large areas with occasional high-rise apartment buildings. Macrocellular systems are often deployed in these areas. The macrocellular system employs high-rise base station antennas, which are located on towers or on rooftops of a high-rise building which is well above the rooftops of surrounding buildings, with its cell radii greater than several kilometers. In contrast, the microcellular system employing low base station antennas (often at the height of a street light) with its cell radii limited within one kilometer, is often deployed in downtown area where high-dense mobile subscribers often exist. The most common macrocellular propagation scenario therefore involves propagation from a base station antenna located above the rooftops of surrounding buildings having nearly uniform height down to a subscriber at street level, which will be the focus of this dissertation.

In a macrocellular propagation environment, the base station antenna is usually located above the rooftops of surrounding buildings, and the mobile subscriber is usually located on streets between these buildings. Therefore the prediction of the field strength reaching a subscriber which is at the street level for an incident wave from a base station antenna involves diffraction over the rooftops, reflection and transmission on and through the walls

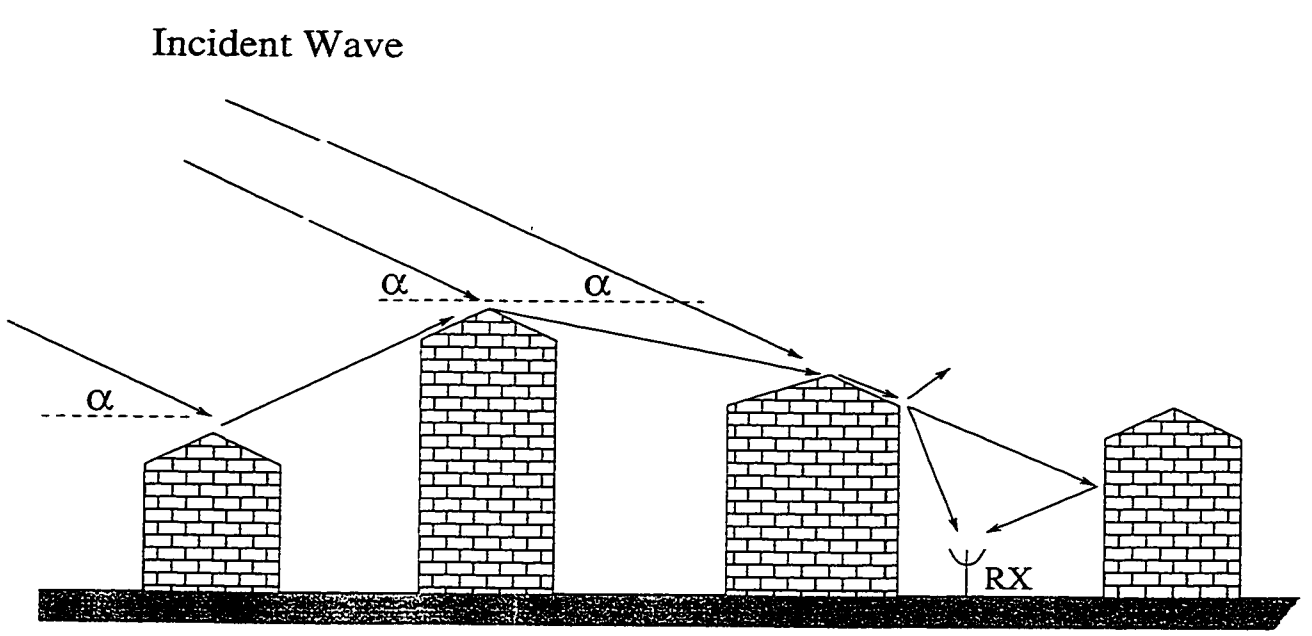

Figure 1.1: Wave past over multiple building rows.

due to the existence of multiple rows of buildings that lie between the subscriber and the transmitting antenna.

The radio signal reaching the subscriber experiences attenuation due to reflection and transmission loss of the signal on and through the walls, and diffraction loss from the rooftops of the buildings that lie between the subscriber and the base station antenna. In most cases, the transmitting antenna is not visible from street level. Buildings are organized along streets with gaps between them that are smaller than the building width, or they form continuous rows. Since gaps between buildings are not aligned with the transmitter from row to row, and because the reflection and transmission loss due to the walls is usually much greater than the diffraction loss from the rooftops of the buildings, when a large number of buildings is involved between the subscriber and the base station antenna, the major contribution to the subscriber at street level is believed to be coming from propagation over the rooftops of buildings. The multi-paths the rooftop fields take to reach street level are suggested in Fig.1.1, and include diffraction at the last row before the mobile receiver, followed by reflection at the next row.

In order to predict the range dependence, the sector average path loss S is defined to be the ratio of the sector average received power to the radiated power for isotropic antenna in free space. The sector average received power is usually defined by averaging the power measured as one end of the radio link is moved over a path whose length is about 20λ or so. With this definition, S may be written as the product off three factors [2]

$$S = P_0 Q^2 P_1. \tag{1.1}$$

Here P_0 represents free-space path loss, which is the ratio of received to radiated power for isotropic antennas in free space, and is given by

$$P_0 = \left(\frac{\lambda}{4\pi R}\right)^2 \tag{1.2}$$

where λ is the wavelength of the operating radio signal, R is the distance between the subscriber and the base station antenna.

The factor Q^2 gives the excess reduction in the rooftop signal at the row just before the subscriber as a result of propagation past previous rows, and P_1 is the reduction due to the diffraction of the rooftop fields down to street level.

The above definition has implied several assumptions. First, the 3-D problem is simplified into a 2-D problem by accounting for the free space attenuation in the term P_0. Second, the excess attenuation due to the presence of the multiple rows of building that the signal has to propagate past before reaching the last row of building before the subscriber was accounted by the term Q^2, which is evaluated by assuming a plane wave propagating past over multiple rows of buildings. The last term P_1 accounts for the reduction of the signal due to the diffraction of the rooftop fields down to street level that are received by the subscriber.

The free space attenuation P_0 can be readily obtained once the operating frequency and the distance between the subscriber and the base station antenna is given. The term P_1, the rooftop diffracted field reaching the subscriber at the street level can be evaluated using standard geometrical optics (GO) and uniform theory of diffraction (UTD) techniques.

The evaluation of the term Q^2 is not so straightforward as of the other two terms. It is often studied by considering a plane wave propagating over an array of parallel half screens, as suggested in Fig. 1.2. The field strength on the tip of the screen just before the subscriber is to be evaluated. Once this field strength is obtained, the power that is received by the subscriber at the street level can be readily evaluated via a standard GO/UTD procedure.

A lot of literature is found concerning the multi-edge diffraction problem. Millington [3] studied the attenuation of radio waves by diffraction over two knife-edges in succession. The method is to take the wavefront above the second knife-edge, obtained by the diffraction of the wave from the source over the first knife-edge, as a source for finding the field at the receiving point by a double application of Huygens' principle. The incident field is assumed to come from a point source. The solution is shown to depend on a Fresnel surface integral.

Furutsu [4] derived a generalized residue series formulation for the propagation of radio waves diffracted by an arbitrary sequence of smooth rounded obstacles. Vogler [5] found that if the radii of the obstacles are allowed to decrease to zero, then the propagation path becomes comparable to a series of perfectly absorbing knife-edges, and the residue series for each obstacle can be transformed into integrals over continuous variables. The attenuation of field strength relative to free space over a path consisting of N knife-edges was expressed by a multiple integral, which is practically difficult to evaluate when $N > 2$.

Lee [6] employed a path integral technique to the calculation of the electromagnetic field on the incident shadow boundary in several edge-diffraction problems involving arbitrary numbers of parallel half-planes. The limitation is that it could only deal with some special cases when the source, receiver and edges of the parallel plane lie in a common plane. The results for these special cases are exact and are often referenced to to verify results from other approximate methods.

Walfisch [1], using a method based on direct numerical evaluation of the Kirchoff-Huygens integral, studied the problem of incident plane wave diffraction when propagating over a series of half-screens. The field in the aperture of the $n = 0$ half-screen is used to compute

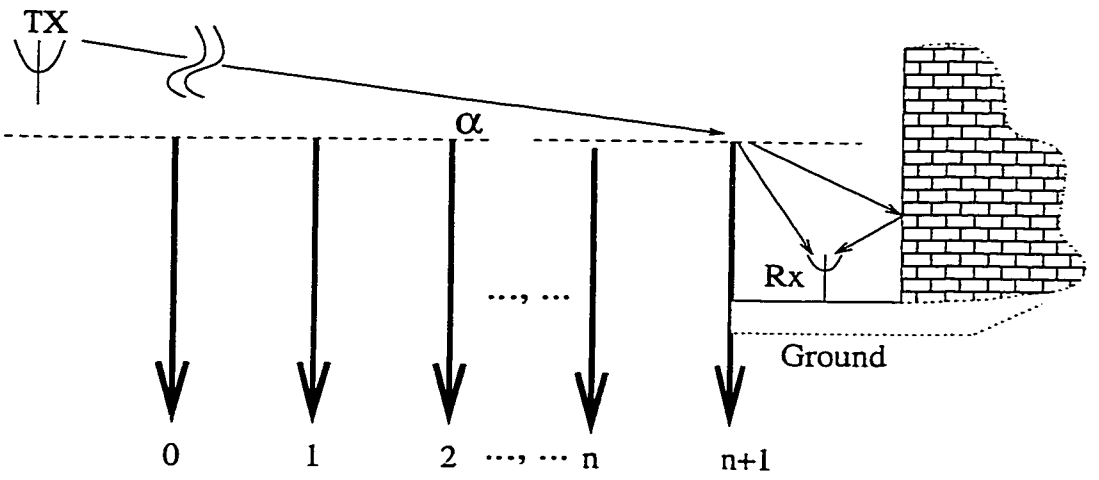

Figure 1.2: Plane wave incident on multiple rows of absorbing half-planes.

the field in the aperture of the $n = 1$ half-screen, and so on. Here n is the index of the half-screens, referring to Fig. 1.2. Finally a recursive relation of the fields between successive screens are obtained. The advantage of the Walfisch model is that it permits the treatment of edges having randomly distributed height without increasing complexity as compared to the case of edges with uniform heights and spacings. Because the integration were expressed numerically from the top of each screen to infinity, which makes the direct implementation difficult, the authors greatly simplified the process by truncating the integral limits using the concept of the Fresnel zone [7] that is, the aperture fields which lie outside the Fresnel zones can be neglected without introducing significant perturbation to the ray field. Although great improvements have been made, such a numerical integration procedure is still time consuming and the formulation is valid only for positive angles of incidence.

Saunders [8] applied Vogler's equation into the study of diffraction by an array of absorbing half-planes with uniform heights and spacings. Using a method of solving integral-equations proposed by Boersma [9], the integral equation for multiple edge diffraction proposed by Vogler is solved for such a special case. The solution is uniformly valid when plane wave incidence is above, level with, or below the plane of the edges. The attenuation function is given by a closed form expression of Fresnel integrals, which is more amenable to efficient

computation than the numerical solution from [1]. A similar result was achieved by Xia later on [10]. Both the Saunders and Xia models are in closed form and have the advantage of being numerically efficient for scattering of incident plane wave when propagating over uniform arrays of half-screens.

Alternatively, UTD has also been applied to the study of radio wave attenuation when propagating over arrays of parallel half-screens. Neve [11] proposed a UTD approach for the computation of forward diffraction of multiple edges. In contrast to the previous formulations, all screens are assumed to be perfectly electric conducting (PEC). Again, back diffracted rays are not considered. It is found that when $\alpha\sqrt{d/\lambda} > 1$ (where d is the spacing between the screens, α is the angle of incidence for the plane wave and λ is the wavelength of plane wave), the deviation between result from UTD and that of Saunders model and Walfisch model is less than 1 dB for an example of uniform array of PEC half-screens. However, the UTD approach gives erroneous results when one or more edges fall into the transition zone of the previous edges.

Andersen [12] tried the UTD technique for diffraction by multiple edges near the transition zone. Slope diffraction was included to give an approximate solution, which coincides well with the exact solution from [6] up to fifteen for the edge numbers. However, it loses its accuracy for large number of edges in the transition zones. It has been shown that Andersen's result for the field at the incident boundary is accurate for field diffraction over multiple screens where the number of screens is not too large. Recall from the UTD approach attempted by [11] who employs a standard UTD procedure, that the result fails for the grazing incidence. The mechanism by which an accurate result could be obtained by the simply inclusion of the slope diffraction field as done by Andersen, remains unclear.

In summary, for radio wave propagation in built-up areas, it is of interest to evaluate the signal intensity which reaches the subscriber on street level. In previous studies, the problem is divided into a two-step procedure. The first is to account for the propagation loss when the wave propagates over many rows of buildings. The field strength on the rooftop of the

last building before the subscriber is evaluated. Second, the field reaches the subscriber at the street level is evaluated using standard GO and UTD techniques. The second step is quite straightforward while the first step is much more involved.

To account for the propagation loss when the signal propagates over multiple rows of buildings, the problem was often simplified as a plane wave propagating over a uniform array of parallel half screens, [1, 8, 11]. The free space path loss of signals for an isotropic antenna was introduced to compensate the over-estimation of the signal strength by using a plane wave incidence and two dimensional geometrical structure. Either multiple physical optics (PO) integrals or a UTD procedure is used to evaluate the field strength on the tips of the half screens. PO has the advantage of being numerically efficient when treating buildings of uniform heights and spacings, also PO processes are capable of dealing with the case of near grazing incidence. However, PO becomes numerically inefficient when treating buildings with arbitrary heights or spacings. UTD is always numerically efficient, and can treat buildings of either uniform or nonuniform heights and spacings, but it loses accuracy when the tips of buildings are located near the transition regions of previous buildings.

Our research will be focused on the study of the field distribution between the buildings within multiple rows of buildings under plane wave incidence. All previous works are based on the geometry configuration of a multiple knife-edges with the lower edges extending to infinity. Therefore the ground effect on the attenuation function when the wave propagates over the multiple buildings was not considered. The wave properties of the building walls and multiple reflections between buildings are also not included in previous research. We propose to use the field integral equation together with the method of moments to solve the problem. The advantage of studying this propagation problem by solving the field integral equation is, the field distribution between the buildings can be evaluated directly, rather than the two-step procedure as suggested in (1.1), that first accounts for the attenuation due to presence of the multiple buildings and then diffracts down to the receiver at the street level. Further, by solving the field integral equation, all the interactions between the walls, ground

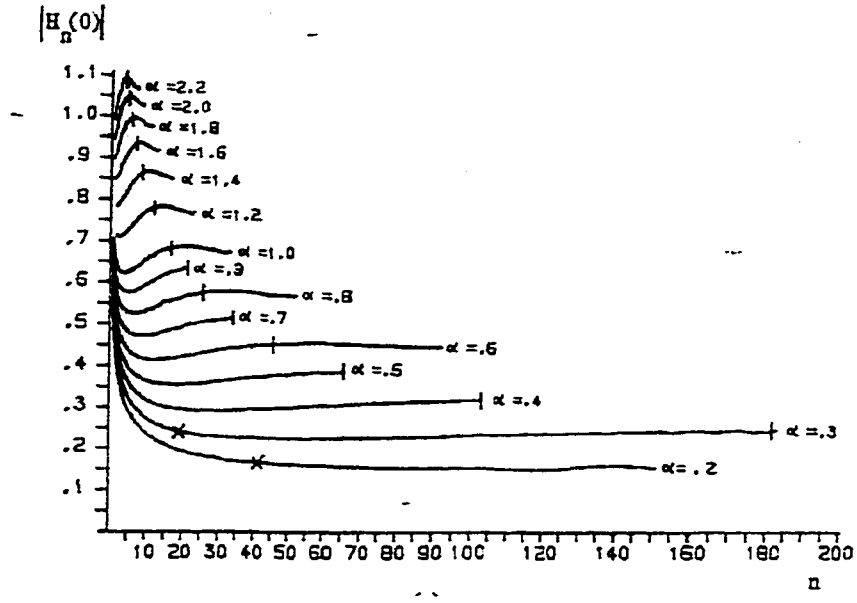

Figure 1.3: Variation of field incident on edges of half-screens as a function of screen number n for various values of the angle of incidence α (Taken from [1]).

and tips of buildings are inherently included in the analysis.

An interesting phenomena was discovered for the field on the tips of the half screens when considering a plane wave propagating over a large number of half screens, that the field strength on the tips tends to approach a constant after the wave has passed a large number of screens. This trend is clearly depicted in Fig. 1.3, where the horizontal axis denotes the index of the edge numbers, the vertical axis is the magnetic field intensity on top of each edge and the various plots represent the field intensity under various values of the incident angles. This phenomena was referred to as the "settling behavior" in [1] and verified in [11]. From Fig. 1.3, it is noticed that the number of edges the wave has to propagate to reach the settled value is dependent on the incident angle. For instance, when incident at 1°, the field has to pass over 15 edges, and for 0.5°, the field has to pass 65 edges to reach their settled values. From this point, we got our initial motivation to investigate the field behavior for the case when the number of edges becomes infinite. Due to the limited computer resources, moment method is incapable of dealing with problems when large numbers of buildings are involved. The phenomena of "settling behavior" for the field on tops of buildings suggested

that the solution for periodic strip arrays may be employed to approximate the solution for a finite array when the number of strips is large. The comparison of the field between a finite and infinite array of parallel strips under transverse magnetic (TM) plane wave incidence showed that such an approximation is quite promising even when the number of strips is only moderately large; results for nine strips were given in [13], where the ground effect is neglected. A key issue is that although a method of moment solution is not possible for a large number of buildings, it is possible for a periodic array which contains an infinite number of buildings, by using the Floquet theory.

The field distribution for infinite periodic strip arrays is formulated using Floquet theory, which enables faster convergence over the original series in the space domain.

In this dissertation, we try to gain some insight into the field distribution behavior when electromagnetic waves propagate past over multiple rows of buildings, by studying the field distribution in periodic arrays of parallel strips and comparing the results against the fields in finite arrays of parallel strips under plane wave incidence. The rows of building are modeled by PEC strips with zero thickness, and the ground plane used to close the bottom ends of the parallel strips, is also PEC. Due to the periodic nature of the structure, and the plane wave incidence, the field distribution is also periodic. It is only necessary to examine the field within a single cell. The problem is formulated using the surface equivalence theorem. The geometrical structures are replaced with equivalent electric currents which radiate in free space. This unknown equivalent current is expanded into a series using appropriate basis functions. The scattered field from this unknown equivalent current can be formulated. Using the boundary condition, an electric field integral equation (EFIE) is established. A system of linear equations is obtained with a method of moments procedure. The equivalent current can be found by solving this equation. Once the equivalent current is found, it is then a straightforward procedure to calculate the scattered field and then the total field at any point in space.

Since the solution for the transverse magnetic (TM) and transverse electric (TE) plane

incidence is orthogonal to each other, both TM and TE polarizations of the incident field are considered.

For the scattering problem of parallel strips with uniform heights, an alternative approach of using the equivalence theorem is the mode matching method, which chooses the aperture magnetic currents as the unknowns. Then matching fields on the aperture gives a magnetic field integral equation (MFIE). The advantage of using the mode matching method is that it permits the use of waveguide modes to expand the fields in the region that is inside, between the parallel strips of PEC. However, we decided not to use such that approach because we wish to develop a general procedure for the scattering problem of parallel strips, where sometimes the waveguide modes are hard to model the aperture fields. For instance, this occurs when there are discontinuities, or aperture on the parallel strips, or when curved surfaces are involved. These would be useful when the effect of windows or irregularities on buildings is desired to be considered.

In the case when the bottom of the periodic arrays of parallel strips is closed with PEC strips, the analysis can be greatly simplified by employing the image theory, however, we have chosen not to do so, because we wish to develop a general method in the future development, that permits other types of surfaces, for instance, rugged or lossy ground in the unit cell of a periodic array.

Chapter 2 will present a point matching solution for the scattering from periodic arrays of parallel strips, with TM plane wave incidence. Although TM incidence has received less attention in mobile radio communication research compared to the TE incidence, (the antennas of the base station are vertically polarized,) we choose to include this part of research not only for the completeness of the analysis but also for the role it served as a preliminary research for the more complicated case of TE incidence. Moreover, the computational data for the TM incidence on periodic arrays of parallel strips is shown to compare favorably against computational data when the periodic array is truncated on both sides.

Chapter 3 will present a method of moments (MM) solution for scattering from periodic

arrays of parallel strips, with TE plane wave incidence. The field distribution for periodic parallel strip arrays is formulated using Floquet theory and solved with a MM procedure. To better model the wave propagation for a vertical antenna in a mobile radio communication environment, the incident field is assumed to be TE, and a ground plane is incorporated into the analysis. By solving the integral equation, the field distribution at any point can be evaluated directly and all the interactions between the parallel strips and the ground plane are inherently included. The solution for the periodic array of parallel strips is compared against the solution for an array which consists of finite numbers of parallel strips, which is obtained by truncating the periodic array on both sides. The solution to this finite array of parallel strips is obtained by using TECYL, [14], an integral equation solution for TE cylinder radiation and scattering. The two solutions agree well when the angle of incidence is off grazing, except at some particular values of incident angle.

The following parts of this dissertation will develop the theory and equations involved in the evaluation of field behavior when a plane wave is incident upon a periodic array of parallel strips. Numerical results are presented and compared with results when the periodic array is truncated on both sides. Chapter 2 will present the analysis and numerical results for TM plane wave incident on periodic array of parallel strips. Chapter 3 will present the analysis and numerical results for TE plane wave incident on periodic array of parallel strips, with the bottom of the parallel strips opened or closed. The derivation for scattering from finite arrays of parallel strips under TM incidence is enclosed in Appendix A. Appendix B will present the mathematical details relating the formulation and derivation in Chapter 3. Appendix C lists some properties relating to convolution as was used in Appendix B. Appendix D includes the formulation for the problem of scattering from planar arrays of parallel cylinders with small radius under TM incidence, as a supplementary material which is not published in [13]. Appendix E lists unpublished material – reference [15].

Chapter 2

Scattering From Periodic Arrays of Parallel Strips, TM Incidence

This chapter presents the point matching solution to the problem of transverse magnetic (TM) plane wave scattering from periodic arrays of parallel strips. The first step is to assume a TM plane wave incidence. Then the surface equivalence theorem [16] is applied to replace the perfect electric conductive strips by free space and the unknown equivalent electric surface current J_z. Due to the fact that the geometry structure is periodic and the incident plane wave is also periodic, the solution for the unknown current is periodic too. We need only assume an unknown J_z on one strip and can have the whole solution by duplicating J_z along the direction of periodicity with appropriate phase shift. The total field in free space is the sum of the field radiated by J_z in free space and the incident field. Imposing the boundary conditions on the surface of parallel strips gives an electric field integral equation (EFIE) containing J_z as an unknown. The unknown current is now expanded along the surface of the strip using pulse basis functions multiplied by unknown complex coefficients. The EFIE can be forced to be valid at *match points* carefully selected on each segments of the strip, known as the point matching method. Therefore a system of linear equations is created. The current coefficients can be found by solving this equation. Once the surface current is found, the fields radiated by this current are readily obtained, and the total field is found by adding the radiated field to the incident field.

The scattering problem when the periodic array is truncated on both sides is also studied.

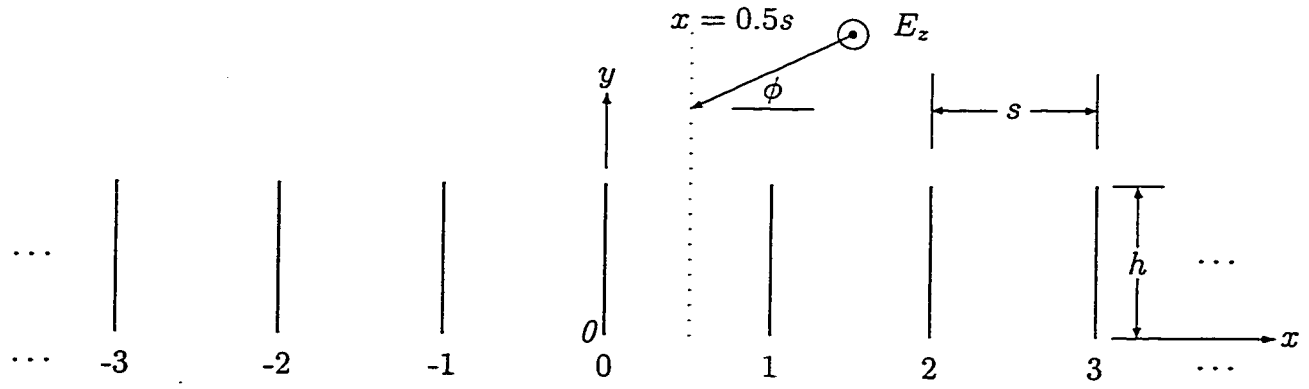

Figure 2.1: TM plane wave incident upon a periodic parallel strip array.

The solution to this problem is formulated in Appendix A, where the surface equivalence theorem together with a point matching procedure is used to calculate the near fields. The reason we choose to use the point matching method is that it provides adequate smoothness for the slightly singular kernel in the TM EFIE (Section 2.3 [17]).

In the following sections, the EFIE for the periodic structure will be established. Pulse basis functions will be employed to expand the unknown current J_z, followed by a point matching procedure to get the current J_z. Examples will be given where the scattered field at appropriate chosen observation points will be calculated and compared with the solution of a seven-cell structure. Good agreement will be demonstrated.

2.1 The Integral Equation

Consider a periodic planar array of vertical-oriented parallel strips, with perfect electric conductivity. The strips are assumed to have zero thickness, and extend to infinity along z-axis and passes through $x_n = ns$ where s denotes the spacing between the parallel strips. With a z-polarized plane wave incident on the array as in Fig.2.1,

$$E_z^i(x, y) = E_0 e^{jk(x\cos\phi + y\sin\phi)} \tag{2.1}$$

where k is the wavenumber of the incident field, $k^2 = \omega^2\mu\varepsilon$, ω is the angular frequency, μ, ϵ are permeability and permittivity in free space, and ϕ is the angle of incidence measured from the $+x$-axis. The time dependence $e^{j\omega t}$ is used and suppressed throughout the analysis.

The surface current density $\mathbf{J}_s$ on the strips has only a z-component. Since the geometry is periodic and the excitation is periodic along x-axis, a periodic solution is possible. The currents on the parallel strips can be expressed as [15]

$$J_s(ns, y) = J_s(y)e^{jnks\cos\phi},\ n = -\infty,\ +\infty \tag{2.2}$$

where $J_s(y)$ is the current on the strips lying on the y-axis.

The field scattered by the nth strip is given by [16]

$$E_n^s(x, y) = -\frac{k\eta}{4}\int_{y'} H_0^{(2)}(kR_n)J_s(y')e^{jkns\cos\phi}\,dy' \tag{2.3}$$

where

$$R_n = \sqrt{(x - ns)^2 + (y - y')^2} \tag{2.4}$$

and $H_0^{(2)}(x)$ is the zeroth order Hankel function of the second kind.

The electric field has only a nonzero z-component, so the subscript z is omitted in the above equations and the following. The total field scattered from the array of parallel strips is obtained by simply summing up the contribution from all the strips

$$\begin{aligned} E^s(x, y) &= \sum_{n=-\infty}^{+\infty} -\frac{k\eta}{4}\int_{y'} H_0^{(2)}(kR_n)J_s(y')e^{jkns\cos\phi}\,dy' \\ &= \int J_s(y')K(x, y - y')dy' \end{aligned} \tag{2.5}$$

where

$$K(x, y - y') = \sum_{n=-\infty}^{+\infty} -\frac{k\eta}{4}H_0^{(2)}(kR_n)e^{jkns\cos\phi} \tag{2.6}$$

The boundary condition requires that

$$E^s + E^i = 0,\ \text{over all strip surfaces} \tag{2.7}$$

where E^s, and E^i represent the scattered and incident field, respectively. Due to the periodical nature, we need only ensure the boundary condition on the one strip lying on y-axis. Using (2.5), we have the EFIE written as

$$\int J_s(y')K(0, y-y')dy' = -E^i(0, y) \tag{2.8}$$

2.2 Floquet Modes Analysis

The function expressed in (2.6) is a series containing Hankel functions which decrease only at $O(n^{-\frac{1}{2}})$ as $n \to \infty$. The Poisson summation formula can be employed to convert the slowly convergent series into a more rapidly convergent series [15].

$$K(x, y-y') = -\frac{jk\eta}{2s} \sum_{n=-\infty}^{+\infty} \frac{e^{-\gamma_n|y-y'|}}{\gamma_n} e^{j\omega_n x} \tag{2.9}$$

where

$$\begin{aligned} \omega_n &= k\cos\phi - \frac{2n\pi}{s} \\ \gamma_n &= \begin{cases} j\sqrt{k^2-\omega_n^2}, & k^2 > \omega_n^2 \\ \sqrt{\omega_n^2-k^2}, & k^2 < \omega_n^2 \end{cases} \end{aligned} \tag{2.10}$$

2.3 Point Matching Method

The point matching method is to expand the unknown equivalent current J_s using pulse basis functions, and enforcing the boundary condition at selected points on each segment. Assume the height of the parallel strips is h, so the surface current J_s is distributed in the domain $[0, h]$. Equally divide the strip that lies on y-axis into P segments, with the coordinates of each node expressed as

$$y_q = \frac{q-1}{P}h, \; q = 1, 2, \cdots, P+1. \tag{2.11}$$

Using the pulse basis functions, the current distribution J_s can be expanded as

$$J_s(y) = \sum_{q=1}^{P} a_q g_q(y) \tag{2.12}$$

where $g_q(y)$ is a pulse function defined as

$$g_q(y) = \begin{cases} 1, & y \in [y_q, y_{q+1}] \\ 0, & y \notin [y_q, y_{q+1}] \end{cases} \tag{2.13}$$

Using current expression in (2.12), the scattered field can be expressed as

$$E^s(x,y) = \sum_{q=1}^{P} a_q \int_{y_q}^{y_{q+1}} K(x, y-y')dy' \tag{2.14}$$

Using (2.14), we have the EFIE rewritten as

$$E^s(0,y) = \sum_{q=1}^{P} a_q \int_{y_q}^{y_{q+1}} K(0, y-y')\, dy' = -E^i(0,y) \tag{2.15}$$

Using point matching, we get a linear system of algebraic equation expression for the boundary condition

$$\sum_{q=1}^{P} Z_{pq} a_q = -E^i(0, y_p), \quad p = 1, 2, \cdots, P \tag{2.16}$$

where y_p are the matching points on the strip. The incident field term on the right is defined by (2.1). The impedance elements Z_{pq} can be expressed as

$$Z_{pq} = \int_{y_q}^{y_{q+1}} K(0, y_p - y')\, dy'. \tag{2.17}$$

Using (2.9), we have

$$Z_{pq} = -\frac{jk\eta}{2s} \sum_{n=-\infty}^{+\infty} \frac{1}{\gamma_n} \int_{y_q}^{y_{q+1}} e^{-\gamma_n |y_p - y'|} dy' \tag{2.18}$$

The matching points are generally chosen at the center point of each segment, as

$$y_p = \frac{2p-1}{2N} h, \; p = 1, 2, \cdots, N \tag{2.19}$$

Performing the integration, we have

$$Z_{pq} = -\frac{jk\eta}{2s} \sum_{n=-\infty}^{+\infty} \frac{1}{\gamma_n^2} \begin{cases} e^{\gamma_n(y_{q+1}-y_p)} - e^{\gamma_n(y_q - y_p)} & p > q \\ e^{-\gamma_n(y_q - y_p)} - e^{-\gamma_n(y_{q+1}-y_p)} & p < q \\ 2\left(1 - e^{-\gamma_n(y_{q+1}-y_q)/2}\right) & p = q \end{cases} \tag{2.20}$$

When the source region and matching points are defined as in (2.11) and (2.19), the expression for Z_{pq} can be further simplified. Starting with (2.20), we have

$$\begin{aligned} y_{q+1} - y_p &= [2(q-p)+1]t, \quad p \neq i \\ y_q - y_p &= [2(q-p)-1]t, \quad p \neq i \end{aligned}$$

where $t = h/2P$, equals half of the segment length. Further, we have

$$Z_{pq} = -\frac{jk\eta}{2s} \sum_{n=-\infty}^{+\infty} \frac{1}{\gamma_n^2} \left(e^{-\gamma_n(2|q-p|-1)t} - e^{-\gamma_n(2|q-p|+1)t} \right) \quad p \neq q \tag{2.21}$$

We can see that Z_{pq} is only a function of $|p-q|$, so $[Z]$ is a Toeplitz matrix. The convergence is ensured by the exponential term for the case when $p \neq q$. When $p = q$, from (2.20), we have $(y_{q+1} - y_q)/2 = t$, which leads to

$$Z_{pp} = -\frac{jk\eta}{2s} \sum_{n=-\infty}^{+\infty} \frac{2}{\gamma_n^2} \left(1 - e^{-\gamma_n t} \right) \tag{2.22}$$

The exponential term keeps decreasing rapidly as $n \to \infty$. The leading term in (2.22) becomes asymptotic as

$$\lim_{n\to\infty} \frac{1}{\gamma_n^2} = \left(\frac{s}{2\pi} \right)^2 \frac{1}{n^2}$$

which is absolutely convergent.

2.4 Scattered Fields

Once the surface current coefficients a_q are solved for, the scattered field can then be evaluated from (2.14)

$$E^s(x,y) = -\frac{jk\eta}{2s} \sum_{q=1}^{N} a_q \sum_{n=-\infty}^{+\infty} \frac{e^{j\omega_n x}}{\gamma_n} \int_{y_q}^{y_{q+1}} e^{-\gamma_n |y-y'|} \, dy'. \tag{2.23}$$

The integral in (2.23) can be evaluated in closed form as follows.

$$\int_{y_q}^{y_{q+1}} e^{-\gamma_n|y-y'|} dy' = \frac{1}{\gamma_n} \begin{cases} e^{-\gamma_n(y-y_{q+1})} - e^{-\gamma_n(y-y_q)}, & y > y_{q+1} \\ e^{-\gamma_n(y_q-y)} - e^{-\gamma_n(y_{q+1}-y)}, & y < y_q \\ 2 - e^{-\gamma_n(y-y_q)} - e^{-\gamma_n(y_{q+1}-y)}, & y_q < y < y_{q+1} \end{cases} \tag{2.24}$$

We have formulated the problem of scattering from periodic array of parallel strips. The equivalent current on the strip $n = 0$ that lies on the y-axis is obtained by solving (2.16),

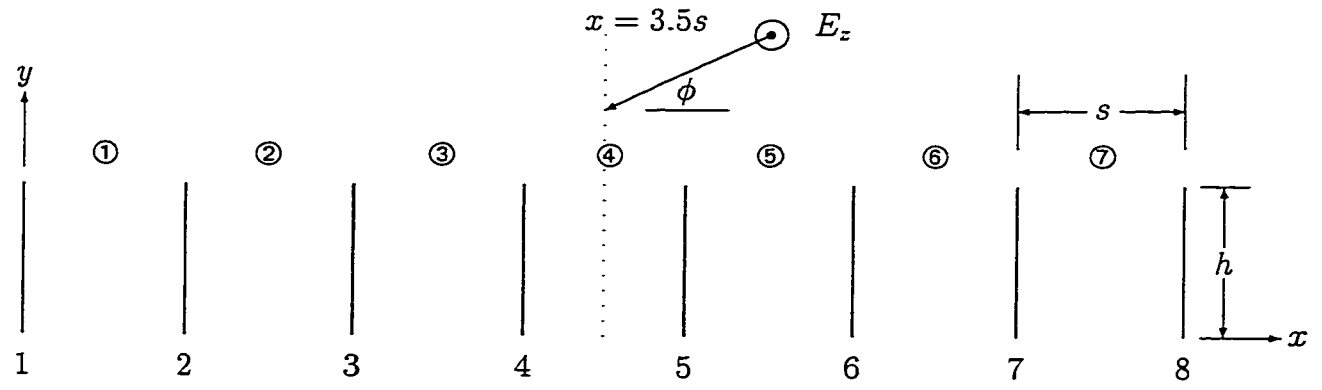

Figure 2.2: TM plane wave incident upon a seven-cell parallel strip array.

to get the current expansion coefficients a_q. Once the current expansion coefficients a_q is obtained, the scattered electric field can be calculated using (2.23). The total electric field is the summation of the scattered field and the incident field.

2.5 Results and Discussion

Let us consider an array containing eight parallel strips forming seven-cell, with a z-polarized field incident from above the array, as illustrated in Fig. 2.2. This array is obtained from the periodic array we discussed in Fig. 2.1 by truncating the numbers of parallel strips on both sides along x-axis. We will evaluate the field distribution in this seven-cell array and compare the results against the field distribution in a periodic array of parallel strips with the same height and spacing. The field distribution within the central cell is probably the least disturbed field by the truncated edges on both ends. Without losing generality, the field distribution along the central line, $x = 3.5s$, in cell ④ of this seven-cell array is calculated, and compared with the field in a periodic structure with the same height h and spacing s.

The field distribution in periodic arrays exhibits a periodic behavior while the observation point moves from one cell to the others. It is sufficient to study the field behavior within one cell. The field points are chosen to lie on the line $x = 0.5s$ in the periodic array of parallel strips.

The field within cell ④ is dominated by the height and spacing of the strip pair standing on both sides, namely strip 4 and strip 5. The presence of the other strips also has a disturbance on the field distribution. One would expect that, the closer the separation the greater the disturbance. From Fig. 2.2, we can expect that strip 6 will have a greater disturbance on the field within cell ④ than strip 7 has. We can also expect that when we add more parallel strips and ground planes on both ends of the structure along x direction, the field within the central cell would asymptotically approach the field distribution of a periodic structure, as the numbers of strips tend to infinity.

Let's consider a typical geometry of a residential area, which contains rows of two story houses. The height is about thirty feet, the spacing between them is about sixty feet. For radio frequency at 1 GHz, if we choose $h = 33\lambda$ and $s = 66\lambda$, where λ is the wavelength of the incident field, the scenario can be well approximated by our model shown in Fig. 2.2.

Fig. 2.3 through Fig. 2.6 show the plot of fields in cell ④ of the seven-cell structure, with various values for the angle of incidence of the incident plane wave. Without losing generality, the field points are selected to move in the y-direction along the central line of cell ④ at $x = 3.5s$ in the seven-cell array. For comparison, the field distribution along the observation line $x = 0.5s$ in the periodic array is also calculated and plotted in the same figures. We chose x to be fixed and y is the variable for the field point, because we anticipate good agreement inside the cell, but not outside the cell.

From all these plots, we see the field distribution in the central cell of the seven-cell structure is very close to the result from a periodic structure.

For great incident angles, such as $\phi = 20°$ and $\phi = 10°$, the field oscillates a lot around the level $|E| = 1$, referring to Fig. 2.3 and Fig. 2.4. For near grazing incidence such as $\phi = 1.0°$ and $\phi = 0.5°$, we see from Fig. 2.5 and Fig. 2.6, the field strength distribution is largely attenuated when the observation point falls into between the top and bottom ends of the strips, $0 < y < h$. This phenomena can be understood by recalling waveguide mode

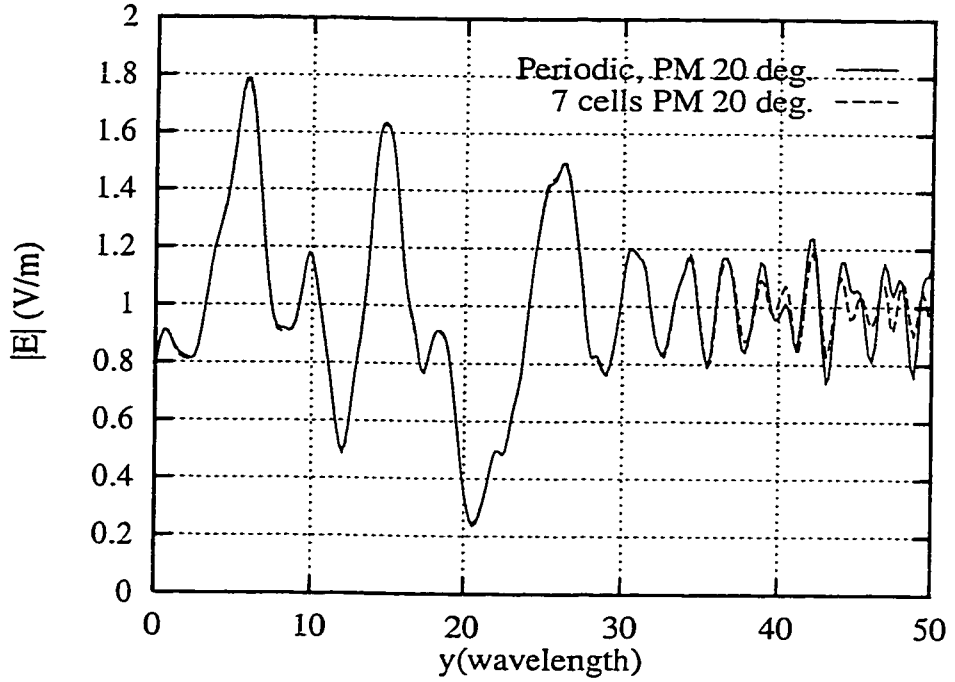

Figure 2.3: Height $h = 33\lambda$, spacing $s = 66\lambda$, incident angle $\phi = 20°$. Observer at $x = 3.5s$, the center line of cell ④ in the seven-cell array, and at $x = 0.5s$ in the periodic array.

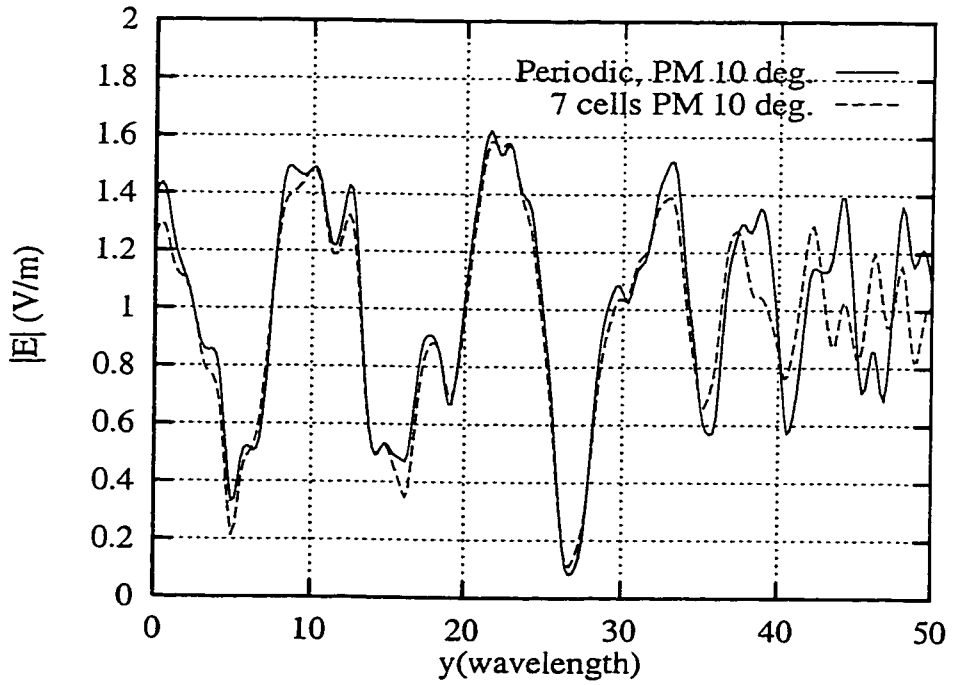

Figure 2.4: Height $h = 33\lambda$, spacing $s = 66\lambda$, incident angle $\phi = 10°$. Observer at $x = 3.5s$, the center line of cell ④ in the seven-cell array, and at $x = 0.5s$ in the periodic array.

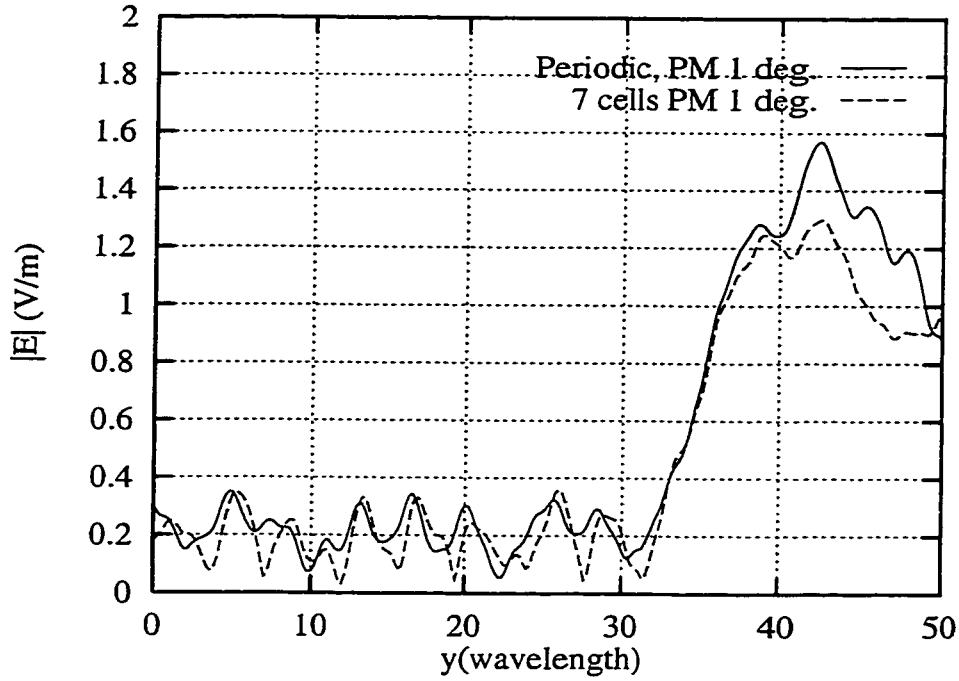

Figure 2.5: Height $h = 33\lambda$, spacing $s = 66\lambda$, incident angle $\phi = 1°$. Observer at $x = 3.5s$, the center line of cell ④ in the seven-cell array, and at $x = 0.5s$ in the periodic array.

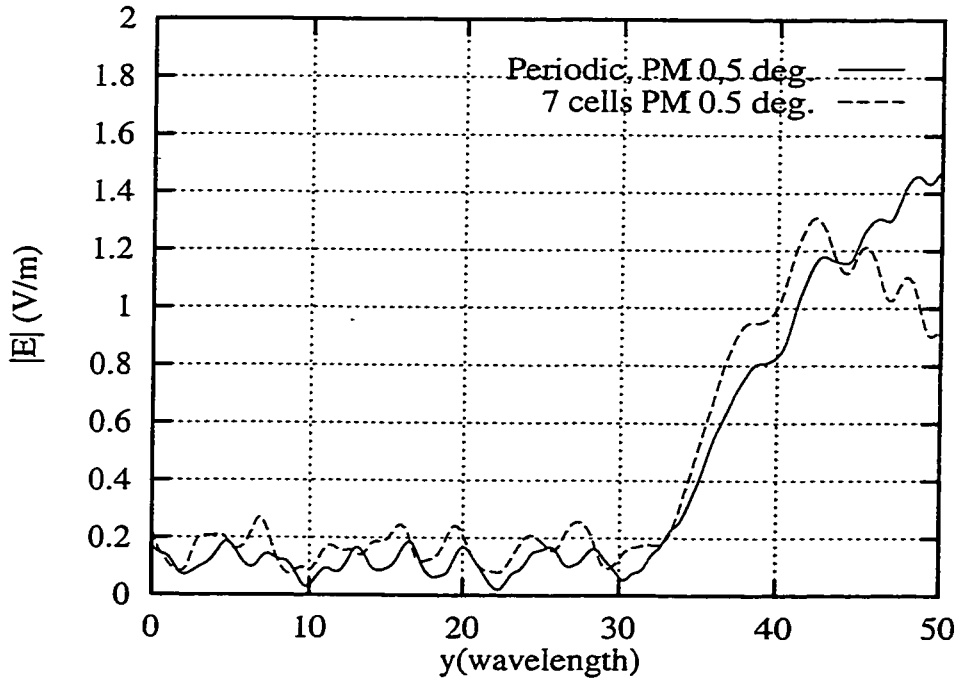

Figure 2.6: Height $h = 33\lambda$, spacing $s = 66\lambda$, incident angle $\phi = 0.5°$. Observer at $x = 3.5s$, the center line of cell ④ in the seven-cell array, and at $x = 0.5s$ in the periodic array.

theory. The wavenumbers in the x- and y-directions are given by

$$k_x = \frac{mx}{s} \qquad m = 1, 2, \cdots \tag{2.25}$$

$$k_y = k\sqrt{1 - \left(\frac{m\lambda}{2s}\right)^2} \tag{2.26}$$

where k is the wavenumber in free space.

In the above examples, $s = 66\lambda$, the highest propagating mode is $m = 131$, which gives the minimum cutoff angle as

$$\phi_0 = \cos^{-1}\frac{k_x}{k} = \cos^{-1}\frac{131}{132} = 7.057°. \tag{2.27}$$

So, when the incident angle $\phi < \phi_0$, there are only evanescent modes existing inside the waveguide, resulting a large attenuation of the field intensity inside the waveguide.

Various angles of incidence were used to calculate the field distribution in the finite and finite arrays of parallel strips, and all yield satisfactory comparison results. The values of incident angles have even been used to make the comparison are $1° < \phi < 30°$, with a step of $\Delta\phi = 1°$.

We also tried a different set of geometrical parameters for the spacing and height of the array of parallel strips. Let us choose $h = -50\lambda$ and $s = 100\lambda$, and make the comparison of field distribution between the seven-cell array and the periodic array.

Fig. 2.7 and Fig. 2.8 show results for the plane wave incident at $\phi = 10°$ and $\phi = 1°$. We see that for $\phi = 10°$, the field distribution oscillates slightly around the level $|E| = 1$, which means that the scattered field does not contribute much to the total field. For the near grazing incidence $\phi = 10°$, the field level is largely attenuated when the observation points fall in between the top and bottom ends of the parallel strips, $-50 < y < 0$. These results have been published by Liu and Paknys [13], where a wire grid model is used to replace the parallel strips. Interested readers can refer to Appendix D for derivation detail which did not appear in [13].

The Poisson summation series contains an infinite number of terms, which have to be truncated while performing numerical computation. The summation index n runs over neg-

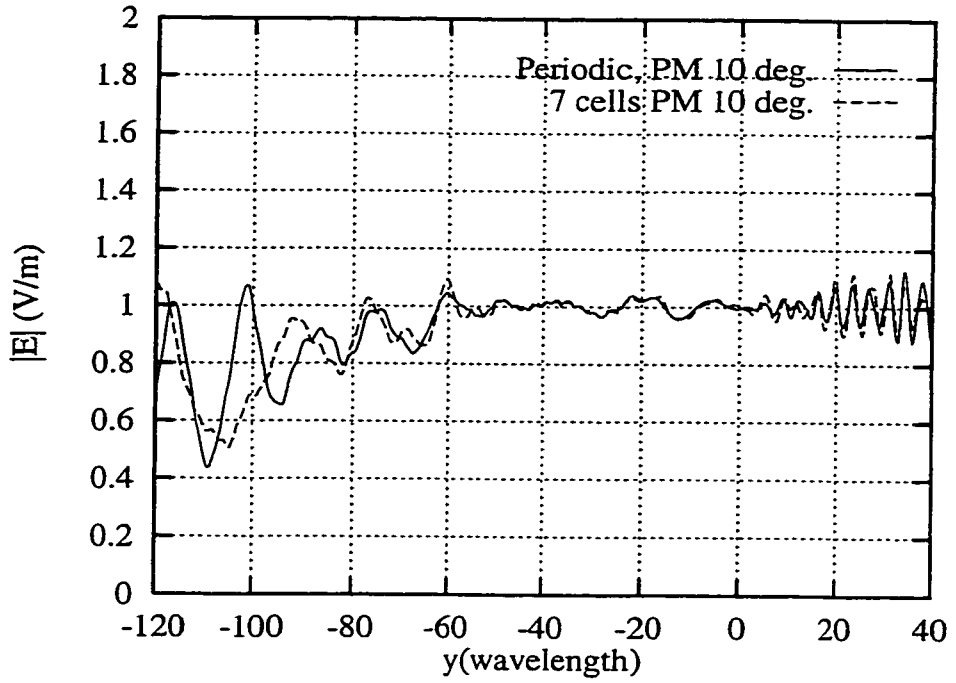

Figure 2.7: Height $h = -50\lambda$, spacing $s = 100\lambda$, incident angle $\phi = 10°$. Observer at $x = 3.5s$, the center line of cell ④ in the seven-cell array, and at $x = 0.5s$ in the periodic array.

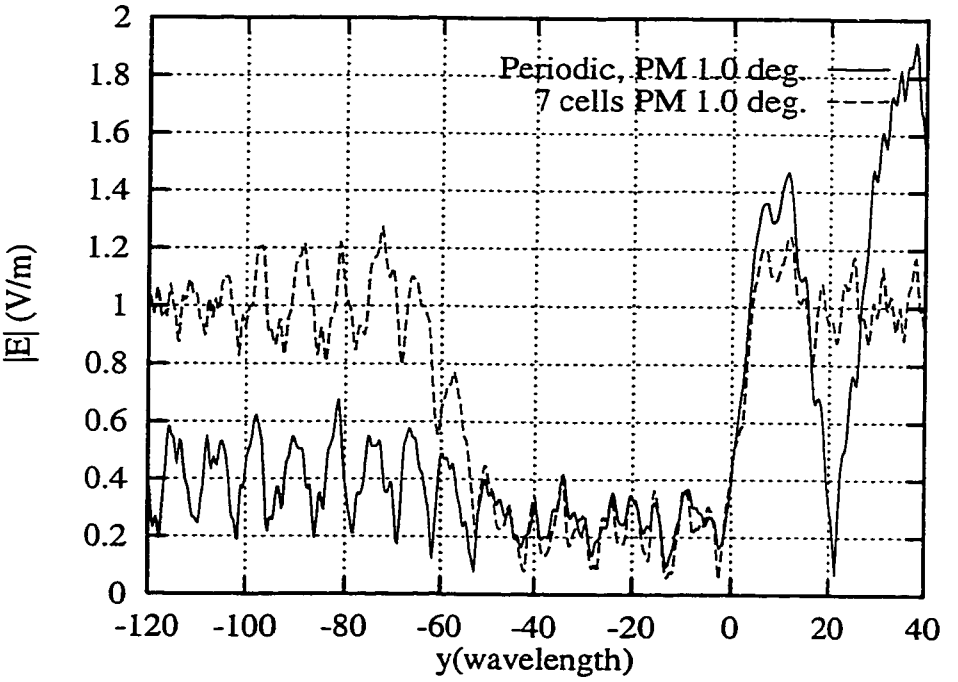

Figure 2.8: Height $h = -50\lambda$, spacing $s = 100\lambda$, incident angle $\phi = 1°$. Observer at $x = 3.5s$, the center line of cell ④ in the seven-cell array, and at $x = 0.5s$ in the periodic array.

ative infinity to positive infinity. While doing the numerical computation, the summation is done by starting from the term $n = 0$, then add the terms $n = 1, 2, \infty$ and $n = -1, -2, -\infty$ separately.

The rule we used to truncate the series is illustrated as follows. Let

$$S = \sum_{n=-\infty}^{+\infty} a_n \tag{2.28}$$

be the series that is desired to be evaluated. Performing the summation over $n < 0$ and $n > 0$ separately by denoting

$$S^+ = \frac{1}{2}a_0 + \sum_{n=1}^{\infty} a_n \qquad S^- = \frac{1}{2}a_0 + \sum_{n=-1}^{-\infty} a_n \tag{2.29}$$

to be the sum over the positive and negative range of n, respectively, we have

$$S = S^+ + S^- \tag{2.30}$$

Let

$$S_N = \sum_{1}^{N} a_n \tag{2.31}$$

be the partial sum of either S^+ or S^-. Set a typical value for the tolerance ϵ, say $\epsilon = 10^{-3}$ and let the summation procedure to stop if

$$\frac{|\sum_{N}^{2N} a_n|}{|S_N|} \leq \epsilon \tag{2.32}$$

is achieved. Then the partial sum S_N is used as an approximation for the exact value S. Otherwise, make N doubled and have the partial sums recalculated until (2.32) is satisfied.

Chapter 3

Scattering From Periodic Arrays of Grounded Parallel Strips, TE Incidence

This chapter presents the method of moments solution to the problem of transverse electric (TE) plane wave scattering from periodic arrays of grounded parallel strips. The first step is to assume TE plane wave incidence. Then the surface equivalence theorem [16] is applied to replace the perfect electric conductive strips and ground plane by free space and the unknown equivalent electric surface current **J**. Due to the fact that the geometry structure is periodic and the incident plane wave is also periodic, the solution of the equivalent surface current is periodic too. We need only assume an unknown equivalent surface current **J** within one cell of the structure. By duplicating **J** along the direction of periodicity with appropriate phase shift, we have the whole solution. The total electric field in free space is the sum of the electric field radiated by **J** in free space and the incident electric field. Imposing the boundary conditions on the surface of parallel strips and the ground plane gives an electric field integral equation (EFIE) containing **J** as an unknown. The unknown current **J** is now expanded along the surfaces of the parallel strips and the ground plane as a sum of overlapped triangular basis functions multiplied by unknown complex coefficients. An inner product is formed between each of the appropriately chosen test functions and the integral equation. Thus a system of linear equations are created. The current coefficients can be found by solving this equation. Once the surface current **J** is found, the fields radiated by

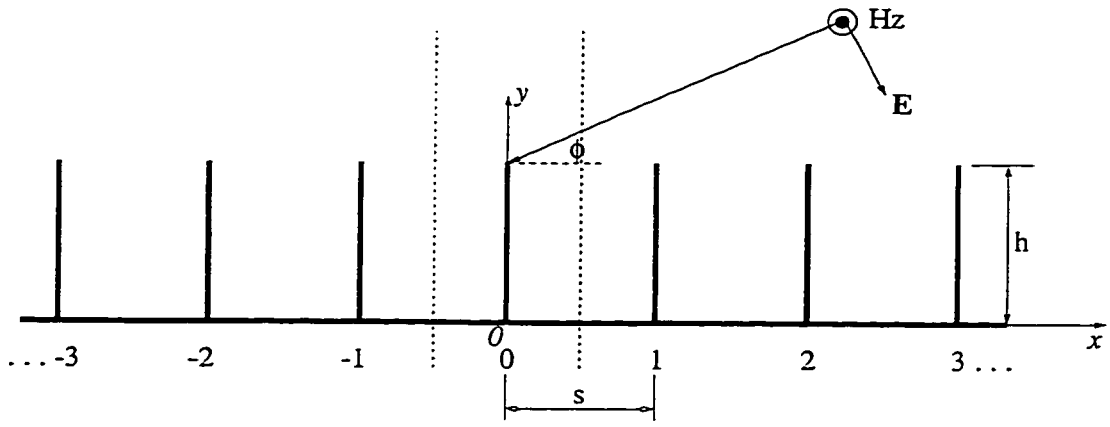

Figure 3.1: Scattering of plane wave on a periodic array of parallel strips, TE incidence.

this current are readily obtained, and the total field is found by adding the radiated field to the incident field.

The scattering problem when the periodic array is truncated on both sides is also studied. The formulation procedure for this finite array is pretty much the same as stated above, except the problem is no longer periodic and the equivalent currents run on all the surfaces of the structure. The solution to this problem is obtained by using TECYL [14], an integral equation solution for TE cylinder radiation and scattering.

In the following sections, the EFIE for the periodic structure will be established and appropriate basis functions will be employed to expand the unknown current **J**, followed by a method of moment solution to get the current **J**. Examples will be given where the scattered field at appropriate chosen observation points will be calculated and compared with the solution of the seven-cell structure from TECYL. Good agreement will be demonstrated. The work in this chapter has been submitted as a paper [18].

3.1 The Integral Equation

Consider a TE polarized plane wave incident from above upon a grounded periodic planar array of parallel strips. Both the ground and the parallel strips are assumed to be perfect electric conductors (PEC). The strips are assumed to have zero thickness, extend to infinity

along z-axis and pass through $x = ns$ where s denotes the spacing between the strips, as illustrated in Fig.3.1. The time dependence $e^{j\omega t}$ is used and suppressed throughout the analysis. The incident magnetic field is

$$H_z^i(x,y) = H_0 e^{jk(x\cos\phi + y\sin\phi)} \tag{3.1}$$
$$H_x = 0, \quad H_y = 0$$

and the electric field components are

$$E_x^i(x,y) = H_z^i(x,y)\eta\sin\phi$$
$$E_y^i(x,y) = -H_z^i(x,y)\eta\cos\phi \tag{3.2}$$
$$E_z = 0$$

where

$$k^2 = \omega^2\mu\varepsilon, \qquad \eta = \sqrt{\frac{\mu}{\epsilon}}, \tag{3.3}$$

where ω is the angular frequency, μ, ϵ are permeability and permittivity in free space, ϕ is the angle of incidence measured from $+x$-axis.

The surface equivalence theorem is employed to solve the problem. Since the geometry is periodic and the excitation is periodic along x-axis, a periodic solution is possible. The currents on the strips and the ground plane can be expressed as

$$\mathbf{J}(x+ns,y) = \mathbf{J}(x,y)e^{jnks\cos\phi}, \qquad n = -\infty,\cdots,+\infty \tag{3.4}$$

where $\mathbf{J}(x,y)$ is the current on the cell $n = 0$ (the structure between the dashed lines in Fig. 3.1).

The vector potential for this equivalent current can be expressed as

$$\mathbf{A} = \int_{l_0} \mathbf{J}(x',y')G_p(x-x',y-y')\,dl \tag{3.5}$$

where l_0 is the contour of surface for the cell $n = 0$, G_p is the Green's function for the periodic array

$$G_p(x-x',y-y') = \sum_{n=-\infty}^{+\infty} -\frac{j\mu}{4}H_0^{(2)}(k\sqrt{(x-x'-ns)^2+(y-y')^2})e^{jkns\cos\phi} \tag{3.6}$$

and $H_0^{(2)}(x)$ represents a Hankel function of the second kind.

Once we have the vector potential, the fields are ready to be expressed using the relationship [16]

$$\begin{aligned} \mathbf{E} &= -j\omega\mathbf{A} + \frac{\nabla\nabla\cdot\mathbf{A}}{j\omega\mu\epsilon} \\ \mathbf{H} &= \frac{1}{\mu}\nabla\times\mathbf{A} \end{aligned} \tag{3.7}$$

When expanded, we have the nonzero field components expressed as

$$E_x = \frac{1}{j\omega\mu\epsilon}\left[\left(k^2+\frac{\partial^2}{\partial x^2}\right)A_x + \frac{\partial^2 A_y}{\partial x\partial y}\right] \tag{3.8}$$

$$E_y = \frac{1}{j\omega\mu\epsilon}\left[\left(k^2+\frac{\partial^2}{\partial y^2}\right)A_y + \frac{\partial^2 A_x}{\partial x\partial y}\right] \tag{3.9}$$

$$H_z = \frac{1}{\mu}\left(\frac{\partial A_y}{\partial x} - \frac{\partial A_x}{\partial y}\right) \tag{3.10}$$

The boundary condition requires that

$$\hat{\mathbf{n}}\times(\mathbf{E}^s+\mathbf{E}^i) = 0, \text{ over all surfaces,} \tag{3.11}$$

where $\mathbf{E}^s$ and $\mathbf{E}^i$ represent the scattered and incident field, respectively. $\hat{\mathbf{n}}$ is the unit vector normal to the surfaces. Due to the periodical nature, we need only to impose the boundary condition on the cell $n = 0$ which lies within $x \in [-s/2, s/2]$ and $y \in [0, h]$. An equivalent expression of (3.11) for TE incidence is

$$\hat{\mathbf{t}}\cdot(\mathbf{E}^s+\mathbf{E}^i) = 0, \tag{3.12}$$

where $\hat{\mathbf{t}}$ is the unit transverse vector that is tangential to the surface.

3.2 Floquet Modes Analysis

The summation series in (3.6) decays only at $O(n^{-\frac{1}{2}})$ as $n \to \infty$. The Poisson summation formula is employed to convert the slowly convergent series into a more rapidly convergent series [19]

$$\sum_{n=-\infty}^{+\infty} H_0(k\sqrt{(x-x'-ns)^2+(y-y')^2})e^{jnks\cos\phi} = \frac{2j}{s}\sum_{n=-\infty}^{+\infty}\frac{e^{-\gamma_n|y-y'|}}{\gamma_n}e^{j\omega_n(x-x')} \tag{3.13}$$

where

$$\begin{aligned} \omega_n &= k\cos\phi - \frac{2n\pi}{s} \\ \gamma_n &= \begin{cases} j\sqrt{k^2-\omega_n^2}, & k^2 > \omega_n^2 \\ \sqrt{\omega_n^2-k^2}, & k^2 < \omega_n^2 \end{cases} \end{aligned} \tag{3.14}$$

Therefore, the Green's function (3.6) for the periodic structure can be expressed as

$$G_p(x-x', y-y') = \frac{\mu}{2s}\sum_{n=-\infty}^{+\infty} \frac{e^{-\gamma_n|y-y'|}}{\gamma_n} e^{j\omega_n(x-x')} \tag{3.15}$$

The converted series is exponentially convergent when $y - y' \neq 0$, and convergent at $O(n^{-1})$ when $y - y' = 0$. We see in both cases the converted series using the Poisson summation formula is advantageous over the original expression.

3.3 Discretization

The EFIE expressions (3.11) or (3.12) need to be discretized in order to be suitable for a computer solution. In order to discretize the EFIE, the equivalent surface current **J** is expanded along the surface where it is distributed, into a sum of independent basis functions multiplied by unknown complex coefficients. The geometry structure in cell $n = 0$ can be discretized using horizontally and vertically oriented strips, with current flowing in x and y directions, respectively. The basis function for the current expansion is triangle basis functions that overlap two adjacent strips [17]. The reason we choose the triangle basis function for the surface current expansion is that, it produces a δ-function after applying the second differentiation as defined in the field relations in (3.9) and (3.10). The behavior of δ-function simplifies the procedure in getting closed form expressions for the impedance elements.

The current continuity at the junction between the horizontal and the vertical strips, namely $(0, 0)$, is enforced by a corner dipole with a triangle basis function straddling over both its horizontal and vertical segment, as shown in Fig. 3.2.

The current continuity at $x = \pm s/2$ is ensured by a basis function that straddles into the adjacent cell, $n = 1$, shown by the dashed line in Fig. 3.2. Therefore by replicating the

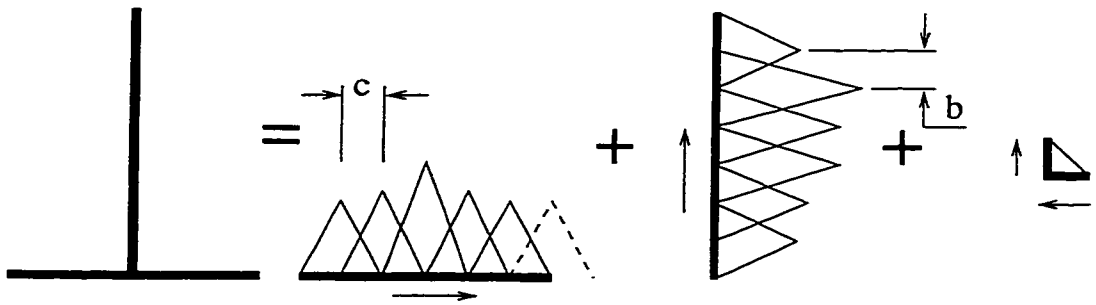

Figure 3.2: Strip model of the surface current on cell $n = 0$, discretized using triangle basis function.

current on the horizontal strip in cell $n = 0$ along the x axis in a period s, continuously flowing current on a ground plane is achieved. The current distribution on cell $n = 0$ can be expressed by

$$\mathbf{J}(x,y) = a_0\mathbf{f}_0(x,y) + \sum_{l=1}^{L} b_l f_l(x)\hat{\mathbf{x}} + \sum_{m=1}^{M} c_m f_m(y)\hat{\mathbf{y}}, \tag{3.16}$$

where $\mathbf{f}_0(x,y)$, $f_l(x)$ and $f_m(y)$ are triangle basis functions defined by

$$\mathbf{f}_0(x,y) = \begin{cases} f_{0x}(x)\hat{\mathbf{x}} & 0 \le x \le c, \\ f_{0y}(y)\hat{\mathbf{y}} & 0 \le y \le b. \end{cases} \tag{3.17}$$

$$f_l(x) = \begin{cases} 1 + \dfrac{x - x_l}{c}, & -c < x - x_l \le 0 \\ 1 - \dfrac{x - x_l}{c}, & 0 < x - x_l \le c \end{cases} \text{. and} \tag{3.18}$$

$$f_m(y) = \begin{cases} 1 + \dfrac{y - y_m}{b}, & -b < y - y_m \le 0 \\ 1 - \dfrac{y - y_m}{b}, & 0 < y - y_m \le b \end{cases} \tag{3.19}$$

and

$$f_{0x}(x) = \left(\frac{x}{c} - 1\right) \quad \text{and} \quad f_{0y}(y) = \left(1 - \frac{y}{b}\right) \tag{3.20}$$

respectively. The coefficients a_0, b_l and c_m are for the current basis on the corner dipole, horizontal and vertical strips, are to be determined. The length of the horizontal strip in cell $n = 0$ is s, we make it equally divided into L segments, with L current modes, each mode occupying two adjacent segments. The spacing between adjacent current modes is

$$c = \frac{s}{L}.$$

The length of the vertical strip is h, equally divided into $M+1$ segments, with M current modes, and each mode occupying two adjacent segments. The spacing between adjacent current modes is

$$b = \frac{h}{M+1}.$$

In Fig. 3.2 we have illustrated a discretization example with $L = 6$ and $M = 6$.

Substituting (3.16) into (3.5), we obtain the vector potential

$$\mathbf{A}(x,y) = a_0\mathbf{A}_0(x,y) + \sum_{l=1}^{L} b_l A_l(x,y)\hat{\mathbf{x}} + \sum_{m=1}^{M} c_m A_m(x,y)\hat{\mathbf{y}} \tag{3.21}$$

where $\mathbf{A}_0(x,y)$ is the vector potential due to the current on the corner dipole. It can be expressed as the sum of it x and y components as

$$\mathbf{A}_0(x,y) = \int \mathbf{f}_0(x',y')G_p(x-x',y-y')\,dl' = A_{0x}(x,y)\hat{\mathbf{x}} + A_{0y}(x,y)\hat{\mathbf{y}}, \tag{3.22}$$

where $A_{0x}(x,y)$ and $A_{0y}(x,y)$ are the x and y component of the vector potential due to the current on the corner dipole. They can be expressed as

$$A_{0x}(x,y) = f_{0x}(x) * G_p(x,y) \tag{3.23}$$

$$A_{0y}(x,y) = f_{0y}(y) * G_p(x,y), \tag{3.24}$$

where f_{0x}, f_{0y} are the x and y components of $\mathbf{f}_0$ defined in (3.17). We note that $*$ denotes the convolution operator.

The two summation terms in (3.21) contain $A_l(x,y)$ and $A_m(x,y)$, which are potentials produced by the equivalent current on the horizontal and vertical strips, respectively. They are expressed as

$$A_l(x,y) = \int f_l(x')G_p(x-x',y)\,dx' = f_l(x) * G_p(x,y) \tag{3.25}$$

$$A_m(x,y) = \int f_m(y')G_p(x,y-y')\,dy' = f_m(y) * G_p(x,y). \tag{3.26}$$

Substituting (3.21) and (3.26) into (3.7), we have the scattered electric field expressed as

$$\begin{aligned}\mathbf{E}^s = &\hat{\mathbf{x}}E^s_{0x}(x,y) + \hat{\mathbf{y}}E^s_{0y}(x,y) \\ &+ \sum_{l=1}^{L} \hat{\mathbf{x}}E^s_{lx}(x,y) + \hat{\mathbf{y}}E^s_{ly}(x,y) \\ &+ \sum_{m=1}^{M} \hat{\mathbf{x}}E^s_{mx}(x,y) + \hat{\mathbf{y}}E^s_{my}(x,y)\end{aligned} \tag{3.27}$$

3.4 Method of Moments Formulation

The integral equation (3.12) can be enforced by weighting the equation with pulse functions whose domain begins in the center of one strip and extends to the center of an adjacent strip, as

$$-\int_l T(t)\hat{\mathbf{t}} \cdot \mathbf{E}^s dt = \int_l T(t)\hat{\mathbf{t}} \cdot \mathbf{E}^i dt \tag{3.28}$$

where l is the contour of the surfaces where the boundary condition is to be ensured, $\hat{\mathbf{t}}$ is the unit tangential vector along l and $T(t)$ is a pulse function to be defined.

Substituting (3.5) and (3.16) into (3.28), we have the following linear algebraic equations

$$\begin{cases} a_0 Z_{00} + \sum_{l=1}^{L} b_l Z_{0l} + \sum_{m=1} c_m Z_{0m} &= V_0 \\ a_0 Z_{p0} + \sum_{l=1}^{L} b_l Z_{pl} + \sum_{m=1} c_m Z_{pm} &= V_p, \quad p = 1, 2, \cdots, L \\ a_0 Z_{q0} + \sum_{l=1}^{L} b_l Z_{ql} + \sum_{m=1} c_m Z_{qm} &= V_q, \quad q = 1, 2, \cdots, M \end{cases} \tag{3.29}$$

We have $L+M+1$ linear equations, ready to solve for the $L+M+1$ expansion coefficients in (3.16). The subscripts of the impedance elements are arranged as Z_{ij}, where i, j refer to the test and source segment, respectively. The right-side of (3.29) represents the excitation voltages on each test segment by the incident field.

The contour of integration l is defined along the tangential line of each segment. In the present problem, only x and y oriented segments are present, therefore the integration will be carried along the $x-$ and $y-$ axis, respectively. For the corner dipole, the contour is

defined to start at $(c/2, 0)$ and ends at $(0, b/2)$. Therefore we have the first row of elements expressed by

$$Z_{0k} = \int T_0(x) E^s_{kx}(x, 0)\, dx - \int T_0(y) E^s_{ky}(0, y)\, dy \qquad k = 0, k = l \text{ or } k = m \tag{3.30}$$

where E^s_{kx} and E^s_{ky} are $x-$ and $y-$ component of the electric field on the corner dipole produced by the equivalent current on either other sources or on itself. Therefore the entries of the impedance matrix can be expressed as

$$Z_{00} = \int T_0(x) E^s_{0x}(x, 0) dx - \int T_0(y) E^s_{0y}(0, y) dy \tag{3.31}$$

$$Z_{p0} = -\int T_p(x) E^s_{0x}(x, 0) dx \tag{3.32}$$

$$Z_{q0} = -\int T_q(y) E^s_{0y}(0, y) dy \tag{3.33}$$

where E^s_{0x} and E^s_{0y} are x and y components of the electric field produced by the current basis function $\mathbf{f}_0(x, y)$.

The excitation voltage on the corner dipole can be expressed as

$$V_0 = -\int T_0(x) E^i_x(x, 0) dx + \int T_0(y) E^i_y(0, y) dy \tag{3.34}$$

In the equation (3.31), $T_0(x)$ and $T_0(y)$ are test functions defined on the $x-$ and $y-$ arms of the corner dipole, as

$$T_0(x) = \begin{cases} 1 & x \in [0, \frac{c}{2}] \\ 0 & \text{else} \end{cases}, \qquad T_0(y) = \begin{cases} 1 & y \in [0, \frac{b}{2}] \\ 0 & \text{else} \end{cases}. \tag{3.35}$$

In equations (3.32) and (3.33), $T_p(x)$ and $T_q(y)$ are test functions defined on the horizontal and vertical strip dipoles as

$$T_p(x) = T(x - x_p) \quad \text{and} \quad T_q(y) = T(y - y_q), \tag{3.36}$$

respectively. Also,

$$T(x) = \begin{cases} 1 & x \in [-\frac{c}{2}, \frac{c}{2}], \\ 0 & \text{else.} \end{cases} \qquad T(y) = \begin{cases} 1 & y \in [-\frac{b}{2}, \frac{b}{2}], \\ 0 & \text{else.} \end{cases} \tag{3.37}$$

Similarly we have the remaining entries of the impedance matrix written as

$$Z_{0l} = \int T_0(x)E^s_{lx}(x,0)dx - \int T_0(y)E^s_{ly}(0,y)dy \tag{3.38}$$

$$Z_{pl} = -\int T_p(x)E^s_{lx}(x,0)dx \tag{3.39}$$

$$Z_{ql} = -\int T_q(y)E^s_{ly}(0,y)dy \tag{3.40}$$

where E^s_{lx} and E^s_{ly} are x and y components of the electric field produced by the current basis function $f_l(x)\hat{\mathbf{x}}$

$$Z_{0m} = \int T_0(x)E^s_{mx}(x,0)dx - \int T_0(y)E^s_{my}(0,y)dy \tag{3.41}$$

$$Z_{pm} = -\int T_p(x)E^s_{mx}(x,0)dx \tag{3.42}$$

$$Z_{qm} = -\int T_q(y)E^s_{my}(0,y)dy \tag{3.43}$$

where E^s_{mx} and E^s_{my} are x and y components of the electric field produced by the current basis function $f_m(y)\hat{\mathbf{y}}$.

The excitation voltage for the segments on the ground plane and the parallel strips can be expressed as

$$V_p = \int T(x-x_p)E^i_x(x,0)\,dx, \qquad p = 1,2,\cdots,L \tag{3.44}$$

$$V_q = \int T(y-y_q)E^i_y(0,y)\,dy, \qquad q = 1,2,\cdots,M \tag{3.45}$$

3.5 The Impedance Matrix Entries

Using the Floquet mode analysis of the previous section, the impedance matrix entries are found to be, as derived in Appendix B

$$\begin{aligned} Z_{00} =& \frac{j\eta}{2ks}\sum_{n=-\infty}^{+\infty}\left\{\frac{3b}{4}\cdot\frac{k^2}{\gamma_n^2} + \frac{1-e^{j\omega_n\frac{c}{2}}}{\gamma_n}\left[\left(\frac{k^2}{\omega_n^2}-1\right)\frac{e^{-j\omega_n c}-1}{j\omega_n c} + \frac{k^2}{\omega_n^2} - \frac{1-e^{-\gamma_n b}}{b\gamma_n}\right]\right. \\ & \left. -\frac{1-e^{-\gamma_n\frac{b}{2}}}{\gamma_n}\left[\left(1+\frac{k^2}{\gamma_n^2}\right)\frac{1-e^{-\gamma_n\frac{b}{2}}}{b\gamma_n} + \frac{k^2}{\gamma_n^2} + \frac{1-e^{-j\omega_n c}}{j\omega_n c}\right]\right\} \end{aligned} \tag{3.46}$$

$$Z_{p0} = \frac{\eta}{ks}\sum_{n=-\infty}^{+\infty}\frac{e^{j\omega_n x_p}}{\gamma_n}\sin\frac{\omega_n c}{2}\left[\left(1-\frac{k^2}{\omega_n^2}\right)\cdot\frac{e^{-j\omega_n c}-1}{j\omega_n c} + \frac{1-e^{-\gamma_n b}}{b\gamma_n} - \frac{k^2}{\omega_n^2}\right] \tag{3.47}$$

$$Z_{q0} = \frac{j\eta}{2ks} \sum_{n=-\infty}^{+\infty} \begin{cases} \dfrac{e^{-\gamma_n(t-\frac{3}{2}b)}}{\gamma_n}(1-e^{-\gamma_n b}) \\ \left[\left(1+\dfrac{k^2}{\gamma_n^2}\right)\dfrac{1-e^{-\gamma_n b}}{b\gamma_n} - \left(\dfrac{1-e^{-j\omega_n c}}{j\omega_n c}+\dfrac{k^2}{\gamma_n^2}\right)e^{-\gamma_n b}\right] & t \geq 2b, \\ \dfrac{k^2}{\gamma_n^2}\dfrac{b}{4} + \dfrac{1-e^{-\gamma_n \frac{b}{2}}}{\gamma_n}\left[\left(1+\dfrac{k^2}{\gamma_n^2}\right)\dfrac{(1-e^{-\gamma_n\frac{b}{2}})(2+e^{-\gamma_n\frac{b}{2}})}{b\gamma_n}\right. & \\ \left. - \left(\dfrac{1-e^{-j\omega_n c}}{j\omega_n c}+\dfrac{k^2}{\gamma_n^2}\right)e^{-\gamma_n\frac{b}{2}}(1+e^{-\gamma_n\frac{b}{2}})\right] & t = b. \end{cases} \tag{3.48}$$

where $t = y_q$.

$$Z_{0l} = \frac{2\eta}{ksc} \sum_{n=-\infty}^{+\infty} \frac{e^{-j\omega_n x_l}}{\gamma_n} \frac{\sin^2\left(\frac{\omega_n c}{2}\right)}{\omega_n} \left[\frac{k^2}{\omega_n^2} + \left(1-\frac{k^2}{\omega_n^2}\right)e^{j\omega_n\frac{c}{2}} - e^{-\gamma_n\frac{b}{2}}\right] \tag{3.49}$$

$$Z_{pl} = \frac{4j\eta}{ksc} \sum_{n=-\infty}^{+\infty} \left(\frac{k^2}{\omega_n^2}-1\right) \frac{\sin^3\frac{\omega_n c}{2}}{\omega_n} \frac{e^{j\omega_n(x_p-x_l)}}{\gamma_n} \tag{3.50}$$

$$Z_{ql} = -\frac{2\eta}{ksc} \sum_{n=-\infty}^{+\infty} \frac{\sin^2\frac{\omega_n c}{2}}{\omega_n} e^{-j\omega_n x_l} \frac{e^{-\gamma_n(y_q+\frac{b}{2})} - e^{-\gamma_n(y_q-\frac{b}{2})}}{\gamma_n} \tag{3.51}$$

$$Z_{0m} = \frac{j\eta}{2ksb} \sum_{n=-\infty}^{+\infty} \frac{Q_n(t)}{\gamma_n^2} \tag{3.52}$$

where

$$Q_n(t) = \begin{cases} e^{-\gamma_n(t-\frac{3}{2}b)}(1-\xi_n)^2(1+\xi_n)^2 & \\ \left[\left(1+\dfrac{k^2}{\gamma_n^2}\right)(1-\xi_n)+\xi_n(1-e^{j\omega_n\frac{c}{2}})\right] & t \geq 2b, \\ \dfrac{(kb)^2}{4}+(1-\xi_n)^2 & \\ \left[\left(1+\dfrac{k^2}{\gamma_n^2}\right)\left(1-\xi_n-\xi_n^2\right)+(1+\xi_n)^2\left(1-e^{j\omega_n\frac{c}{2}}\right)\right] & t = b. \end{cases} \tag{3.53}$$

where $t = y_m$ and $\xi_n = e^{-\gamma_n\frac{b}{2}}$.

$$Z_{pm} = -\frac{\eta}{ksb}\sum_{n=-\infty}^{+\infty}\frac{e^{-\gamma_n(y_m-b)}}{\gamma_n^2}(1-e^{-\gamma_n b})^2\sin\frac{\omega_n c}{2}e^{j\omega_n x_p} \tag{3.54}$$

$$Z_{qm} = \frac{j\eta}{2ksb}\sum_{n=-\infty}^{+\infty}\frac{Q_n(t)}{\gamma_n^2} \tag{3.55}$$

where $t = y_q - y_m$ and

$$Q_n(t) = \begin{cases} \left(1+\dfrac{k^2}{\gamma_n^2}\right)e^{-\gamma_n(|t|-\frac{3b}{2})}\left(1-e^{-\gamma_n b}\right)^3 & |t| \geq 2b \\ \dfrac{1}{4}k^2b^2 + \left(1+\dfrac{k^2}{\gamma_n^2}\right)\left(1-e^{-\gamma_n\frac{b}{2}}\right)^2\left(2-2e^{-\gamma_n b}-e^{-\gamma_n\frac{3b}{2}}\right) & |t| = b \\ \dfrac{3k^2b^2}{2} - 2\left(1+\dfrac{k^2}{\gamma_n^2}\right)\left(1-e^{-\gamma_n\frac{b}{2}}\right)^2\left(2+e^{-\gamma_n\frac{b}{2}}\right) & |t| = 0 \end{cases} \tag{3.56}$$

The excitation voltages on the corner dipole, segment on ground plane and parallel strips are expressed as

$$V_0 = \frac{j\eta H_0}{k}\left[\left(e^{jk\frac{c}{2}\cos\phi}-1\right)\tan\phi + \left(e^{jk\frac{b}{2}\sin\phi}-1\right)\cot\phi\right], \tag{3.57}$$

$$V_p = \frac{2\eta}{k}\tan\phi\sin\left(\frac{kc}{2}\cos\phi\right)H^i(x_p,0), \qquad p = 1,2,\cdots,L. \tag{3.58}$$

and

$$V_q = -2\eta\cot\phi\sin\left(\frac{kb}{2}\sin\phi\right)H^i(0,y_q), \qquad q = 1,2,\cdots,M. \tag{3.59}$$

respectively.

The impedance matrix entries and the excitation voltages are readily evaluated using (3.46) through (3.59). The linear system algebraic equation (3.29), can be solved and the coefficients (a_0, b_l, c_m) for the equivalent surface electric currents is obtained. Substituting (a_0, b_l, c_m) into (3.16), the expression for the unknown equivalent surface current can be evaluated.

3.6 Scattered Fields

Once the surface equivalent currents are obtained, the scattered fields can be evaluated. The scattered magnetic field can be evaluated by substituting (3.16), (3.5) and (3.6) into (3.10), as

$$H_z^s = \frac{1}{\mu}\left(\frac{\partial A_y}{\partial x} - \frac{\partial A_x}{\partial y}\right) \tag{3.60}$$

The total field comes from three parts: current on the corner dipole, current on the ground plane and current on the vertical strips, respectively. We write the scattered magnetic field as three parts,

$$H^s = H_0^s + H_g^s + H_p^s \tag{3.61}$$

where H_0^s, H_g^s and H_s^s denote the scattered magnetic field due to current on the corner dipole, current on the ground plane and current on the parallel strips, respectively. The subscript z is suppressed here and thereafter, since the magnetic field has only a nonzero z-component in our analysis. The magnetic field from the currents on the corner dipoles is

$$H_0^s(x,y) = \frac{1}{2s}a_0 \sum_{n=-\infty}^{+\infty} e^{j\omega_n x} \begin{cases} Q_n(y) & y \geq b \\ 2\left(1-\frac{y}{b}\right)\frac{j\omega_n}{\gamma_n^2} + Q_n(y) & y < b \end{cases} \tag{3.62}$$

where

$$Q_n(y) = \frac{j\omega_n}{b\gamma_n^3}e^{-\gamma_n|y-b|} + \left[\frac{e^{-j\omega_n c}-1}{\omega_n^2 c} - \frac{j\omega_n}{\gamma_n^2}\left(\frac{1}{b\gamma_n} + \frac{k^2}{\omega_n^2}\right)\right]e^{-\gamma_n y} \tag{3.63}$$

We see that when $y > b$, (3.62) is exponentially convergent. For the case $y = b$, the convergence rate is at $O(n^{-2})$, while for the case $y < b$, it is only $O(n^{-1})$ as $n \to \infty$.

The scattered magnetic field from currents on horizontal oriented strips is, for $y \geq 0$

$$H_g^s(x,y) = \frac{c}{2s}\sum_{l=1}^{L} a_l \sum_{n=-\infty}^{+\infty} e^{j\omega_n(x-x_l)}e^{-\gamma_n y}\left(\frac{\sin\alpha_n}{\alpha_n}\right)^2 \tag{3.64}$$

where

$$\alpha_n = \frac{\omega_n c}{2}.$$

We see the terms in the series decays at least at $O(n^{-2})$, which happens when $y = 0$, otherwise exponential decay is ensured as $n \to \infty$.

The scattered magnetic field from currents on parallel strips is

$$H_p^s(x,y) = \frac{j}{2s} \sum_{m=1}^{M} a_m \sum_{n=-\infty}^{\infty} \frac{\omega_n}{\gamma_n^2} e^{j\omega_n x} S_n(t) \tag{3.65}$$

where $t = y - y_m$ and

$$S_n(t) = \begin{cases} \dfrac{e^{-\gamma_n|t|}}{b\gamma_n}\left(e^{\gamma_n b} - 2 + e^{-\gamma_n b}\right), & |t| \geq b \\ 2\left(1 - \dfrac{|t|}{b}\right) + \dfrac{1}{b\gamma_n}\left[e^{\gamma_n(|t|-b)} - 2e^{-\gamma_n|t|} + e^{-\gamma_n(|t|+b)}\right], & |t| \leq b \end{cases} \tag{3.66}$$

The series in equation (3.65) decays exponentially when $|t| > b$ but only decays at $O(n^{-1})$ when $|t| \leq b$ as $n \to \infty$.

An accelerating method [17] was applied to ensure proper numerical convergence in the calculation of the scattered field while using (3.62), (3.64) and (3.65). Mathematical details for the calculation of the scattered fields and impedance can be found in Appendix B.

3.7 Results and Discussion

The field distribution in periodic arrays exhibits a periodic behavior while the observation point moves from one cell to the other. It is sufficient to study the field behavior within one cell.

Let's consider a typical geometry of a residential area, which contains rows of two story houses. The height is about thirty feet, the spacing between them is about sixty feet. For radio frequency at 1 GHz, if we choose $h = 33\lambda$ and $s = 66\lambda$, where λ is the wavelength of the incident field, the scenario can be well approximated by our model shown in Fig. 3.1.

For comparison, the field in an array containing a finite number of grounded parallel strips was calculated. As an example, the geometry of an array containing eight strips is shown in Fig. 3.3. The whole structure was divided into seven cells by the eight strips. The calculation is made possible by using TECYL [14], a method of moments code for cylinders

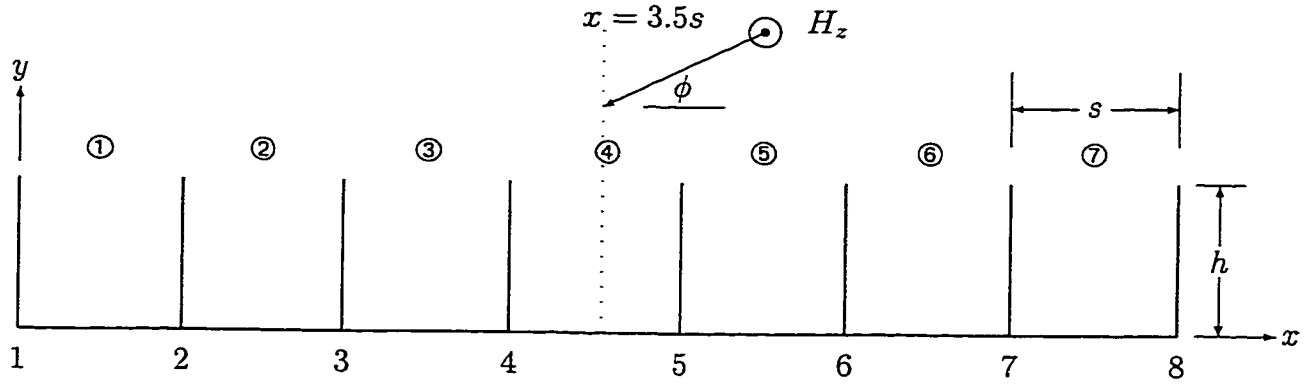

Figure 3.3: TE plane wave incident upon a grounded seven-cell parallel strips array.

under TE illumination. The study of field behavior is focused at the central cell of this finite length array. The field distribution within the central cell is probably the least disturbed field by the truncated edges on both ends. We will compare the field within the cell ④ of the seven-cell structure with the field in a periodic structure with the same height h and spacing s.

The field within cell ④ is dominated by the height and spacing of the strip pair standing on both sides and the ground plane. The presence of the other strips also create a disturbance on the field distribution. One would expect that, the closer the separation the greater the disturbance. From Fig. 3.3, we can expect that strip 6 will have a greater disturbance on the field within cell ④ than strip 7 has. We can also expect that when we add more parallel strips and ground planes on both ends of the structure along x direction, the field within the central cell would asymptotically approach the field distribution of a periodic structure, as the numbers of strips tend to infinity.

In the following example, a segment length of 0.1λ is used to divide the surface of the structure. Fig. 3.4 through Fig. 3.6 show the plot of fields in cell ④ of the seven-cell structure. The ground plane is absent. Without losing generality, the field points are selected to move in the y-direction along the central line of cell ④ at $x = 3.5s$. For comparison, the field distribution along the observation line $x = 0.5s$ in the periodic array is also calculated and

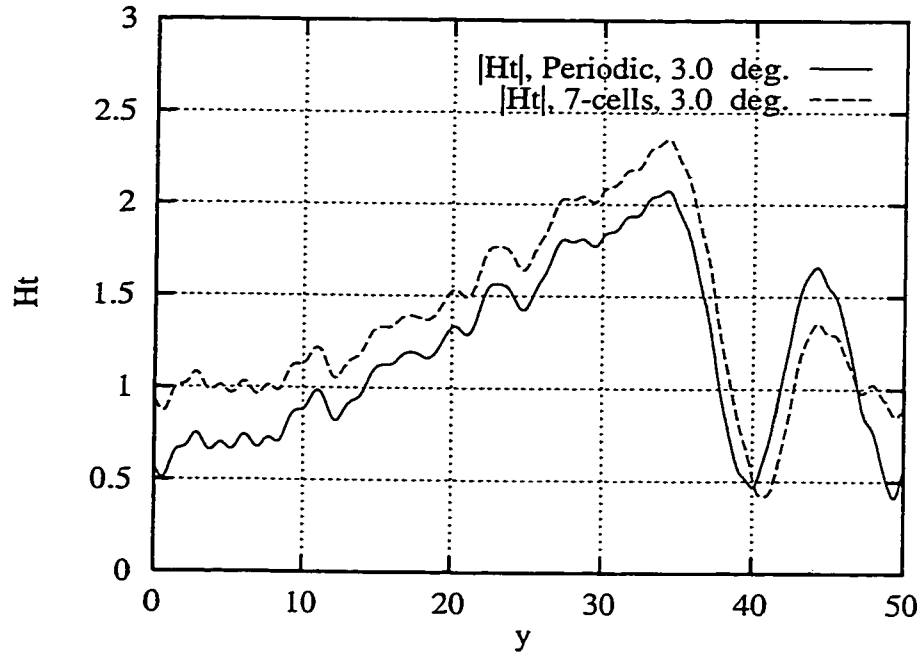

Figure 3.4: Height $h = 33\lambda$, spacing $s = 66\lambda$, incident angle $\phi = 3°$. Observer at $x = 3.5s$, the center line of cell ④ in the seven-cell array, and at $x = 0.5s$ in the periodic array. Ground plane is absent.

plotted in the same figure. We chose x to be fixed and y is the variable for the field point, because we anticipate good agreement inside the cell, but not outside the cell.

From Fig. 3.4, we see the field distribution in the central cell of the seven-cell structure is very close to the result from a periodic structure.

For smaller incident angles, such as $\phi = 1°$, we see from Fig. 3.5 that the difference between the two plots becomes larger. For near grazing incidence such as $\phi = 0.5°$, we see from Fig. 3.6 the plot of the field for the seven-cell structure is very different from the plots for the field in the periodic structure.

Fig. 3.7 through Fig. 3.9 plot the field distribution in both the seven-cell and the periodic structure, with the lower ends of the parallel strip array closed with a perfectly conductive plane. The other parameters remain unchanged as used in Fig. 3.4 through Fig. 3.6. Compared with the results from that without the ground plane, similar trends are observed. When the incident angle is away from grazing, say $\phi = 3°$, the two plots are so close to each

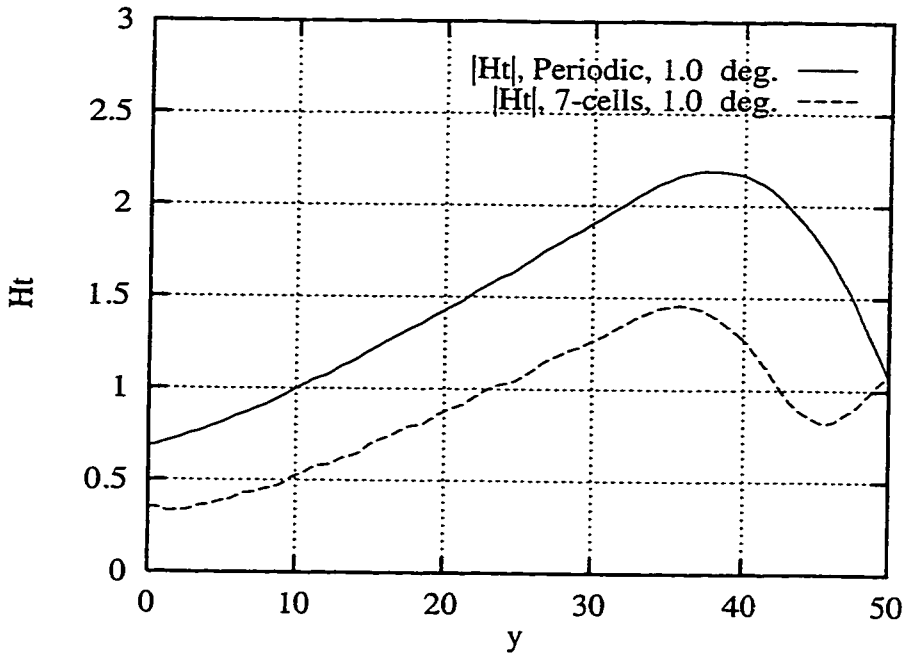

Figure 3.5: Height $h = 33\lambda$, spacing $s = 66\lambda$, incident angle $\phi = 1°$. Observer at $x = 3.5s$, the center line of cell ④ in the seven-cell array, and at $x = 0.5s$ in the periodic array. Ground plane is absent.

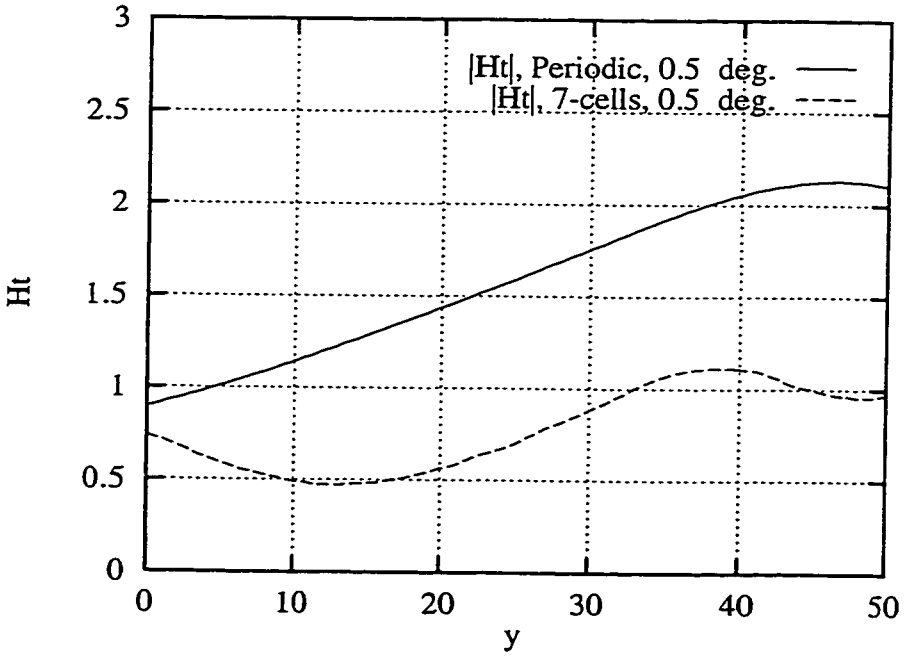

Figure 3.6: Height $h = 33\lambda$, spacing $s = 66\lambda$, incident angle $\phi = 0.5°$. Observer at $x = 3.5s$, the center line of cell ④ in the seven-cell array, and at $x = 0.5s$ in the periodic array. Ground plane is absent.

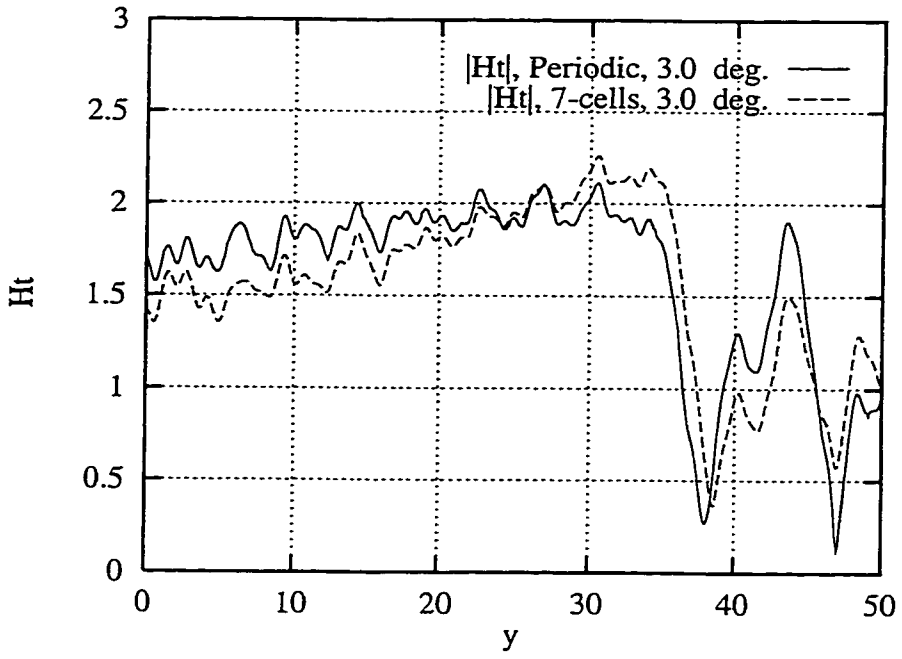

Figure 3.7: Height $h = 33\lambda$, spacing $s = 66\lambda$, incident angle $\phi = 3°$. Observer at $x = 3.5s$, the center line of cell ④ in the seven-cell array, and at $x = 0.5s$ in the periodic array. Ground plane is present.

other that the result from the periodic structure can be virtually used to approximate the field in the seven-cell structure. $0 \leq y \leq h$.

When approaching grazing incidence, the deviation between the two plots becomes large. Also noticed is that when the observation point is close to the ground plane, the field levels are higher than the corresponding cases without the ground plane. This is reasonable since the image effect of the ground plane strengthens the magnetic field strength in the upper half space.

Another interesting phenomena for near grazing incidence is that the field intensity does not show much fluctuation and attenuation when the observer moves inside between the parallel strips, as it did when in the case of TM incidence. This trend can be clearly seen from Fig. 3.6 and Fig. 3.9.

From either the case with or without the ground plane, we noticed the field behavior in a periodic array deviates from the field in their corresponding seven-cell array for low

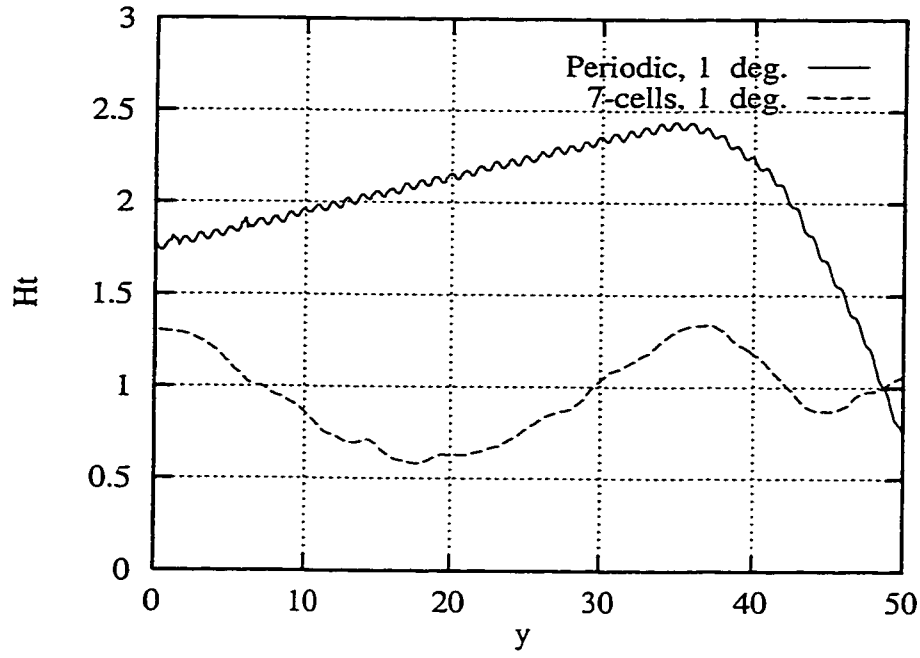

Figure 3.8: Height $h = 33\lambda$, spacing $s = 66\lambda$, incident angle $\phi = 1°$. Observer at $x = 3.5s$, the center line of cell ④. in the seven-cell array, and at $x = 0.5s$ in the periodic array Ground plane is present.

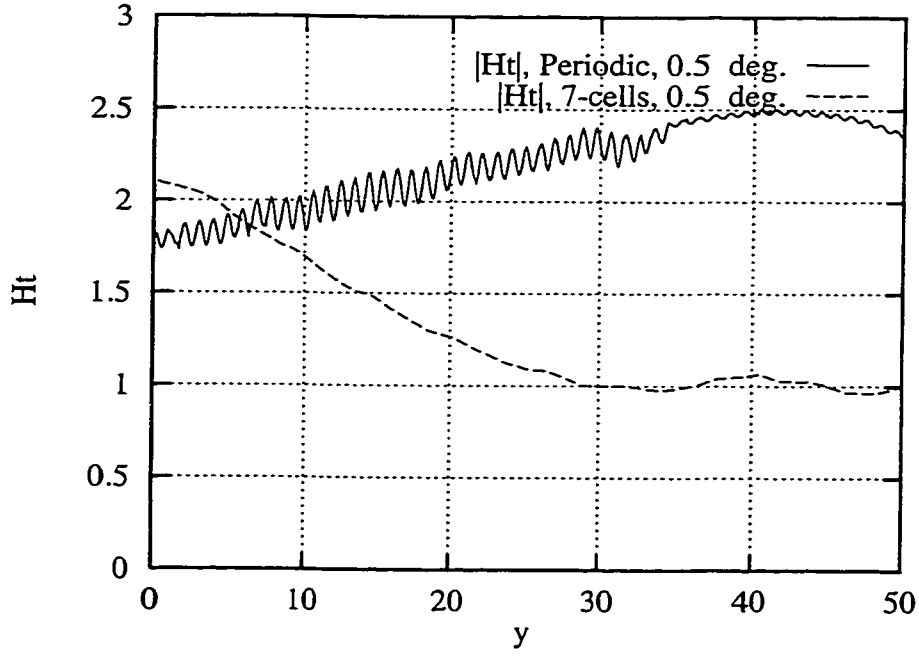

Figure 3.9: Height $h = 33\lambda$, spacing $s = 66\lambda$, incident angle $\phi = 0.5°$. Observer at $x = 3.5s$, the center line of cell ④ in the seven-cell array, and at $x = 0.5s$ in the periodic array. Ground plane is present.

incident angles. This behavior was understood in [1] where plane wave forward scattering from uniform arrays of absorbing half screens were studied. The settled value of the field strength on the tip of each screen can be achieved when the first Fresnel zone about the ray through the $n = N_0$ edge just clears the $n = 0$ edge. The screen number N_0 is given by [1]

$$N_0 = \frac{\lambda}{s}\cot^2\phi \tag{3.67}$$

In our calculation examples, $s = 66\lambda$; a brief table was made from (3.67) to show the dependency of N_0 on ϕ; refer to Table 3.1. When the observation points are selected in cell ④, we have four strips on both sides of them. The minimum value for the incident angle required by (3.67) is 4°. This can be seen from the result in either Fig. 3.4 or Fig. 3.7 where we have virtually identical results for the periodic array and a finite strip array, with the number of strips as small as eight.

In solving the EFIE for the periodic array, only the equivalent current distributed in one cell need to be solved for, unlike in the problem for a finite strip array where the current distribution in every cell need be solved for. We noted the computation time for the examples discussed above. The program we compiled for the computation of the periodic array of grounded parallel strips under TE plane wave incidence is named PAGPS. The program we use for computation of the array containing finite numbers of parallel strips with ground plane is TECYL. The computer we used to run these two programs is a PENTIUM 1 GHz. For the two plots shown in Fig. 3.8, running TECYL took 9h18m while running PAGPS took 0h26m.

Besides the aforementioned examples, we also made computation using other values of the incident angles of the incident field. Fig. 3.10 through Fig. 3.13 show computational results for the plane wave incident at 10°, 20° and 30°, respectively. We see the comparison

ϕ	0.5°	1°	2°	3°	4°	5°	6°	7°
N_0	198	49	12	5	3	1	1	1

Table 3.1: The number of screens needed for the field to achieve settled values.

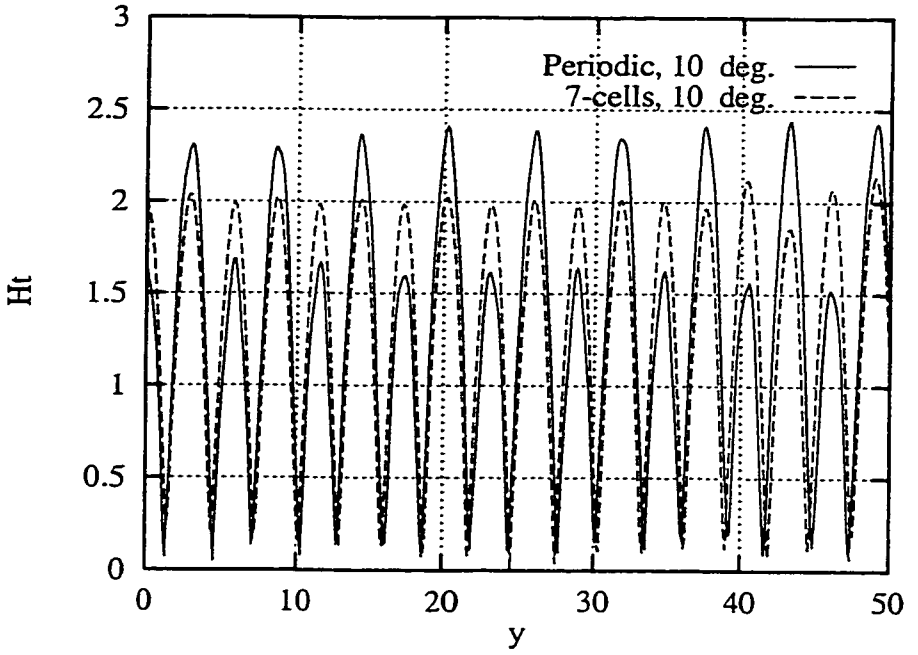

Figure 3.10: Height $h = 33\lambda$, spacing $s = 66\lambda$, incident angle $\phi = 10°$. Observer at $x = 3.5s$, the center line of cell ④ in the seven-cell array, and at $x = 0.5s$ in the periodic array. Ground plane is present.

between the results from the periodic array and the seven-cell array is good. All these examples uses $\beta = 2k\lambda/s$ for the periodic array in the convergence accelerating procedure (refer to Appendix B for the definition of β).

Numerical examples have been shown to support our initial motivation of using the solution for a periodic array to approximate the solution for a finite array. During the process we tried to exhaust the range of incident angles from $\phi = 1°$ through $\phi = 30°$, in a step of $\Delta\phi = 1°$, however, there are cases for some incident angles, the deviation between the two plots is large. Fig. 3.14 through Fig. 3.16 show the results for the plane wave of incident at 17°, 15° and 9°. Large deviation can be seen for the field distribution when the observation point moves below $y = h$ for $\phi = 17°$, $\phi = 9°$ and throughout the whole observation range for $\phi = 15°$. What causing these bad results at some particular incident angles remains unclear.

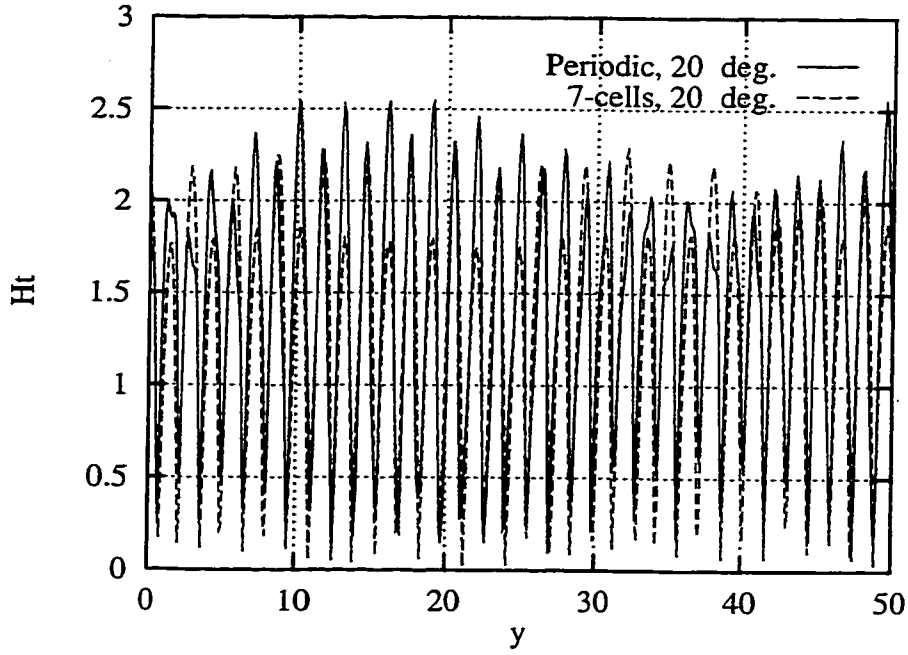

Figure 3.11: Height $h = 33\lambda$, spacing $s = 66\lambda$, incident angle $\phi = 20°$. Observer at $x = 3.5s$, the center line of cell ④ in the seven-cell array, and at $x = 0.5s$ in the periodic array. Ground plane is present.

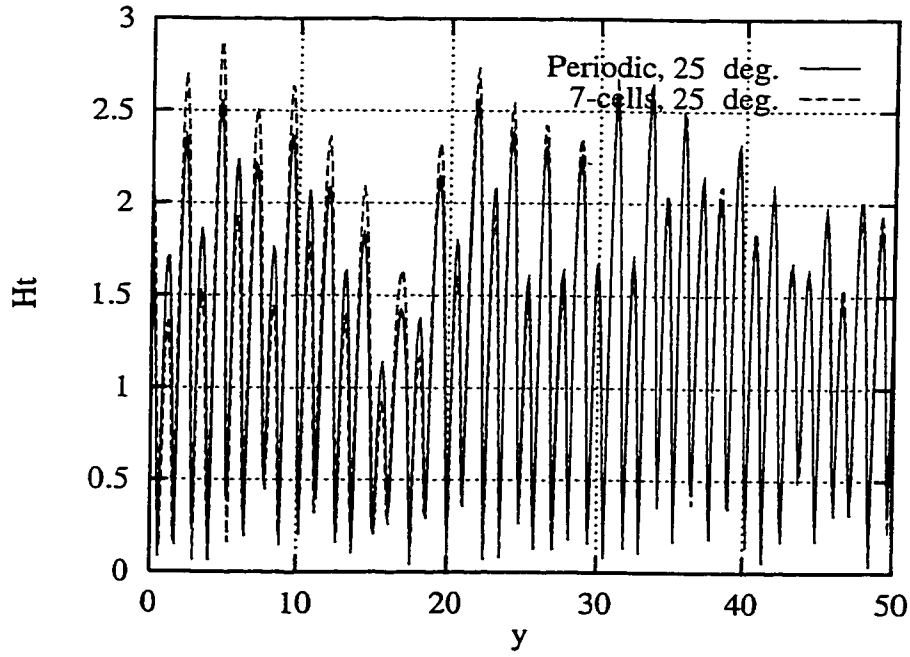

Figure 3.12: Height $h = 33\lambda$, spacing $s = 66\lambda$, incident angle $\phi = 25°$. Observer at $x = 3.5s$, the center line of cell ④ in the seven-cell array, and at $x = 0.5s$ in the periodic array. Ground plane is present.

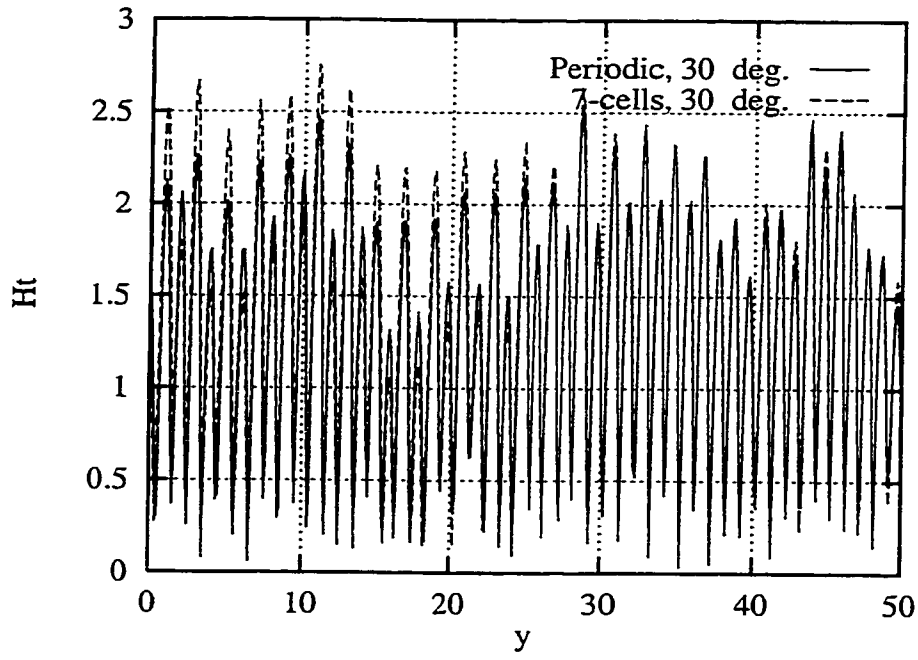

Figure 3.13: Height $h = 33\lambda$, spacing $s = 66\lambda$, incident angle $\phi = 30°$. Observer at $x = 3.5s$, the center line of cell ④ in the seven-cell array, and at $x = 0.5s$ in the periodic array. Ground plane is present.

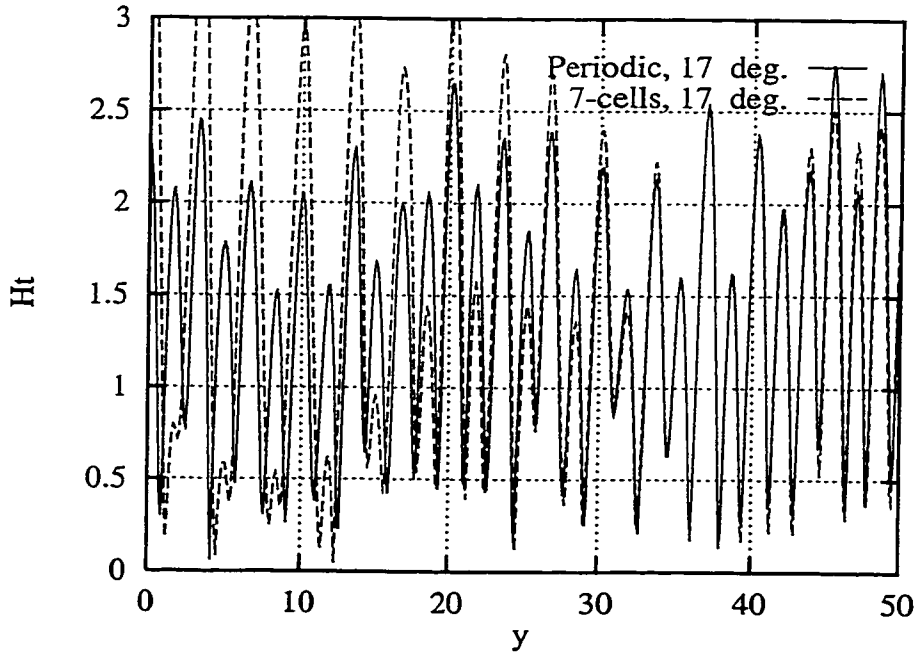

Figure 3.14: Height $h = 33\lambda$, spacing $s = 66\lambda$, incident angle $\phi = 17°$. Observer at $x = 3.5s$, the center line of cell ④ in the seven-cell array, and at $x = 0.5s$ in the periodic array. Ground plane is present.

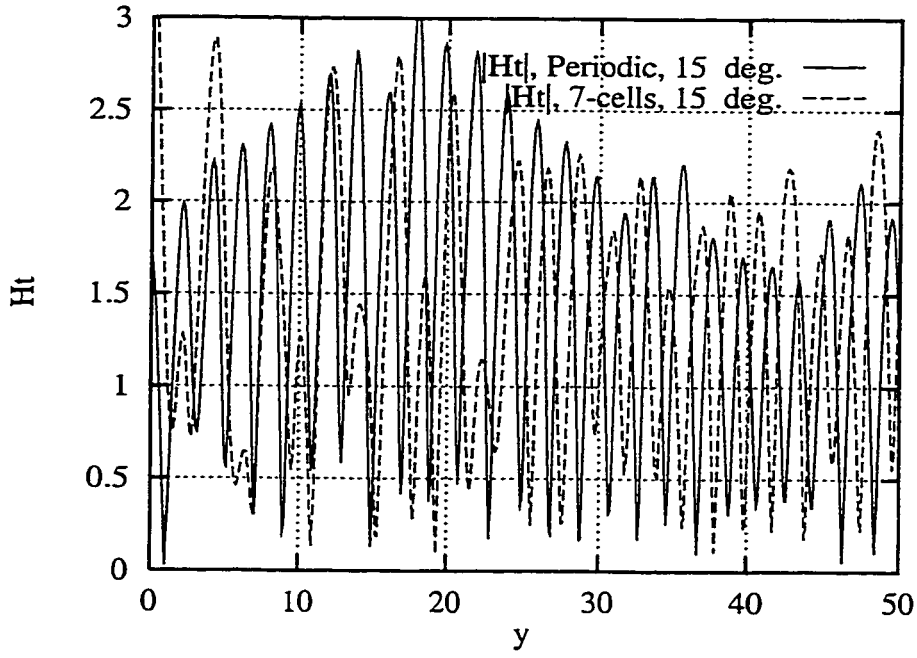

Figure 3.15: Height $h = 33\lambda$, spacing $s = 66\lambda$, incident angle $\phi = 15°$. Observer at $x = 3.5s$, the center line of cell ④ in the seven-cell array, and at $x = 0.5s$ in the periodic array. Ground plane is present.

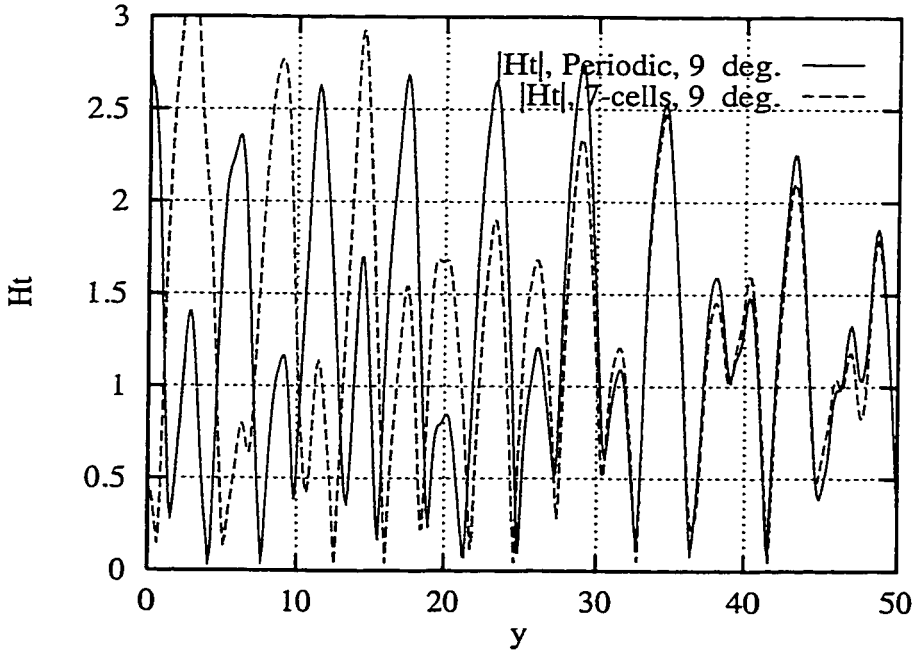

Figure 3.16: Height $h = 33\lambda$, spacing $s = 66\lambda$, incident angle $\phi = 9°$. Observer at $x = 3.5s$, the center line of cell ④ in the seven-cell array, and at $x = 0.5s$ in the periodic array. Ground plane is present.

Chapter 4

Conclusion and Further Development

Studies were made for a plane wave propagating over a periodic array of parallel strips and over an array containing a finite number of parallel strips. Both TM and TE plane wave incidence were considered. A method of moments solution for arrays of parallel strips is computationally costly, either on memory or CPU time when the array contains a large number of parallel strips. On the other hand, using the method of moments solution for periodic arrays of parallel strips, only the surface current in one cell needs to be solved for, thus greatly reducing the number of unknown coefficients for the surface current. Numerical examples were given using geometrical parameters of a typical residential area. The field distribution in a periodic array was calculated. Also the field distribution was calculated when the periodic array was truncated on both sides. The results showed that the two solutions were close to each other when the incident angle was not so small and the Fresnel zone criterion was obeyed. Hence it is practical to use solutions for periodic arrays of parallel strips to approximate the solutions for arrays which contain large numbers of parallel strips. The extent of this approximation accuracy depends on the number of strips in the finite parallel strip array and the angle of incidence. Therefore we conclude that except for some particular incident angles, when the incident wave is away from grazing, the periodic solution can be used to well approximate the solution even when the number of strips is only moderately large.

Previous work was focused on finding the field strength that hits the tips of the parallel

half planes that represent the buildings. This field would then be used to compute the field at the street level. In contrast, the present work examines the field directly at the street level, using a rigorous method of moments formulation. Similar to previous work, it was found that low angles of incidence require a large number of buildings in the model to achieve the "settled values" for the field, whereas at high angles only a few is needed.

The present analysis is based on arrays of PEC strips of zero thickness. Apparently two possible aspects of generalization can be made from the present model.

One is to introduce a lossy dielectric material into the analysis. By doing so, impedance sheets can be used to construct the model of the building and ground [20, 21]. The other is to replace the parallel strips and ground plane with objects that have more general shapes. For instance, one could model the buildings with rectangular cylinders, to allow rugged surface for the ground and to introduce windows on the walls of buildings in order to better model the environment in the real world.

For the bad results we found in our numerical example for the TE incidence, we currently have no satisfactory explanation, and further research would be needed.

Bibliography

[1] J. Walfisch and H. L. Bertoni. A theoretical model of uhf propagation in urban environments. *IEEE Trans. Antennas Propagat.*, 36(12):1788–1796, 1988.

[2] L. R. Maciel H. L. Bertoni, W. Honcharenko and H. H. Xia. Uhf propagation prediction for wireless personal communications. *Proceedings of the IEEE*, 82(9):1333–1359, September 1994.

[3] R. Hewitt G. Millington and F. S. Immirzi. Double knife-edge diffraction in field-strength predictions. *Proceedings IEE*, Monograph(507 E):419–429, 1962.

[4] K. Furutsu. On the theory of radio waves propagation over inhomogeneous earth. *J. Res. Nat. Bur. Stand.*, 67:39–62, 1963. Sec. D.

[5] L. E. Vogler. An attenuation function for multiple knife-edge diffraction. *Radio Sci.*, 17:1541–1546, 1982.

[6] S. W. Lee. Path integrals for solving some electromagnetic edge diffraction problems. *J. Mathematical Physics*, 19:1414–1422, 1978.

[7] A. Hessel H. L. Bertoni, L. B. Felsen. Local properties of radiation in lossy media. *IEEE Trans. Antennas and Propagat.*, 19(2):226–237, March 1971.

[8] S. R. Saunders and F. R. Bonar. Explicit multiple building diffraction attenuation function for mobile radio wave propagation. *Electronics Letter*, 27:1276–1277, 1991.

[9] J. Boersma. On certain multiple integrals occurring in a waveguide scattering problem. *SIAM J. Math. Anal.*, 9:377–393, 1978.

[10] H. H. Xia and H. L. Bertoni. Diffraction of cylindrical and plane waves by an array of absorbing half-screens. *IEEE Trans. Antennas Propagat.*, 40(2):170–177, 1992.

[11] M. J. Neve and G. B. Rowe. Contributions towards the development of a utd-based model for cellular radio propagation prediction. *IEE Proc. -Microw. Antennas and Propagat.*, 141(5):407–414, October 1994.

[12] J. B. Andersen. Transition zone diffraction by multiple edges. *IEE Proc. -Microw. Antennas and Propagat.*, 141(5):367–371, October 1994.

[13] H. Liu and R. Paknys. Comparison of field between finite and infinite array of parallel strips. In *Antem 2000 – Symposium on Antenna Technology and Applied Electromagnetics*, pages 349–352, Winnipeg, Manitoba, Canada, July 30–Aug 2, 2000.

[14] J. H. Richmond. An integral-equation solution for TE cylinder radiation and scattering. Technical report, The Ohio State University Electroscience Laboratory, Columbus, Ohio 43212, 1972. Report 2902-7.

[15] J. H. Richmond. Periodic planar array of parallel cylinders with small radius, TM polarization. Ohio State University Lecture Notes EE814 (See Appendix E), 1985.

[16] C. A. Balanis. *Advanced Engineering Electromagnetics.* John Willy & Sons Inc, 1989.

[17] S. L. Ray A. F. Peterson and R. Mittra. *Computational Methods For Electromagnetics.* The IEEE/OUP Series on Electromagnetic Wave Theory. IEEE Press, 1998.

[18] H. Liu and R. Paknys. Scattering from periodic array of grounded parallel strips, TE incident. *IEEE Trans. Antennas and Propagations*, 2001. submitted for publication.

[19] A. Papoulis. *The Fourier Integral And Its Applications.* Electronic Science Series. McGraw-Hill, 1962.

[20] R. F. Harrington and J. R. Mautz. An impedance sheet approximation for thin dielectric shells. *IEEE Trans. Antennas Propagat.*, 23(7):531–534, 1975.

[21] T. B. A. Senior. Backscattering from resistive strips. *IEEE Trans. Antennas Propagat.*, 27(6):808–813, November 1979.

[22] I. S. Gradshteyn and I. M. Ryzhik. *Table of Integrals, Series and Products.* Academic Press, 1994. Section 8.522.

Appendix A

Scattering From Arrays of Parallel Strips, TM polarization

Consider a TM polarized plane wave incident upon an array of parallel strips of perfect electric conductive, with uniform spacing, as shown in Fig. A.1. The number of parallel strips is N_x. The strips are assumed to have zero thickness, extends to infinity along z-axis and passes through $x_n = ns$ where s denotes the spacing between the strips, and $n = 0, 1, 2, \cdots, N_x - 1$, with a z-polarized plane wave incident upon the array,

$$E_z^i(x, y) = E_0 e^{jk(x\cos\phi + y\sin\phi)} \tag{A.1}$$

where k is the wavenumber of the incident field, $k^2 = \omega^2\mu\varepsilon$, ω is the angular frequency and μ, ϵ are permeability and permittivity in free space, ϕ is the angle of incidence measured from the $+x$ axis. The time dependence $e^{j\omega t}$ is assumed and suppressed throughout our analysis.

The surface equivalence theorem is employed to solve the problem. The surface current density $\mathbf{J}_s$ is assumed on the strips, and it has only a nonzero z-component. The field scattered by this surface current is given by [16]

$$E^s(x, y) = -\frac{k\eta}{4}\iint_{x'y'} J(x', y') H_0^{(2)}(k\sqrt{(x - x')^2 + (y - y')^2})\, dx'dy' \tag{A.2}$$

where $H_0^{(2)}(x)$ is the zeroth order Hankel function of the second kind. Since the electric field and the equivalent surface current have only nonzero z-components, the subscript z is suppressed in the above equation and in the following analysis.

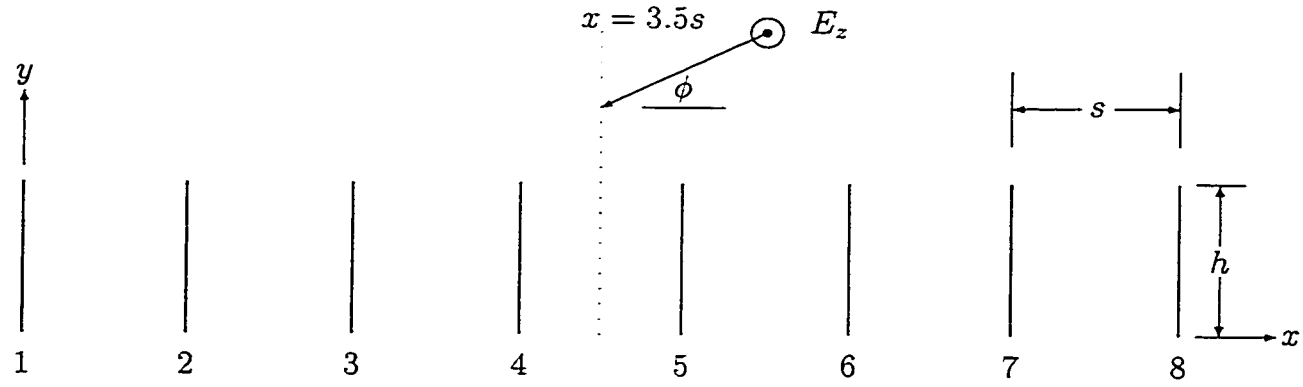

Figure A.1: TM plane wave incident upon a finite parallel strip array.

The point matching method described in Chapter 2.3 is used to formulate the scattered field. Assume the height of the parallel strips is h, so the surface current J_s is distributed in the domain $x = ns,\ n = 1, 2, \cdots, N_x - 1$ and $y \in [0, h]$. Equally divide the strips into N_y-segments, with the coordinates of each node expressed as

$$y_j = \frac{j-1}{N_y} h,\ j = 1, 2, \cdots, N_y + 1. \tag{A.3}$$

Using the pulse basis functions, the current distribution J_s can be expanded as

$$J(x, y) = \sum_{i=1}^{N_x} \sum_{j=1}^{N_y} a_{ij} \delta(x - x_i) g_j(y) \tag{A.4}$$

where $x_i = (i-1)s,\ i = 1, 2, \cdots, N_x$ and $g_j(y)$ is a pulse function defined as

$$g_j(y) = \begin{cases} 1, & y \in [y_j, y_{j+1}] \\ 0, & y \notin [y_j, y_{j+1}] \end{cases} \tag{A.5}$$

Using the current expression in (A.4), the scattered field can be expressed as

$$E^s(x, y) = -\frac{k\eta}{4} \sum_{i=1}^{N_x} \sum_{j=1}^{N_y} a_{ij} \int H_0^{(2)}(k\sqrt{(x - x_i)^2 + (y - y')})\, dy' \tag{A.6}$$

Merging the subscripts i, j into q, we have (A.6) rewritten as

$$E^s(x, y) = -\frac{k\eta}{4} \sum_{q=1}^{N} a_q \int_{y_q - b}^{y_q + b} H_0^{(2)}(k\sqrt{(x - x_q)^2 + (y - y')})\, dy'. \tag{A.7}$$

where (x_q, y_q) is the coordinate of the central point of each segment. It is defined together with the index q as

$$x_q = (i-1)s \tag{A.8}$$

$$y_q = (2j-1)b \tag{A.9}$$

$$q = j + (i-1)N_y \tag{A.10}$$

where $i = 1, 2, \cdots, N_x$, $j = 1, 2, \cdots, N_y$ and b is the half-length of the segment

$$b = \frac{h}{2N_y} \tag{A.11}$$

Using the field expression (A.7) and applying the point matching method by selecting the matching points as the central point of each segment, we have the EFIE written as

$$\sum_{q=1}^{N} Z_{pq} a_q = V_p, \quad p = 1, 2, \cdots, N \tag{A.12}$$

where $N = N_x N_y$ and

$$Z_{pq} = -\frac{k\eta}{4} \sum_{q=1}^{N} a_q \int_{y_q-b}^{y_q+b} H_0^{(2)}(k\sqrt{(x_p - x_q)^2 + (y_p - y')}) \, dy'. \tag{A.13}$$

The excitation voltage is

$$V_p = -E^i(x_p, y_p) \tag{A.14}$$

It is noticed that Z_{pq} is symmetric. Now equation (A.12) can be solved and the unknown coefficient a_q is obtained.

Once the surface current coefficients a_q are solved for, the scattered field can then be evaluated by using (A.7).

In summary, using the surface equivalence theorem, the surface electric current is assumed to flow on strips. The PEC strips are replaced with free space, leaving the equivalent current radiating in free space. The strips are divided into small segments. The unknown equivalent current is now expanded along the surfaces of the parallel strips as a sum of pulse basis functions multiplied by unknown complex coefficients. The EFIE is established by enforcing

the boundary condition at the matching points of each segment. A system of linear equation is then established to solve for the unknown complex coefficients of for the equivalent surface current. Once the equivalent surface current is found, the fields radiated by this current are readily obtained, and the total field is found by adding the radiated field to the incident field.

Appendix B

Mathematical Details and Convergence Acceleration

The purpose of this appendix is to present in detail the scattered fields and the matrix elements in the MM analysis. It is derived for the problem of TE plane wave incident upon periodic array of grounded parallel strips in Chapter 3.

We have already seen that the scattered fields expressed by the Poisson summation formula does not analytically converge in some cases, referring to (3.65). Furthermore, expression (3.62), (3.64) and most of the impedance elements exhibit convergent at $O(n^{-2})$ as $n \to \infty$ under some circumstances. These expressions are absolutely convergent mathematically, but are numerically slow. Special treatment is necessary to make them amenable to numerical calculation. Look at a simple example of the series

$$\sum_{n=1}^{\infty} \frac{1}{n^2}, \tag{B.1}$$

which converges at $O(n^{-2})$ as $n \to \infty$. If we specify a tolerance of $\epsilon = 10^{-3}$, and using the criteria expression (2.32) (listed below for convenience)

$$\frac{|\sum_{N}^{2N} a_n|}{|S_N|} \leq \epsilon, \tag{B.2}$$

numerical test shows it requires $N = 763$ terms to be added to achieve the accuracy. For the specific series in our problem, the terms needed would probably not reach such a big number, because the terms in the Poisson summation formula (3.13) is oscillating about n.

Nevertheless a general procedure of convergence accelerating described by Peterson *et al.* [17] is adopted to our problem to deal with all these cases.

Starting from the periodic Greens function (3.13), the expression is rewritten in such a way that part of it is expressed in the original space domain, while the remaining part is expressed via the Poisson summation formula. Starting from (3.15), an alternative expression may be written as

$$G_p(x,y) = G_a(x,y) + G_b(x,y) \tag{B.3}$$

and

$$G_b(x,y) = \mathcal{F}^{-1}\left\{G_p(\omega) - G_a(\omega)\right\} \tag{B.4}$$

where $G_p(\omega)$ and $G_a(\omega)$ are Fourier transforms of $G_p(x,y)$ and $G_a(x,y)$, respectively. The symbol $\mathcal{F}^{-1}$ denotes inverse Fourier transform. $G_a(x,y)$ can be chosen as

$$G_a(x-x',y-y') = \sum_{n=-\infty}^{+\infty} -\frac{j\mu}{4} H_0^{(2)}(-j\beta\sqrt{(x-x'-ns)^2+(y-y')^2})e^{jkns\cos\phi} \tag{B.5}$$

We use the relation

$$H_0^{(2)}(-jx) = \frac{-2}{j\pi} K_0(x) \tag{B.6}$$

$$G_a(x-x',y-y') = \sum_{n=-\infty}^{+\infty} \frac{\mu}{2\pi} K_0(\beta\sqrt{(x-x'-ns)^2+(y-y')^2})e^{jkns\cos\phi} \tag{B.7}$$

where $K_0(x)$ is the modified Hankel function. Observe that $G_a(x,y)$ is obtained by replacing the real-valued wavenumber k in $G_p(x,y)$ with the imaginary quantity $-j\beta$. $G_b(x,y)$ in (B.4) is expressed using the Poisson summation formula as

$$G_b(x,y) = \mathcal{F}^{-1}\left\{G_p(\omega) - G_a(\omega)\right\} = \frac{\mu}{2s}\sum_{n=-\infty}^{+\infty}\left(\frac{e^{-\gamma_n|y-y'|}}{\gamma_n} - \frac{e^{-\alpha_n|y-y'|}}{\alpha_n}\right)e^{j\omega_n(x-x')} \tag{B.8}$$

where

$$\alpha_n = \sqrt{\omega_n^2+\beta^2}$$

We notice that the Green's function is decomposed into two parts. The first part is an arbitrarily chosen function which is evaluated in the original space domain. The second part is a difference between the original Green's function and the chosen function, which is evaluated in the transformed spectral domain.

The following sections are organized according to the nature of the equivalent currents. The first section is for fields generated by the current on parallel strips, the impedance on segments on ground plane and on the corner dipole by this vertical current. The second section calculates fields generated by the current on ground plane, the impedance on segments on parallel strips and on the corner dipole by this horizontal current. The third section deals with fields generated by the current on the corner dipole, the impedance on segments on ground plane and on parallel strips by this current. Also, we will apply the accelerating method discussed above to the calculation of these MM matrix elements.

B.1 Fields From Parallel Strips

Fields from $f_m(y)\hat{\mathbf{y}}$ are given by

$$E_{mx}(x,y) = \frac{1}{j\omega\mu\epsilon}\frac{\partial^2}{\partial x \partial y}A_m(x,y), \qquad E_{my}(x,y) = \frac{1}{j\omega\mu\epsilon}\left(k^2 + \frac{\partial^2}{\partial y^2}\right)A_m(x,y) \quad \text{(B.9)}$$

$$H_{mz}(x,y) = \frac{1}{\mu}\frac{\partial}{\partial x}A_m(x,y) \quad \text{(B.10)}$$

where $A_m(x,y)$ is given by (3.26), the vector potential produced by the current $f_m(y)\hat{\mathbf{y}}$ on parallel strips.

B.1.1 Impedance Matrix Entries Z_{qm}

The impedance element Z_{qm} is the weighted field on segment q produced by the current on segment m. It can be expressed as

$$\begin{aligned} Z_{qm} &= \int T_q(y) E_{my}(x,y)dy \\ &= -\frac{1}{j\omega\mu\epsilon}\int T_q(y)\left(k^2 + \frac{\partial^2}{\partial y^2}\right)A_m(x,y)dy \end{aligned} \quad \text{(B.11)}$$

where $T_q(y)$ is the test function defined on segment q of the parallel strip.

According to (3.36) on page 33, let $u = y - y_q$, we have

$$\begin{aligned}\int T_q(y)\left(k^2+\frac{\partial^2}{\partial y^2}\right)A_m(x,y)dy &= \int T(u)\left(k^2+\frac{\partial^2}{\partial u^2}\right)A(x,u+t)du,\\ &= T(t)*\left(k^2+\frac{\partial^2}{\partial t^2}\right)*A(x,t)\end{aligned} \tag{B.12}$$

where $t = y_q - y_m$. The final expression in (B.12) is obtained by replacing u with $-u$ and using the fact that $T(-u) = T(u)$.

Using (3.26), we have

$$A(x,t) = f(t) * G_p(x,t) \tag{B.13}$$

where $A(x,t)$ is the vector potential due to the current $f(t)$ on parallel strips, and $f(t)$ is the basis function for current on the vertical strip and is defined by (3.19) with $y_m = 0$. Therefore Z_{qm} can be written as

$$\begin{aligned}Z_{qm} &= -\frac{1}{j\omega\mu\epsilon}\left(k^2+\frac{\partial^2}{\partial t^2}\right)T(t)*f(t)*G_p(x,t)\\ &= \frac{j\eta}{2ks}\left(k^2+\frac{\partial^2}{\partial t^2}\right)\sum_{n=-\infty}^{+\infty}\frac{e^{j\omega_n x}}{\gamma_n}T(t)*f(t)*e^{-\gamma_n|t|}.\end{aligned} \tag{B.14}$$

In the above equation, the Poisson summation expression is used for the periodic Green's function. Also note that $x = 0$. Using the definition of $T(y)$ and $f_m(y)$ in(3.37) and (3.19) for $T(t)$ and $f(t)$, respectively, and performing the convolution with respect to t, we have

$$Z_{qm} = \frac{j\eta}{2ksb}\sum_{n=-\infty}^{+\infty}\frac{Q(t,\gamma_n)}{\gamma_n^2} \tag{B.15}$$

where $t = y_p - y_m$ and

$$Q(t,\gamma_n) = \begin{cases}\left(1+\dfrac{k^2}{\gamma_n^2}\right)e^{-\gamma_n(|t|-\frac{3b}{2})}\left(1-e^{-\gamma_n b}\right)^3 & |t|\geq 2b\\ \dfrac{1}{4}k^2b^2+\left(1+\dfrac{k^2}{\gamma_n^2}\right)\left(1-e^{-\gamma_n\frac{b}{2}}\right)^2\left(2-2e^{-\gamma_n b}-e^{-\gamma_n\frac{3b}{2}}\right) & |t|=b\\ \dfrac{3k^2b^2}{2}-2\left(1+\dfrac{k^2}{\gamma_n^2}\right)\left(1-e^{-\gamma_n\frac{b}{2}}\right)^2\left(2+e^{-\gamma_n\frac{b}{2}}\right) & |t|=0\end{cases} \tag{B.16}$$

We see the series is exponentially convergent when $|t| \geq 2b$ and at $O(n^{-2})$ when $|t| < 2b$ as $n \to \infty$.

For cases when $|t| = b$ and $t = 0$, an additional order of convergence can be achieved by using the decomposition of the Green's function defined in (B.4). We express Z_{qm} as

$$Z_{qm} = Z^a_{qm} + Z^b_{qm} \tag{B.17}$$

where

$$Z^a_{qm} = -\frac{1}{j\omega\mu\epsilon}\left(k^2 + \frac{\partial^2}{\partial t^2}\right) T(t) * f(t) * G_a(x,t) \tag{B.18}$$

$$Z^b_{qm} = -\frac{1}{j\omega\mu\epsilon}\left(k^2 + \frac{\partial^2}{\partial t^2}\right) T(t) * f(t) * G_b(x,t). \tag{B.19}$$

Using (B.7), write Z^a_{qm} as

$$Z^a_{qm} = \frac{j\eta}{2\pi k}\sum_{n=-\infty}^{+\infty}\left(k^2 I_1 + \frac{1}{b} I_2\right) \tag{B.20}$$

where

$$I_1 = \int_{y=0}^{b}\int_{x=0}^{b}\left(1 - \frac{x}{b}\right)\left[f_n\left(t + \frac{b}{2} + x - y\right) + f_n\left(t + \frac{b}{2} - x - y\right)\right] dxdy \tag{B.21}$$

$$I_2 = \int_0^b \left[f_n\left(t + \frac{3}{2}b - x\right) - 2f_n\left(t + \frac{b}{2} - x\right) + f_n\left(t - \frac{b}{2} - x\right)\right] dx$$

and

$$f_n(x) = K_0\left(\beta\sqrt{(ns)^2 + x^2}\right). \tag{B.22}$$

The 2-D integral in (B.22) can be converted into a 1-dimensional integral by variable substitution. The converted integral can be written as

$$I_1 = \int_0^b \left(\frac{b}{2} + x - \frac{x^2}{b}\right) f_n\left(t + \frac{b}{2} - x\right) dx + \int_0^b \frac{b}{2}\left(1 - \frac{x}{b}\right)^2 f_n\left(t + \frac{b}{2} + x\right) dx + \int_0^b \frac{b}{2}\left(1 - \frac{x}{b}\right)^2 f_n\left(t - \frac{b}{2} - x\right) dx. \tag{B.23}$$

Since

$$K_0(x) \sim \sqrt{\frac{\pi}{2x}} e^{-x} \text{ as } x \to \infty, \tag{B.24}$$

therefore the summation in (B.20) exhibits exponential decay as $n \to \infty$. Substituting (B.8) into (B.19), we have

$$\begin{aligned} Z^b_{qm} &= \frac{j\eta}{2ks}\left(k^2 + \frac{\partial^2}{\partial t^2}\right) \sum_{n=-\infty}^{+\infty} e^{j\omega_n(x-x')} T(t) * f(t) * \left(\frac{e^{-\gamma_n|t|}}{\gamma_n} - \frac{e^{-\alpha_n|t|}}{\alpha_n}\right) \\ &= \frac{j\eta}{2ks} \sum_{n=-\infty}^{+\infty} e^{j\omega_n(x-x')} P_n(t) \end{aligned} \tag{B.25}$$

where

$$P_n(t) = \begin{cases} \left[\left(\frac{kb}{2}\right)^2 + 2\right]\left(\frac{1}{\gamma_n^2} - \frac{1}{\alpha_n^2}\right) - \left(\frac{p_1(u_n)}{\gamma_n^2} - \frac{p_1(v_n)}{\alpha_n^2}\right) \\ \quad +2k^2\left(\frac{1}{\gamma_n^4} - \frac{1}{\alpha_n^4}\right) - k^2\left(\frac{p_1(u_n)}{\gamma_n^4} - \frac{p_1(v_n)}{\alpha_n^4}\right) & |t| = b \\ \left[\frac{3}{2}(kb)^2 - 4\right]\left(\frac{1}{\gamma_n^2} - \frac{1}{\alpha_n^2}\right) + 2\left(\frac{p_0(u_n)}{\gamma_n^2} - \frac{p_0(v_n)}{\alpha_n^2}\right) \\ \quad -4k^2\left(\frac{1}{\gamma_n^4} - \frac{1}{\alpha_n^4}\right) + 2k^2\left(\frac{p_0(u_n)}{\gamma_n^4} - \frac{p_0(v_n)}{\alpha_n^4}\right) & |t| = 0 \end{cases} \tag{B.26}$$

and

$$\begin{aligned} p_1(x) &= x(4 - 3x^2 + x^4) \\ p_0(x) &= x(3 - x^2) \\ u_n &= e^{-\gamma_n \frac{b}{2}} \\ v_n &= e^{-\alpha_n \frac{b}{2}}. \end{aligned} \tag{B.27}$$

We see the terms in the difference part described by (B.26) decays as $O(n^{-4})$ as $\to \infty$. The convergence of the difference part has been improved as compared with the original expression in (3.56), which only decreases as $O(n^{-2})$ as $n \to \infty$.

B.1.2 Excitation Voltage V_q

The exciting voltage defined in (3.45) is the line integral of the incident electric field along the surface of the vertical strip in segment q. Substituting the definition of $T_q(y)$ in (3.36)

and the incident field in (3.2) into (3.45), we have

$$V_q = -\eta H_0 \cos\phi e^{jkx\cos\phi} \int_{\epsilon-\frac{b}{2}}^{\epsilon+\frac{b}{2}} e^{jky\sin\phi} dy \tag{B.28}$$

where $\epsilon = y_q$, is used for notational convenience. Performing the integration, we have

$$V_q = -\frac{2\eta}{k\tan\phi} \sin\left(k\frac{b}{2}\sin\phi\right) H^i(x, y_q). \tag{B.29}$$

B.1.3 Scattered Fields H_p^s

Once the surface equivalent currents are obtained, the scattered fields from the parallel strips can be evaluated. The scattered magnetic field has only a nonzero z-component

$$H_z^s(x,y) = \frac{1}{\mu}\frac{\partial A_y(x,y)}{\partial x}, \tag{B.30}$$

where $A_y(x,y)$ is the y-component of vector potential due to electric current on parallel strips. It is expressed as the superposition of vector potential produced by each current basis function as indicated in (3.21) on page 31. Using (3.21) and (3.26) on page 31, we have the magnetic field from the parallel strips expressed as

$$H_z^s(x,y) = \frac{1}{\mu}\frac{\partial}{\partial x}\sum_{m=1}^{M} c_m f_m(y) * G_p(x,y). \tag{B.31}$$

Using the Poisson summation expression for $G_p(x,y)$ in (3.15) on page 29, we have

$$H_z^s(x,y) = \frac{j}{2s}\sum_{m=1}^{M} c_m \sum_{n=-\infty}^{\infty} \frac{\omega_n}{\gamma_n} e^{j\omega_n x} f_m(y) * e^{-\gamma_n|y|}. \tag{B.32}$$

Using the definition of $f_m(y)$ in (3.19) on page 30 and perform the convolution, we have

$$H_z^s(x,y) = \frac{j}{2s}\sum_{m=1}^{M} a_m \sum_{n=-\infty}^{\infty} \frac{\omega_n}{\gamma_n^2} e^{j\omega_n x} S_n(t) \tag{B.33}$$

where

$$S_n(t) = \begin{cases} \dfrac{e^{-\gamma_n|t|}}{b\gamma_n}\left(e^{\gamma_n b} - 2 + e^{-\gamma_n b}\right), & |t| \geq b \\ 2\left(1 - \dfrac{|t|}{b}\right) + \dfrac{1}{b\gamma_n}\left[e^{\gamma_n(|t|-b)} - 2e^{-\gamma_n|t|} + e^{-\gamma_n(|t|+b)}\right] & |t| \leq b \end{cases} \tag{B.34}$$

Again $t = y_q - y_m$ here. The series in equation (B.33) decays exponentially when $|t| > b$, at $O(n^{-2})$ when $|t| = b$ and only decays at $O(n^{-1})$ when $|t| < b$. Again, the accelerating method described in the beginning of Appendix B is employed when $|t| < b$. Decomposing H_z^s into two parts, we have

$$H_z^s = H_a + H_b \tag{B.35}$$

where H_a will be evaluated in space domain, while the differential term H_b will be evaluated in the transformed domain.

Using (3.26) on page 31 with $G_p(x, y)$ replaced by $G_a(x, y)$, we have

$$H_a(x, y) = \frac{1}{\mu}\frac{\partial}{\partial x}\sum_{m=1}^{M} c_m f_m(y) * G_a(x, y). \tag{B.36}$$

Substituting (B.7) into the above equation and being aware that $x' = 0$ here, we have

$$H_a = \frac{1}{2\pi}\frac{\partial}{\partial x}\sum_{m=1}^{M} c_m f_m(y) * \sum_{n=-\infty}^{+\infty} K_0(\beta\sqrt{(x - ns)^2 + y^2})e^{jnks\cos\phi}. \tag{B.37}$$

Performing the convolution and the partial differentiation on x, we have the field written as

$$H_a(x, y) = \frac{1}{2\pi}\sum_{m=1}^{M} c_m \sum_{n=-\infty}^{+\infty} h_n(x, y)e^{jnks\cos\phi}, \tag{B.38}$$

and

$$h_n(x, y) = -\beta(x - ns)\int_0^b \left(1 - \frac{\tau}{b}\right)\left[\frac{K_1(\beta R_n^+)}{R_n^+} + \frac{K_1(\beta R_n^-)}{R_n^-}\right] d\tau \tag{B.39}$$

where

$$R_n^{\pm} = \sqrt{(x - ns)^2 + (t \pm \tau)^2} \tag{B.40}$$

and $t = y_q - y_m$. In (B.39), h_n can be evaluated via numerical integration. The integrand contains a modified Hankel functions of the first kind, which exhibits exponential decay when the argument increases. Therefore h_n exhibits exponential decreases as $n \to \infty$.

Similar to (B.36) the difference term $H_b(x,y)$ can be expressed as

$$H_b(x,y) = \frac{1}{\mu}\frac{\partial}{\partial x}\sum_{m=1}^{M} c_m f_m(y) * G_b(x,y). \tag{B.41}$$

Substituting the expression of $G_b(x,y)$ as in (B.8) into the above equation, and noticing that $G_b(x,y)$ is the difference of two terms in which the second term has a similar expression as the first one, except γ_n is replaced by α_n. We have the difference term written as

$$H_b(x,y) = \frac{j}{2s}\sum_{m=1}^{M} c_m \sum_{n=-\infty}^{+\infty} \omega_n e^{j\omega_n x}\left(\frac{S_n(t)}{\gamma_n^2} - \frac{S_n'(t)}{\alpha_n^2}\right) \tag{B.42}$$

where $S_n(t)$ is defined in (B.34), $S_n'(t)$ has the same expression as $S_n(t)$ except γ_n is replaced by α_n. Writing it in detail, we have

$$H_b(x,y) = \frac{j}{2s}\sum_{m=1}^{M} c_m \sum_{n=-\infty}^{+\infty} \omega_n e^{j\omega_n x}\begin{cases} P_n(t,\alpha_n,\gamma_n), & t \geq b \\ 2\left(1-\frac{t}{b}\right)\left(\frac{1}{\gamma_n^2}-\frac{1}{\alpha_n^2}\right) + P_n(t,\alpha_n,\gamma_n), & t \leq b \end{cases} \tag{B.43}$$

where

$$P_n(t,\alpha_n,\gamma_n) = \frac{1}{b}\left[f_n(\gamma_n) - f_n(\alpha_n)\right] \tag{B.44}$$

and

$$f_n(\xi) = \frac{e^{-\xi_n|t-b|} - 2e^{-\xi_n t} + e^{-\xi_n(t+b)}}{\xi_n^3}. \tag{B.45}$$

The bottom case in (B.43) decays at $O(n^{-4})$ while the top case decays exponentially as $n \to \infty$.

B.1.4 Weighted Fields on Horizontal Strips Z_{pm}

The impedance element Z_{pm} is the weighted field on segment p of the horizontal strip due to current segment m of the vertical strip, and can be expressed as

$$Z_{pm} = -\int T_p(x) E_{mx}^s(x,0)\, dx \tag{B.46}$$

where $T_p(x)$ is the test function defined in (3.37), E_{mx} is the electric field produced by the current on the parallel strips which is expressed in (B.10).

Using the vector potential expression (3.26) and the Poisson summation expression for the periodic Green's function, we have

$$Z_{pm} = -\frac{1}{j\omega\mu\epsilon}\int T_p(x)\frac{\partial^2 A_m(x,y)}{\partial x\partial y}dx \tag{B.47}$$

$$= \frac{j\eta}{2ks}\sum_{n=-\infty}^{+\infty}\frac{1}{\gamma_n}\int T_p(x)\frac{\partial}{\partial x}e^{j\omega_n(x-x')}dx\cdot\int f_m(y')\frac{\partial}{\partial y}e^{-\gamma_n|y-y'|}dy' \tag{B.48}$$

where $f(y)$ is the basis function defined in (3.19). Performing the integrals under the condition $y_m \geq b$, we have

$$\int T_p(x)\frac{\partial}{\partial x}e^{j\omega_n(x-x')}dx = 2j\sin\frac{\omega_n c}{2}e^{j\omega_n(x_p-x')} \tag{B.49}$$

$$\int f_m(y')\frac{\partial}{\partial y}e^{-\gamma_n|y-y'|}dy' = \frac{e^{-\gamma_n(y_m-b)}}{b\gamma_n}(1-e^{-\gamma_n b})^2 \tag{B.50}$$

Notice that $x' = 0 = y$ here. Therefore the impedance is expressed as

$$Z_{pm} = -\frac{\eta}{ksb}\sum_{n=-\infty}^{+\infty}\frac{e^{-\gamma_n(y_m-b)}}{\gamma_n^2}(1-e^{-\gamma_n b})^2\sin\frac{\omega_n c}{2}e^{j\omega_n x_p}. \tag{B.51}$$

We see that terms in the summation series of (B.51) is exponentially decayed when $y_m > b$, and is at $O(n^{-2})$ when $y_m = b$. An additional order of convergence can be achieved by using the decomposition of the Green's function defined in (B.4). We express Z_{pm} as

$$Z_{pm} = Z_{pm}^a + Z_{pm}^b \tag{B.52}$$

where

$$Z_{pm}^a = -\frac{1}{j\omega\mu\epsilon}\sum_{n=-\infty}^{+\infty}\int T_p(x)\frac{\partial^2}{\partial x\partial y}\int J_m(y')G_a(x,y-y')\,dy'dx. \tag{B.53}$$

Using (B.7), we write Z_{pm}^a as

$$Z_{pm}^a = \frac{j\eta}{2\pi kb}\sum_{n=-\infty}^{+\infty}I_n e^{jnks\cos\phi} \tag{B.54}$$

and

$$I_n = \int_0^b \left(f_n(\frac{c}{2},b-y) - f_n(\frac{c}{2},b+y) - f_n(-\frac{c}{2},b-y) + f_n(-\frac{c}{2},b+y)\right)dy \tag{B.55}$$

where

$$f_n(x,y) = K_0(\beta\sqrt{(x_p - ns + x)^2 + y^2}). \tag{B.56}$$

The difference part is obtained in a similar procedure as in obtaining (B.43), and is expressed as

$$\begin{aligned} Z^b_{pm} = &-\frac{\eta}{ksb}\sum_{n=-\infty}^{+\infty}\sin\frac{\omega_n c}{2}e^{j\omega_n x_p} \\ &\cdot\left[\left(\frac{1}{\gamma_n^2}-\frac{1}{\alpha_n^2}\right) - 2\left(\frac{e^{-\gamma_n b}}{\gamma_n^2}-\frac{e^{-\alpha_n b}}{\alpha_n^2}\right) + \frac{e^{-2\gamma_n b}}{\gamma_n^2}-\frac{e^{-2\alpha_n b}}{\alpha_n^2}\right] \end{aligned} \tag{B.57}$$

We see that the terms in (B.57) decrease as $O(n^{-4})$ as $n \to \infty$.

B.1.5 Weighted Fields on The Corner Dipole Z_{0m}

The impedance element Z_{0m} is the weighted field on the corner dipole due to the current on parallel strips. It is obtained in a similar way as we did in Section B.1.1, except with a different test function. It is written as

$$Z_{0m} = -\int_l T(t)\hat{\mathbf{t}}\cdot\mathbf{E}^s dt \tag{B.58}$$

where $\mathbf{E}$ is the field produced by the current on parallel strips, $T(t)$ is the test function on the corner dipole which is expressed by $T_0(x)$ and $T_0(y)$ separately for the x- and y- arms of the corner dipole, as defined in (3.35). The line integral is defined along the surface of the corner dipole. l denotes the the contour of the whole corner dipole and $\hat{\mathbf{t}}$ is the tangential vector along l, refer to Fig. B.1 for illustration.

Using the field expressions (B.10) and the test function (3.35), we have

$$Z_{0m} = \int T_0(x)E^s_{mx}(x,0)dx - \int T_0(y)E^s_{my}(0,y)\,dy. \tag{B.59}$$

Write it in detail, we have

$$Z_{0m} = \frac{1}{j\omega\mu\epsilon}\left[\int T_0(x)\frac{\partial^2}{\partial x\partial y}A_m(x,y)dx - \int T_0(y)\left(k^2+\frac{\partial^2}{\partial y^2}\right)A_m(x,y)dy\right] \tag{B.60}$$

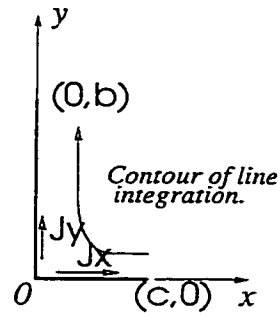

Figure B.1: Surface Current on Corner Dipole.

Using the vector potential expression (3.26) and the Poisson summation expression for the periodic Green's function, we have

$$Z_{0m} = -\frac{j\eta}{2ks}\sum_{n=-\infty}^{+\infty}\frac{1}{\gamma_n}\left\{\int T_0(x)\frac{\partial}{\partial x}e^{j\omega_n(x-x')}\,dx\cdot\frac{\partial}{\partial y}f(y-y_m)*e^{-\gamma_n|y-y_m|}\right.$$
$$\left.-e^{j\omega_n(x-x')}\int T_0(y)\left(k^2+\frac{\partial^2}{\partial y^2}\right)f(y-y_m)*e^{-\gamma_n|y-y_m|}\,dy\right\}. \quad \text{(B.61)}$$

Making further manipulations, we have

$$\int T_0(x)\frac{\partial}{\partial x}e^{j\omega_n(x-x')}dx = -\int T_0'(x)e^{j\omega_n(x-x')}dx, \quad \text{(B.62)}$$
$$\frac{\partial}{\partial y}f(y-y_m)*e^{-\gamma_n|y-y_m|} = f'(y-y_m)*e^{-\gamma_n|y-y_m|}, \quad \text{(B.63)}$$

and

$$\int T_0(y)\left(k^2+\frac{\partial^2}{\partial y^2}\right)f(y-y_m)*e^{-\gamma_n|y-y_m|}dy \quad \text{(B.64)}$$
$$= T_0(y_m)*\left(k^2+\frac{\partial^2}{\partial y_m^2}\right)f(y_m)*e^{-\gamma_n|y_m|}dy$$

Therefore the impedance element can be expressed as

$$Z_{0m} = \frac{j\eta}{2ksb}\sum_{n=-\infty}^{+\infty}\frac{Q_n(t)}{\gamma_n^2} \quad \text{(B.65)}$$

and

$$Q_n(t) = \begin{cases} e^{-\gamma_n(t-\frac{3}{2}b)}(1-\alpha)^2(1+\alpha)^2\left[\left(1+\frac{k^2}{\gamma_n^2}\right)(1-\alpha)+\alpha(1-e^{j\omega_n\frac{c}{2}})\right] & t\geq 2b \\ \left(\frac{kb}{2}\right)^2+(1-\alpha)^2 & \\ \qquad\cdot\left\{\left(1+\frac{k^2}{\gamma_n^2}\right)\left(1-\alpha-\alpha^2\right)+(1+\alpha)^2\left(1-e^{j\omega_n\frac{c}{2}}\right)\right\} & t=b \end{cases} \quad \text{(B.66)}$$

where

$$t = y_m, \quad \text{and } \alpha = e^{-\gamma_n \frac{b}{2}}. \tag{B.67}$$

We see that when $t = b$, the terms in Z_{0m} decay at $O(n^{-2})$ as $n \to \infty$. An additional order of convergence can be achieved by using the decomposition of the Green's function defined in (B.4). We can express Z_{0m} as

$$Z_{0m} = Z^a_{0m} + Z^b_{0m}. \tag{B.68}$$

Similar to (B.61), Z^a_{0m} can be written as

$$Z^a_{0m} = \frac{j\eta}{2\pi k} \sum_{n=-\infty}^{+\infty} \left(k^2 I_1^y + \frac{1}{b} I_2^y - \frac{1}{b} I^x \right) e^{jnks\cos\phi} \tag{B.69}$$

where

$$I_1^y = \int_{y=0}^{\frac{b}{2}} \int_{x=0}^{b} \left(1 - \frac{x}{b}\right) [f_n(0, b + x - y) + f_n(0, b - x - y)]\, dxdy \tag{B.70}$$

$$I^x = \int_0^b \left[f_n(\frac{c}{2}, -b + y') - f_n(\frac{c}{2}, -b - y') - f_n(0, -b + y') + f_n(0, -b - y') \right] dy' \tag{B.71}$$

$$I_2^y = \int_0^b \left[f_n(0, \frac{b}{2} - b + y') - f_n(0, \frac{b}{2} - b - y') - f_n(0, -b + y') + f_n(0, -b - y') \right] dy'. \tag{B.72}$$

Merging I^x with I_2^y and denoting $I^{xy} = I^x - I_2^y$, we have

$$I^{xy} = \int_0^b \left[f_n(\frac{c}{2}, -b + y') - f_n(\frac{c}{2}, -b - y') - f_n(0, -\frac{b}{2} + y') + f_n(0, -\frac{b}{2} - y') \right] dy' \tag{B.73}$$

where

$$f_n(u, v) = K_0(\beta\sqrt{(u - ns)^2 + v^2}). \tag{B.74}$$

Now (B.69) becomes

$$Z^a_{0m} = \frac{j\eta}{2\pi k} \sum_{n=-\infty}^{+\infty} \left(k^2 I_1^y - \frac{1}{b} I^{xy} \right) e^{jnks\cos\phi}. \tag{B.75}$$

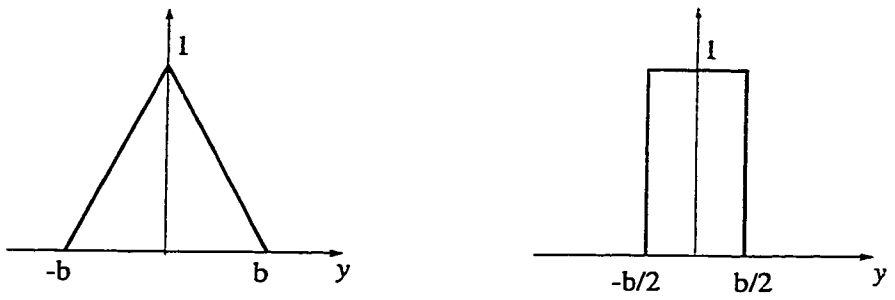

Figure B.2: Triangle function and pulse function.

The 2-D integral in I_1^y can be converted into 1-D integrals. We denote

$$I_1^y = I_1 + I_2 \tag{B.76}$$

where

$$\begin{aligned} I_1 &= \int_{y=0}^{\frac{b}{2}} \int_{x=0}^{b} \left(1 - \frac{x}{b}\right) f_n(0, b + x - y) dx dy \\ I_2 &= \int_{y=0}^{\frac{b}{2}} \int_{x=0}^{b} \left(1 - \frac{x}{b}\right) f_n(0, b - x - y) dx dy. \end{aligned} \tag{B.77}$$

I_1 and I_2 can be expressed as 1-D integrals via coordinate rotation. Denoting $I_1 = I_{11} + I_{12} + I_{13}$ and $I_2 = I_{21} + I_{22} + I_{23}$, we have the results written as

$$\begin{aligned} I_{11} &= \int_0^{\frac{b}{2}} x \left(1 - \frac{x}{2b}\right) f_n(0, x + \frac{b}{2}) dx \\ I_{12} &= \int_0^{\frac{b}{2}} \frac{b}{2} \left(\frac{3}{4} - \frac{x}{b}\right) f_n(0, x + b) dx \\ I_{13} &= \int_0^{\frac{b}{2}} \frac{b}{2} \left(\frac{1}{2} - \frac{x}{b}\right)^2 f_n(0, x + \frac{3}{2}b) dx \\ I_{21} &= \int_0^{\frac{b}{2}} x \left(1 - \frac{x}{2b}\right) f_n(0, b - x) dx \\ I_{22} &= \int_0^{\frac{b}{2}} \frac{b}{2} \left(\frac{3}{4} - \frac{x}{b}\right) f_n(0, \frac{b}{2} - x) dx \\ I_{23} &= \int_0^{\frac{b}{2}} \frac{b}{2} \left(\frac{1}{2} - \frac{x}{b}\right)^2 f_n(0, -x) dx. \end{aligned} \tag{B.78}$$

B.2 Fields From the Ground Plane

$$E_{lx} = \frac{1}{j\omega\mu\epsilon}\left(k^2 + \frac{\partial^2}{\partial x^2}\right) A_l(x,y), \quad E_{ly} = \frac{1}{j\omega\mu\epsilon}\frac{\partial^2}{\partial x \partial y} A_l(x,y) \tag{B.79}$$

$$H_{lz} = -\frac{1}{\mu}\frac{\partial A_l(x,y)}{\partial y} \tag{B.80}$$

B.2.1 Impedance Matrix Entries Z_{pl}

The entry in the impedance matrix relating to the averaged field on section p due to current on section l is given by

$$\begin{aligned} Z_{pl} &= -\int T_p(x) E^s_{lx}(x,0)dx \qquad \text{(B.81)} \\ &= -\frac{1}{j\omega\mu\epsilon}\int T_p(x)\left[k^2 + \frac{\partial^2}{\partial x^2}\right] A_l(x,y)dx \\ &= -\frac{1}{j\omega\mu\epsilon}\int T_p(x)\left[k^2 + \frac{\partial^2}{\partial x^2}\right] \int f_l(x') G_p(x-x',y)dx'dx \\ &= -\frac{1}{j\omega\mu\epsilon} T(x) * \left[k^2 + \frac{\partial^2}{\partial x^2}\right] f(x) * G_p(x,y) \\ &= \frac{j\eta}{2ks}\sum_{n=-\infty}^{+\infty} \frac{e^{-\gamma_n|y|}}{\gamma_n} T(x) * f(x) * \left[k^2 + \frac{\partial^2}{\partial x^2}\right] e^{j\omega_n x} \end{aligned}$$

where $x = x_p - x_l$. The convolution is carried out on x-axis. The test and basis functions are defined as pulse and triangle function depicted in Fig. B.2, except the parameter c is used here instead of b.

We define the Fourier transform pair as

$$F(\omega) = \int_{-\infty}^{+\infty} f(x) e^{-j\omega x} dx \tag{B.82}$$

$$f(x) = \frac{1}{2\pi}\int_{-\infty}^{+\infty} F(\omega) e^{j\omega x} d\omega \tag{B.83}$$

and using the convolution theorem, we can express (B.82) as

$$Z_{pl} = \frac{j\eta}{2ks}\sum_{n=-\infty}^{+\infty} \frac{e^{-\gamma_n|y|}}{\gamma_n}\left(k^2 - \omega_n^2\right) T(\omega_n) F(\omega_n) e^{j\omega_n x} \tag{B.84}$$

where

$$T(\omega) = 2\frac{\sin\frac{\omega c}{2}}{\omega} = c\frac{\sin\alpha}{\alpha} \tag{B.85}$$

$$F(\omega) = \frac{4}{c}\frac{\sin^2\frac{\omega c}{2}}{\omega^2} = c\left(\frac{\sin\alpha}{\alpha}\right)^2 \tag{B.86}$$

and $\alpha = \omega c/2$. Writing it in detail, and noting that $y = 0$ here, we have

$$Z_{pl} = \frac{4j\eta}{ksc}\sum_{n=-\infty}^{+\infty}\left(\frac{k^2}{\omega_n^2} - 1\right)\frac{\sin^3\frac{\omega_n c}{2}}{\omega_n}\frac{e^{j\omega_n(x_p - x_l)}}{\gamma_n}. \tag{B.87}$$

We see the terms in (B.87) decay only as $O(n^{-2})$ as $n \to \infty$. We can rewrite it as

$$Z_{pl} = Z_{pl}^a + Z_{pl}^b \tag{B.88}$$

where

$$Z_{pl}^a = \frac{j\eta}{2\pi k}\sum_{n=-\infty}^{+\infty}\left(k^2 I_1 + \frac{1}{c}I_2\right)e^{jnks\cos\phi} \tag{B.89}$$

and where

$$I_1 = \int_0^c\int_0^c\left(1 - \frac{x}{c}\right)\left[f(t_n - \frac{c}{2} + x + x') + f(t_n - \frac{c}{2} + x - x')\right]dxdx' \tag{B.90}$$

$$I_2 = \int_0^c\left[f(t_n + \frac{c}{2} + x) - 2f(t_n - \frac{c}{2} + x) + f(t_n - \frac{c}{2} - x)\right]dx$$

with $t_n = x_p - x_l - ns$ and $f(x) = K_0(\beta|x|)$.

Similarly, the 2-D integrals in I_1 can be converted into 1-D integrals as

$$I_1 = I_{11} + I_{12} + I_{13} + I_{14} \tag{B.91}$$

where

$$I_{11} = \int_0^c x\left(1 - \frac{x}{2c}\right)f(t_n - \frac{c}{2} + x)dx \tag{B.92}$$

$$I_{12} = \int_0^c \frac{c}{2}\left(1 - \frac{x}{c}\right)^2 f(t_n + \frac{c}{2} + x)dx$$

$$I_{13} = \int_0^c x\left(1 - \frac{x}{2c}\right)f(t_n + \frac{c}{2} - x)dx$$

$$I_{14} = \int_0^c \frac{c}{2}\left(1 - \frac{x}{c}\right)^2 f(t_n - \frac{c}{2} - x)dx.$$

The difference part is expressed as

$$Z_{pl}^{b} = \frac{4j\eta}{ksc}\sum_{n=-\infty}^{+\infty}\left(\frac{k^2}{\omega_n^2}-1\right)\frac{e^{j\omega_n(x_p-x_l)}}{\omega_n}\sin^3\frac{\omega_n c}{2}\left(\frac{1}{\gamma_n}-\frac{1}{\alpha_n}\right). \tag{B.93}$$

We see the terms in (B.93) decay as $O(n^{-4})$ as $n \to \infty$.

B.2.2 Excitation Voltage V_p

$$\begin{aligned} V_p &= \int T(x-x_p)\hat{\mathbf{x}}\cdot\mathbf{E}^i(x,0)dx \\ &= \frac{2\eta}{k}\tan\phi\sin\left(\frac{kc}{2}\cos\phi\right)H^i(x_p,0), \quad p=1,2,\cdots,L. \end{aligned} \tag{B.94}$$

B.2.3 Scattered Fields H_g^s

The scattered magnetic field is

$$H_z^s = -\frac{1}{\mu}\frac{\partial A_x}{\partial y}. \tag{B.95}$$

Using the current expansion and Poisson sum for the Green's function, we have

$$H_z^s = -\frac{1}{2s}\sum_{l=1}^{L}a_l\frac{\partial}{\partial y}\sum_{n=-\infty}^{+\infty}\frac{e^{-\gamma_n|y|}}{\gamma_n}\int f(\tau)e^{j\omega_n(x-x_l-\tau)}d\tau. \tag{B.96}$$

For $y \geq 0$ we can have the scattered field written as

$$H_z^s(x,y) = \frac{c}{2s}\sum_{l=1}^{L}a_l\sum_{n=-\infty}^{+\infty}e^{j\omega_n(x-x_l)}e^{-\gamma_n y}\left(\frac{\sin\alpha_n}{\alpha_n}\right)^2 \tag{B.97}$$

where

$$\alpha_n = \frac{\omega_n c}{2}.$$

We see the terms in the series decays at least at $O(n^{-2})$, which happens when $y = 0$, otherwise exponential decaying is ensured.

B.2.4 Weighted Fields on Parallel Strips Z_{ql}

The weighted field on segment q due to current segment l is similar to (B.82), as

$$\begin{aligned} Z_{ql} &= -\frac{1}{j\omega\mu\epsilon}\int T_q(y)\frac{\partial^2}{\partial x\partial y}A_l(x,y)dy \qquad \text{(B.98)} \\ &= -\frac{1}{j\omega\mu\epsilon}\int T_q(y)\frac{\partial^2}{\partial x\partial y}\int f(x'-x_l)G_p(x-x',y)dx'dy \\ &= \frac{j\eta}{2ks}\sum_{n=-\infty}^{+\infty}\frac{1}{\gamma_n}\int T_q(y)\frac{\partial}{\partial y}e^{-\gamma_n|y-y'|}dy\cdot\int f_l(x')\frac{\partial}{\partial x}e^{j\omega_n(x-x')}dx' \end{aligned}$$

where $T(y)$ and $f(x)$ are test and basis function defined in y and x axis. Performing the integral under the condition $y_q \geq b$, we have

$$\int T_q(y)\frac{\partial}{\partial y}e^{-\gamma_n|y-y'|}dy = e^{-\gamma_n(y_q+\frac{b}{2})} - e^{-\gamma_n(y_q-\frac{b}{2})} \qquad \text{(B.99)}$$

$$\begin{aligned} \int f_l(x')\frac{\partial}{\partial x}e^{j\omega_n(x-x')}dx' &= j\omega_n F_l(\omega_n)e^{j\omega_n(x-x_l)} \qquad \text{(B.100)} \\ &= j\frac{4}{c}\cdot\frac{\sin^2\left(\frac{\omega_n c}{2}\right)}{\omega_n}e^{j\omega_n(x-x_l)} \\ &= j2\cdot\frac{\sin^2\alpha_n}{\alpha_n}e^{j\omega_n(x-x_l)}. \qquad \text{(B.101)} \end{aligned}$$

Note that $x = y' = 0$ here, therefore

$$Z_{ql} = -\frac{\eta}{ks}\sum_{n=-\infty}^{+\infty}\frac{\sin^2\alpha_n}{\alpha_n}e^{-j\omega_n x_l}\frac{e^{-\gamma_n(y_q+\frac{b}{2})} - e^{-\gamma_n(y_q-\frac{b}{2})}}{\gamma_n} \qquad \text{(B.102)}$$

where

$$\alpha_n = \frac{\omega_n c}{2}.$$

We see that terms in the summation series of (B.102) are exponentially decaying.

B.2.5 Weighted Fields on the Corner Dipole Z_{0l}

$$\begin{aligned} Z_{0l} &= -\int \mathbf{E}_l\cdot\hat{\mathbf{t}}dl = -\int \mathbf{E}_l\cdot(\hat{\mathbf{x}}dx+\hat{\mathbf{y}}dy) \qquad \text{(B.103)} \\ &= \int_0^{\frac{c}{2}} E^s_{lx}(x,0)dx - \int_0^{\frac{b}{2}} E^s_{0y}(0,y)dy \\ &= Z_x + Z_y \end{aligned}$$

where E_{lx} and E_{ly} are field due to the currents on x axis, except the x-arm of the corner dipole. $T_0(x)$ and $T_0(y)$ are pulse functions defined in the Section B.3. The contour of integration is defined in Fig. B.1. The entry in the impedance matrix relating to the averaged field on the corner dipole due to current on section l is given by

$$Z_{0l} = -\frac{1}{j\omega\mu\epsilon}\left[\int T_0(x)\left(k^2+\frac{\partial^2}{\partial x^2}\right)A_l(x,y)dx + \int T_0(y)\frac{\partial^2}{\partial x\partial y}A_l(x,y)dy\right]. \quad \text{(B.104)}$$

Looking at the two integrals, we have

$$\begin{aligned}
&\int T_0(x)\left(k^2+\frac{\partial^2}{\partial x^2}\right)A_l(x,y)dx \qquad \text{(B.105)}\\
&\quad = \int T_0(x)\left(k^2+\frac{\partial^2}{\partial x^2}\right)f(x-x_l) * G_p(x-x_l,y)dx\\
&\quad = T_0(t) * \left(k^2+\frac{\partial^2}{\partial x^2}\right)f(t) * G_p(t,y)\\
&\quad = \mathcal{F}^{-1}\left\{T_0(\omega)\left(k^2+\frac{\partial^2}{\partial x^2}\right)F(\omega)\tilde{G}_p(\omega,y)\right\}
\end{aligned}$$

where $t=-x_l$, and $\tilde{G}_p(\omega,y)$ is the Fourier Transform of $G_p(t,y)$ and

$$\int T_0(y)\frac{\partial^2}{\partial x\partial y}A_l(x,y)dy = \frac{\mu}{2s}\sum_{n=-\infty}^{+\infty}\frac{1}{\gamma_n}\int T_0(y)\frac{\partial}{\partial y}e^{-\gamma_n|y-y'|}dy\cdot \int f(x'-x_l)\frac{\partial}{\partial x}e^{j\omega_n(x-x')}dx'. \quad \text{(B.106)}$$

These integrals can be evaluated in closed form, as follows

$$\int T_0(y)\frac{\partial}{\partial y}e^{-\gamma_n|y-y'|}dy = e^{-\gamma_n|\frac{1}{2}b-y'|} - e^{-\gamma_n|y'|} \quad \text{(B.107)}$$

$$\int f(x'-x_l)\frac{\partial}{\partial x}e^{j\omega_n(x-x')}dx' = j\omega_n F(\omega_n)e^{j\omega_n(x-x_l)} \quad \text{(B.108)}$$

$$\begin{aligned}
Z_x^{(1)} &= \frac{jk\eta}{2s}\sum_{n=-\infty}^{+\infty}\frac{e^{-j\omega_n x_l}}{\gamma_n}F(\omega_n)T^*(\omega_n) \qquad \text{(B.109)}\\
&= -\frac{2k\eta}{sc}\sum_{n=-\infty}^{+\infty}\frac{e^{-j\omega_n x_l}}{\gamma_n}\frac{\sin^2\left(\frac{\omega_n c}{2}\right)}{\omega_n^3}\left(e^{j\omega_n\frac{c}{2}}-1\right)\\
&= -\frac{2\eta}{ksc}\sum_{n=-\infty}^{+\infty}\frac{e^{-j\omega_n x_l}}{\gamma_n}\frac{\sin^2\left(\frac{\omega_n c}{2}\right)}{\omega_n}\frac{k^2}{\omega_n^2}\left(e^{j\omega_n\frac{c}{2}}-1\right)
\end{aligned}$$

$$Z_x^{(2)} = -\frac{2\eta}{ksc}\sum_{n=-\infty}^{+\infty}\frac{e^{-j\omega_n x_l}}{\gamma_n}\frac{\sin^2\left(\frac{\omega_n c}{2}\right)}{\omega_n}\left(1-e^{j\omega_n\frac{c}{2}}\right) \tag{B.110}$$

$$Z_y = \frac{2\eta}{ksc}\sum_{n=-\infty}^{+\infty}\frac{e^{-j\omega_n x_l}}{\gamma_n}\frac{\sin^2\left(\frac{\omega_n c}{2}\right)}{\omega_n}\left(1-e^{-\gamma_n\frac{b}{2}}\right). \tag{B.111}$$

Now we sum the three terms up, noting that the first terms in $Z_x^{(2)}$ and Z_y cancel with each other, we have

$$Z_{0l} = \frac{2\eta}{ksc}\sum_{n=-\infty}^{+\infty}\frac{e^{-j\omega_n x_l}}{\gamma_n}\frac{\sin^2\left(\frac{\omega_n c}{2}\right)}{\omega_n}\left[\frac{k^2}{\omega_n^2}+\left(1-\frac{k^2}{\omega_n^2}\right)e^{j\omega_n\frac{c}{2}}-e^{-\gamma_n\frac{b}{2}}\right]. \tag{B.112}$$

We see the terms in (B.112) decay only as $O(n^{-2})$ as $n\to\infty$. We rewrite Z_{ol} as two parts

$$Z_{0l} = Z_{0l}^a + Z_{0l}^b. \tag{B.113}$$

We write Z_{0l}^a as

$$Z_{0l}^a = \frac{j\eta}{2\pi k}\sum_{n=-\infty}^{+\infty} I_n e^{jnks\cos\phi} \tag{B.114}$$

where

$$I_n = -k^2 I_1 + \frac{1}{c}I_2 \tag{B.115}$$

and

$$I_1 = \int_{y=0}^{\frac{c}{2}}\int_{x=0}^{c}\left(1-\frac{x}{c}\right)\left[f_n(t_n+x-y,0)+f_n(t_n-x-y,0)\right]dxdx' \tag{B.116}$$

$$I_2 = \int_0^c\left[f_n(t_n-x,\frac{b}{2})-f_n(t_n+x,\frac{b}{2})-f_n(t_n-\frac{c}{2}-x,0)+f_n(t_n-\frac{c}{2}+x,0)\right]dx$$

with $t_n = x_l + ns$, and $f_n(x,y) = K_0(\beta\sqrt{x^2+y^2})$.

Similarly, the 2-D integrals in I_1 can be expressed as 1-D integrals via coordinate rotation. Denoting

$$I_1 = I_{11} + I_{12} + I_{13} + I_{21} + I_{22} + I_{23} \tag{B.117}$$

we have the results written as

$$
\begin{aligned}
I_{11} &= \int_0^{\frac{c}{2}} x\left(1-\frac{x}{2c}\right) f_n(t_n-\frac{c}{2}+x,0)dx \qquad \text{(B.118)}\\
I_{12} &= \int_0^{\frac{c}{2}} \frac{c}{2}\left(\frac{3}{4}-\frac{x}{c}\right) f_n(t_n+x,0)dx\\
I_{13} &= \int_0^{\frac{c}{2}} \frac{c}{2}\left(\frac{1}{2}-\frac{x}{c}\right)^2 f_n(t_n+\frac{c}{2}+x,0)dx\\
I_{21} &= \int_0^{\frac{c}{2}} x\left(1-\frac{x}{2c}\right) f_n(t_n-x,0)dx\\
I_{22} &= \int_0^{\frac{c}{2}} \frac{c}{2}\left(\frac{3}{4}-\frac{x}{c}\right) f_n(t_n-\frac{c}{2}-x,0)dx\\
I_{23} &= \int_0^{\frac{c}{2}} \frac{c}{2}\left(\frac{1}{2}-\frac{x}{c}\right)^2 f_n(t_n-c-x,0)dx.
\end{aligned}
$$

B.3 Fields From the Corner Dipole

The field components produced by the x and y segments are

$$
\begin{aligned}
E_x(x,y) &= \frac{1}{j\omega\mu\epsilon}\left[\left(k^2+\frac{\partial^2}{\partial x^2}\right)A_{0x}(x,y)+\frac{\partial^2}{\partial x\partial y}A_{0y}(x,y)\right] \qquad \text{(B.119)}\\
E_y(x,y) &= \frac{1}{j\omega\mu\epsilon}\left[\left(k^2+\frac{\partial^2}{\partial y^2}\right)A_{0y}(x,y)+\frac{\partial^2}{\partial x\partial y}A_{0x}(x,y)\right] \qquad \text{(B.120)}\\
H_z(x,y) &= \frac{1}{\mu}\left(\frac{\partial}{\partial x}A_{0y}(x,y)-\frac{\partial}{\partial y}A_{0x}(x,y)\right). \qquad \text{(B.121)}
\end{aligned}
$$

B.3.1 Impedance Matrix Entries Z_{00}

Applying test functions on both sides of the above equation, we have

$$
-\int_l T(t)\mathbf{E}^s\cdot\hat{\mathbf{t}}dt=\int_l T(t)\mathbf{E}^i\cdot\hat{\mathbf{t}}dt \qquad \text{(B.122)}
$$

where l denotes the the contour of the whole corner dipole, $\hat{\mathbf{t}}$ is the tangential vector along l. Refer to Fig. B.1 for illustration. We select the test function $T(t)$ in such a way that the integral yields the average of the field along the contour of the whole corner dipole.

$$
\begin{aligned}
Z_{00} &= \int_0^{\frac{1}{2}c} E_x^s dx-\int_0^{\frac{1}{2}b} E_y^s dy\\
&= \int_0^{\frac{c}{2}} E_x^x dx+\int_0^{\frac{c}{2}} E_x^y dx-\int_0^{\frac{b}{2}} E_y^y dy-\int_0^{\frac{b}{2}} E_y^x dy\\
&= Z_{xx}+Z_{xy}+Z_{yy}+Z_{yx}
\end{aligned}
$$

where Z_{xx} and Z_{xy} denotes the averaged field on x-segment of the corner dipole generated by J_x and J_y, respectively. Similarly, Z_{yy} and Z_{yx} denote the averaged field on y-segment of the corner dipole generated by J_y and J_x, respectively.

Further, we denote $Z_{xx} = Z_{xx}^{(1)} + Z_{xx}^{(2)}$. Performing the double integration, we have

$$\begin{aligned} Z_{xx}^{(1)} &= \frac{k\eta}{2s}\sum_{n=-\infty}^{+\infty}\frac{1-e^{j\omega_n c/2}}{\omega_n\gamma_n}\left(\frac{e^{-j\omega_n c}-1}{\omega_n^2 c}-\frac{1}{j\omega_n}\right) \qquad \text{(B.123)}\\ &= \frac{j\eta}{2ks}\sum_{n=-\infty}^{+\infty}\frac{1-e^{j\omega_n c/2}}{\gamma_n}\frac{k^2}{\omega_n^2}\left(\frac{e^{-j\omega_n c}-1}{j\omega_n c}+1\right) \\ Z_{xx}^{(2)} &= -\frac{j\eta}{2ks}\sum_{n=-\infty}^{+\infty}\frac{1-e^{j\omega_n c/2}}{\gamma_n}\left(\frac{e^{-j\omega_n c}-1}{j\omega_n c}+1\right) \qquad \text{(B.124)}\\ Z_{xy} &= -\frac{j\eta}{2ks}\sum_{n=-\infty}^{+\infty}\frac{1-e^{j\omega_n c/2}}{\gamma_n}\left(\frac{1-e^{-\gamma_n b}}{b\gamma_n}-1\right). \qquad \text{(B.125)} \end{aligned}$$

It is noticed that the first term in $Z_{xx}^{(2)}$ is canceled with the first term in Z_{xy}, which yields

$$Z_{xx}^{(2)} + Z_{xy} = -\frac{j\eta}{2ks}\sum_{n=-\infty}^{+\infty}\frac{1-e^{j\omega_n c/2}}{\gamma_n}\left(\frac{e^{-j\omega_n c}-1}{j\omega_n c}+\frac{1-e^{-\gamma_n b}}{b\gamma_n}\right). \qquad \text{(B.126)}$$

Similarly, we denote $Z_{yy} = Z_{yy}^{(1)} + Z_{yy}^{(2)}$. Performing the double integration, we have

$$\begin{aligned} Z_{yy}^{(1)} &= \frac{jk\eta}{2s}\sum_{n=-\infty}^{+\infty}\frac{Q(\gamma_n)}{\gamma_n^2} \qquad \text{(B.127)}\\ &= \frac{j\eta}{2ks}\sum_{n=-\infty}^{+\infty}\frac{k^2}{\gamma_n^2}Q(\gamma_n) \\ Z_{yy}^{(2)} &= -\frac{j\eta}{2ks}\sum_{n=-\infty}^{+\infty}\frac{1-e^{-\gamma_n b/2}}{\gamma_n}\left(1+\frac{1-e^{-\gamma_n b/2}}{b\gamma_n}\right) \qquad \text{(B.128)}\\ Z_{yx} &= \frac{j\eta}{2ks}\sum_{n=-\infty}^{+\infty}\frac{1-e^{-\gamma_n b/2}}{\gamma_n}\left(1+\frac{e^{-j\omega_n c}-1}{j\omega_n c}\right) \qquad \text{(B.129)} \end{aligned}$$

where

$$Q(\gamma_n) = \frac{3b}{4} - \frac{1-e^{-\gamma_n\frac{b}{2}}}{\gamma_n}\left(1+\frac{1-e^{-\gamma_n\frac{b}{2}}}{b\gamma_n}\right).$$

We also notice that the first term in $Z_{yy}^{(2)}$ is canceled with the first term in Z_{yx}, which yields

$$Z_{yy}^{(2)} + Z_{yx} = \frac{j\eta}{2ks}\sum_{n=-\infty}^{+\infty}\frac{1-e^{-\gamma_n b/2}}{\gamma_n}\left(\frac{e^{-j\omega_n c}-1}{j\omega_n c}-\frac{1-e^{-\gamma_n b/2}}{b\gamma_n}\right). \qquad \text{(B.130)}$$

Summing up, (B.123) becomes

$$Z_{00} = \frac{j\eta}{2ks}\sum_{n=-\infty}^{+\infty}\left\{\frac{3b}{4}\cdot\frac{k^2}{\gamma_n^2}+\frac{1-e^{j\omega_n\frac{c}{2}}}{\gamma_n}\left[\left(\frac{k^2}{\omega_n^2}-1\right)\frac{e^{-j\omega_n c}-1}{j\omega_n c}+\frac{k^2}{\omega_n^2}-\frac{1-e^{-\gamma_n b}}{b\gamma_n}\right]\right.$$
$$\left.-\frac{1-e^{-\gamma_n\frac{b}{2}}}{\gamma_n}\left[\left(1+\frac{k^2}{\gamma_n^2}\right)\frac{1-e^{-\gamma_n\frac{b}{2}}}{b\gamma_n}+\frac{k^2}{\gamma_n^2}+\frac{1-e^{-j\omega_n c}}{j\omega_n c}\right]\right\}.$$

It is noticed that the terms in the above series converges at $O(n^{-2})$ as $n \to \infty$. An additional order of convergence can be achieved by using the decomposition of the Green's function defined in (B.4). We express Z_{00} as

$$Z_{00} = Z_{00}^a + Z_{00}^b. \tag{B.131}$$

Next, we write Z_{00}^a as

$$Z_{00}^a = \frac{j\eta}{2\pi k}\sum_{n=-\infty}^{+\infty} I_n e^{jnks\cos\phi} \tag{B.132}$$

where

$$I_n = k^2\left(I_1^x + I_1^y\right) + \frac{1}{c}I^x + \frac{1}{b}I^y \tag{B.133}$$

and

$$\begin{aligned}
I_1^x &= \int_{y=0}^{\frac{c}{2}}\int_{x=0}^{c}\left(1-\frac{x}{c}\right)K_0(\beta|ns+x-y|)dxdy \qquad \text{(B.134)}\\
I_1^y &= \int_{y=0}^{\frac{b}{2}}\int_{x=0}^{b}\left(1-\frac{x}{b}\right)K_0(\beta\sqrt{(ns)^2+(x-y)^2})dxdy\\
I^x &= \int_0^c\left[f_n(x,\frac{b}{2})-f_n(x-\frac{c}{2},0)\right]dx\\
I^y &= \int_0^b\left[f_n(-\frac{c}{2},y)-f_n(0,y-\frac{b}{2})\right]dy
\end{aligned}$$

and

$$f_n(x,y) = K_0\left(\beta\sqrt{(ns+x)^2+y^2}\right). \tag{B.135}$$

Similarly, the 2-D integrals in I_1 can be expressed as 1-D integrals via coordinate rotation. Denoting

$$I_1^x = I_{11}^x + I_{12}^x + I_{13}^y \text{ and } I_1^y = I_{11}^y + I_{12}^y + I_{13}^y \tag{B.136}$$

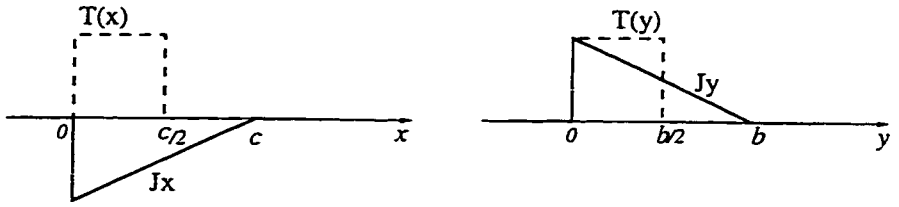

Figure B.3: Current basis and test function on the corner dipole.

we have the results written as

$$
\begin{aligned}
I_{11}^{x} &= \int_0^{\frac{c}{2}} x\left(1-\frac{x}{2c}\right) f_n(-\frac{c}{2}+x,0)dx \\
I_{12}^{x} &= \int_0^{\frac{c}{2}} \frac{c}{2}\left(\frac{3}{4}-\frac{x}{c}\right) f_n(x,0)dx \\
I_{13}^{x} &= \int_0^{\frac{c}{2}} \frac{c}{2}\left(\frac{1}{2}-\frac{x}{c}\right)^2 f_n(\frac{c}{2}+x,0)dx \\
I_{11}^{y} &= \int_0^{\frac{b}{2}} x\left(1-\frac{x}{2b}\right) f_n(0,,x-\frac{b}{2})dx \\
I_{12}^{y} &= \int_0^{\frac{b}{2}} \frac{b}{2}\left(\frac{3}{4}-\frac{x}{b}\right) f_n(0,x)dx \\
I_{13}^{y} &= \int_0^{\frac{b}{2}} \frac{b}{2}\left(\frac{1}{2}-\frac{x}{b}\right)^2 f_n(0,x+\frac{b}{2})dx.
\end{aligned}
\tag{B.137}
$$

B.3.2 Excitation Voltage V_0

The excitation voltage is defined as a line integral of the tangential incident electric field on the surface of the corner dipole, as expressed in the LHS of (B.122).

$$
\begin{aligned}
V_0 &= \int_l T(t)\mathbf{E}^i \cdot \hat{\mathbf{t}} dt \\
&= \int_{\frac{c}{2}}^{0} E_x dx + \int_0^{\frac{b}{2}} E_y dy \\
&= \frac{j\eta H_0}{k}\left[\left(e^{jk\frac{c}{2}\cos\phi}-1\right)\tan\phi + \left(e^{jk\frac{b}{2}\sin\phi}-1\right)\cot\phi\right].
\end{aligned}
\tag{B.138}
$$

The basis and test functions applied on the x and y arms are depicted in Fig. B.3.

B.3.3 Scattered Fields H_0^s

The magnetic field from the currents on corner dipoles is

$$H_z = \frac{1}{\mu}\left(\frac{\partial A_y}{\partial x} - \frac{\partial A_x}{\partial y}\right). \tag{B.139}$$

Now we formulate the contributions from A_y and A_x separately in the following sections.

Field From J_x

$$\begin{aligned} H_z(x,y) &= -\frac{1}{2s}a_0 \sum_{n=-\infty}^{+\infty} \frac{\partial}{\partial y}\frac{e^{-\gamma_n|y-y'|}}{\gamma_n} \int f_0(x')e^{j\omega_n(x-x')}dx' \\ &= -\frac{1}{2s}a_0 \sum_{n=-\infty}^{+\infty} \frac{\partial}{\partial y}\frac{e^{-\gamma_n|y-y'|}}{\gamma_n} f_o(x) * e^{j\omega_n x} \\ &= -\frac{1}{2s}a_0 \sum_{n=-\infty}^{+\infty} \frac{\partial}{\partial y}\frac{e^{-\gamma_n y}}{\gamma_n} F(\omega_n)e^{j\omega_n x} \\ &= \frac{1}{2s}a_0 \sum_{n=-\infty}^{+\infty} \left(\frac{e^{-j\omega_n c}-1}{\omega_n^2 c} - \frac{1}{j\omega_n}\right) e^{j\omega_n x}e^{-\gamma_n y}. \end{aligned} \tag{B.140}$$

Note in the above, we have used the fact that $y' = 0$ and assumed $y \geq 0$. Also the Fourier transform is defined in (B.83), and the convolution theorem is applied.

Field From J_y

$$\begin{aligned} H_z(x,y) &= \frac{1}{2s}a_0 \sum_{n=-\infty}^{+\infty} \frac{1}{\gamma_n}\frac{\partial}{\partial x}e^{j\omega_n(x-x')} \int f_0(y')e^{-\gamma_n|y-y'|}dy' \\ &= \frac{j}{2s}a_0 \sum_{n=-\infty}^{+\infty} \frac{\omega_n}{\gamma_n}e^{j\omega_n(x-x')} \int f_0(y')e^{-\gamma_n|y-y'|}dy'. \end{aligned}$$

The integral can be evaluated in closed form for $y \leq 0$, as

$$\int f_0(y')e^{-\gamma_n|y-y'|}dy' = \frac{1}{\gamma_n}\begin{cases} \left(\dfrac{e^{\gamma_n b}-1}{b\gamma_n} - 1\right)e^{-\gamma_n y} & y \geq b \\ 2\left(1-\dfrac{y}{b}\right) + \dfrac{e^{\gamma_n(y-b)}}{b\gamma_n} - \left(1+\dfrac{1}{b\gamma_n}\right)e^{-\gamma_n y} & y < b. \end{cases} \tag{B.141}$$

Therefore the scattered magnetic field from J_y is, (note $x' = 0$ here)

$$H_z(x,y) = \frac{j}{2s} a_0 \sum_{n=-\infty}^{+\infty} \frac{\omega_n}{\gamma_n^2} e^{j\omega_n x} \begin{cases} \left(\frac{e^{\gamma_n b} - 1}{b\gamma_n} - 1\right) e^{-\gamma_n y} & y \geq b \\ 2\left(1 - \frac{y}{b}\right) + \frac{e^{\gamma_n (y-b)}}{b\gamma_n} & \\ \qquad - \left(1 + \frac{1}{b\gamma_n}\right) e^{-\gamma_n y} & y < b. \end{cases} \tag{B.142}$$

The Total Field From Corner Dipoles

Using (B.141) and (B.142), we have the scattered magnetic field by the corner dipole

$$H_z^s = \frac{1}{2s} a_0 \sum_{n=-\infty}^{+\infty} e^{j\omega_n x} \begin{cases} Q_n & y \geq b \\ 2\left(1 - \frac{y}{b}\right) \frac{j\omega_n}{\gamma_n^2} + Q_n & y < b \end{cases} \tag{B.143}$$

where

$$Q_n = \frac{j\omega_n}{b\gamma_n^3} e^{-\gamma_n |y-b|} + \left[\frac{e^{-j\omega_n c} - 1}{\omega_n^2 c} - \frac{j\omega_n}{\gamma_n^2}\left(\frac{1}{b\gamma_n} + \frac{k^2}{\omega_n^2}\right)\right] e^{-\gamma_n y}. \tag{B.144}$$

We see that for the case $y > b$, exponential convergence is ensured. For the case $y = b$, the convergence rate is at $O(n^{-2})$, while for the case $y < b$, is only $O(n^{-1})$. Again, the accelerating procedure is employed, we write

$$H_z^s = H^a + H^b. \tag{B.145}$$

Next, we write H^a as

$$H^a = \frac{a_0}{2\pi} \sum_{n=-\infty}^{+\infty} (I_n^x + I_n^y) e^{jnks\cos\phi} \tag{B.146}$$

where

$$\begin{aligned} I_n^x &= -\beta y \int_0^c \left(1 - \frac{x'}{c}\right) \frac{K_1(\beta R_x)}{R_x} dx' \\ I_n^y &= -\beta (x - ns) \int_0^b \left(1 - \frac{y'}{b}\right) \frac{K_1(\beta R_y)}{R_y} dy' \end{aligned} \tag{B.147}$$

and

$$\begin{aligned} R_x &= \sqrt{(x - x' - ns)^2 + y^2} \\ R_y &= \sqrt{(x - ns)^2 + (y - y')^2}. \end{aligned} \tag{B.148}$$

The difference part which is evaluated in the spectral domain comes out to be

$$H^b(x,y) = \frac{1}{2s}a_0 \sum_{n=-\infty}^{+\infty} e^{j\omega_n x} \begin{cases} Q_n^b(y,\omega_n,\gamma_n,\alpha_n) & y \geq b \\ 2\left(1-\frac{y}{b}\right)j\omega_n\left(\frac{1}{\gamma_n^2}-\frac{1}{\alpha_n^2}\right) & \\ \quad + Q_n^b(y,\omega_n,\gamma_n,\alpha_n) & y < b \end{cases} \tag{B.149}$$

where

$$\begin{aligned} Q_n^b(y,\omega_n,\gamma_n,\alpha_n) &= \frac{j\omega_n}{b}\left(\frac{e^{-\gamma_n|y-b|}-e^{-\gamma_n y}}{\gamma_n^3} - \frac{e^{-\alpha_n|y-b|}-e^{-\alpha_n y}}{\alpha_n^3}\right) \\ &+ \frac{e^{-j\omega_n c}-1}{\omega_n^2 c}\left(e^{-\gamma_n y}-e^{-\alpha_n y}\right) + \frac{1}{j\omega_n}\left(\frac{k^2}{\gamma_n^2}e^{-\gamma_n y}+\frac{\beta^2}{\alpha_n^2}e^{-\alpha_n y}\right). \end{aligned} \tag{B.150}$$

We see that for the case $y > b$, the terms exhibit exponential decay, for the case $y = b$, decrease as $O(n^{-4})$ and for case $y < b$, decrease as $O(n^{-3})$ as $n \to \infty$.

B.3.4 Weighted Fields on Horizontal Strips Z_{p0}

$$Z_{p0} = -\int T_p(x)E_x(x,y)dx$$

where $T_p(x)$ is the weighting function, and E_x is the x-component of the field from the corner dipole.

The field from the corner dipole consists of contributions from the horizontal and vertical current components, and is given by

$$E_x^{J_x} = -\frac{\eta}{4k}\left(k^2+\frac{\partial^2}{\partial x^2}\right)\int J_x(x')\sum_{n=-\infty}^{+\infty} H_0^{(2)}(kR_n)e^{jnk_x s}dx' \tag{B.151}$$

$$E_x^{J_y} = -\frac{\eta}{4k}\frac{\partial^2}{\partial x\partial y}\int J_y(y')\sum_{n=-\infty}^{+\infty} H_0^{(2)}(kR_n)e^{jnk_x s}dy'. \tag{B.152}$$

Applying the Poisson summation, we have

$$E_x^{J_x} = -\frac{j\eta}{2ks}\left(k^2+\frac{\partial^2}{\partial x^2}\right)\int J_x(x')\sum_{n=-\infty}^{+\infty}\frac{e^{j\omega_n(x-x')}}{\gamma_n}e^{-\gamma_n|y-y'|}dx' \tag{B.153}$$

$$E_x^{J_y} = -\frac{j\eta}{2ks}\frac{\partial^2}{\partial x\partial y}\int J_y(y')\sum_{n=-\infty}^{+\infty}\frac{e^{j\omega_n(x-x')}}{\gamma_n}e^{-\gamma_n|y-y'|}dy'. \tag{B.154}$$

We denote $Z_{pv} = Z_x + Z_y$, which accounts for the contributions from J_x and J_y, respectively. We have

$$Z_x = \frac{j\eta}{2ks}\sum_{n=-\infty}^{+\infty}\frac{e^{-\gamma_n|y-y'|}}{\gamma_n}\int T(x-x_p)\int J_x(x')\left[k^2+\frac{\partial^2}{\partial x^2}\right]e^{j\omega_n(x-x')}dx'dx \quad \text{(B.155)}$$

$$Z_y = \frac{j\eta}{2ks}\sum_{n=-\infty}^{+\infty}\int T(x-x_p)\int J_y(y')\frac{\partial^2}{\partial x\partial y}\frac{e^{j\omega_n(x-x')}}{\gamma_n}e^{-\gamma_n|y-y'|}dy'dx. \quad \text{(B.156)}$$

The expression can be written as a convolution form

$$Z_x = \frac{j\eta}{2ks}\sum_{n=-\infty}^{+\infty}\frac{e^{-\gamma_n|y-y'|}}{\gamma_n}T(t)*J_x(t)\left[k^2+\frac{\partial^2}{\partial t^2}\right]e^{j\omega_n t} \quad \text{(B.157)}$$

$$Z_y = \frac{j\eta}{2ks}\sum_{n=-\infty}^{+\infty}\frac{1}{\gamma_n}T(t)*\frac{\partial}{\partial t}e^{j\omega_n t}\cdot J_y(y)*\frac{\partial}{\partial y}e^{-\gamma_n|y-y'|} \quad \text{(B.158)}$$

where $t = x_p$, $y = y' = 0$. Performing the convolution, we have

$$Z_x = \frac{j\eta}{2ks}\sum_{n=-\infty}^{+\infty}\frac{e^{-\gamma_n|y-y'|}}{\gamma_n}T(\omega_n)J_x(\omega_n)\left(k^2-\omega_n^2\right)e^{j\omega_n t} \quad \text{(B.159)}$$

$$= \frac{\eta}{ks}\sum_{n=-\infty}^{+\infty}\frac{e^{j\omega_n x_p}}{\gamma_n}\sin\frac{\omega_n c}{2}\left[\left(1-\frac{k^2}{\omega_n^2}\right)\frac{e^{-j\omega_n c}-1}{j\omega_n c}+1-\frac{k^2}{\omega_n^2}\right] \quad \text{(B.160)}$$

$$Z_y = \frac{j\eta}{2ks}\sum_{n=-\infty}^{+\infty}\frac{j\omega_n}{\gamma_n}T(\omega_n)e^{j\omega_n t}\cdot J_x'(y)*e^{-\gamma_n|y|} \quad \text{(B.161)}$$

$$= \frac{\eta}{ks}\sum_{n=-\infty}^{+\infty}\frac{e^{j\omega_n x_p}}{\gamma_n}\sin\frac{\omega_n c}{2}\left(\frac{1-e^{-\gamma_n b}}{b\gamma_n}-1\right). \quad \text{(B.162)}$$

Using Z_x and Z_y, we have

$$Z_{p0} = \frac{\eta}{ks}\sum_{n=-\infty}^{+\infty}\frac{e^{j\omega_n x_p}}{\gamma_n}\sin\frac{\omega_n c}{2}\left[\left(1-\frac{k^2}{\omega_n^2}\right)\cdot\frac{e^{-j\omega_n c}-1}{j\omega_n c}+\frac{1-e^{-\gamma_n b}}{b\gamma_n}-\frac{k^2}{\omega_n^2}\right]. \quad \text{(B.163)}$$

B.3.5 Weighted Fields on Parallel Strips Z_{q0}

The weighted field on segment q of the parallel stripe due to the current on corner dipole is given by

$$Z_{q0} = -\int T(y-y_q)\hat{\mathbf{y}}\cdot\mathbf{E}(0,y)dy \quad \text{(B.164)}$$

where $T(y-y_q)$ is the test function applied on segment q, and $\mathbf{E}$ is the electric field produced by the corner dipoles. Note the corner dipole has current of both x and y components, the

above expression can be written as

$$Z_{q0} = -\int T(y-y_q)\hat{\mathbf{y}}\cdot\mathbf{E}^y(0,y)dy - \int T(y-y_q)\hat{\mathbf{y}}\cdot\mathbf{E}^x(0,y)dy = Z_y + Z_x \tag{B.165}$$

where $\mathbf{E}^y$ and $\mathbf{E}^x$ are fields produced by the current on the y and x arm of the corner dipole, respectively. Using the decomposition shown in (B.165), we evaluate the contribution from J_y and J_x separately.

Contribution From J_y

$$Z_y = \frac{j\eta}{2ks}\sum_{n=-\infty}^{+\infty}\frac{e^{j\omega_n(x-x')}}{\gamma_n}\int\int T(y-y_q)J(y')\left[k^2+\frac{\partial^2}{\partial y^2}\right]e^{-\gamma_n|y-y'|}\,dy'dy. \tag{B.166}$$

Note that $x = x' = 0$ here. Performing the double integration, we have

$$Z_y = \frac{j\eta}{2ks}\sum_{n=-\infty}^{+\infty}Q_n^y(\gamma_n) \tag{B.167}$$

where

$$Q_n^y = \begin{cases} \dfrac{e^{-\gamma_n\left(t-\frac{3}{2}b\right)}}{\gamma_n}\left(1+\dfrac{k^2}{\gamma_n^2}\right)\left(1-e^{-\gamma_n b}\right)\left(\dfrac{1-e^{-\gamma_n b}}{b\gamma_n}-e^{-\gamma_n b}\right) & t \geq 2b, \\ \dfrac{k^2 b}{4\gamma_n^2}+\dfrac{1-e^{-\gamma_n\frac{b}{2}}}{\gamma_n}\left(1+\dfrac{k^2}{\gamma_n^2}\right) & \\ \qquad\left[\dfrac{\left(1-e^{-\gamma_n\frac{b}{2}}\right)\left(2+e^{-\gamma_n\frac{b}{2}}\right)}{b\gamma_n}-e^{-\gamma_n\frac{b}{2}}\left(1+e^{-\gamma_n\frac{b}{2}}\right)\right] & t = b. \end{cases} \tag{B.168}$$

and $t = y_q$.

Contribution From J_x

$$Z_x = \frac{j\eta}{2ks}\sum_{n=-\infty}^{+\infty}\int_{x'}J(x')\frac{\partial}{\partial x}\frac{e^{j\omega_n(x-x')}}{\gamma_n}dx'\int_y T(y-y_q)\frac{\partial}{\partial y}e^{-\gamma_n|y-y'|}dy. \tag{B.169}$$

We note that $x = y' = 0$ here. Performing the double integration, we have

$$Z_x = \frac{j\eta}{2ks}\sum_{n=-\infty}^{+\infty}\frac{e^{-\gamma_n(t-\frac{b}{2})}}{\gamma_n}(e^{-\gamma_n b}-1)\left(\frac{1-e^{-j\omega_n c}}{j\omega_n c}-1\right). \tag{B.170}$$

Merging Z_x with Z_y, we have

$$Z_{q0} = \frac{j\eta}{2ks} \sum_{n=-\infty}^{+\infty} \begin{cases} \dfrac{e^{-\gamma_n(t-\frac{3}{2}b)}}{\gamma_n}(1-e^{-\gamma_n b}) \\ \left[\left(1+\dfrac{k^2}{\gamma_n^2}\right)\dfrac{1-e^{-\gamma_n b}}{b\gamma_n} - \left(\dfrac{1-e^{-j\omega_n c}}{j\omega_n c}+\dfrac{k^2}{\gamma_n^2}\right)e^{-\gamma_n b}\right] & t \geq 2b, \\ \dfrac{k^2}{\gamma_n^2}\dfrac{b}{4} + \dfrac{1-e^{-\gamma_n \frac{b}{2}}}{\gamma_n}\left[\left(1+\dfrac{k^2}{\gamma_n^2}\right)\dfrac{(1-e^{-\gamma_n \frac{b}{2}})(2+e^{-\gamma_n \frac{b}{2}})}{b\gamma_n}\right. & \text{(B.171)} \\ \left. - \left(\dfrac{1-e^{-j\omega_n c}}{j\omega_n c}+\dfrac{k^2}{\gamma_n^2}\right)e^{-\gamma_n \frac{b}{2}}(1+e^{-\gamma_n \frac{b}{2}})\right] & t = b. \end{cases}$$

Appendix C

Some Properties Relating to Convolution

In the formulation of the impedance elements and the scattered fields, we will encounter the evaluation of some integrals which are given below for quick reference.

In derivation of impedance between segments on parallel strips, we encountered the following integral, refer to (B.14)

$$Z_{qm} = -\frac{1}{j\omega\mu\epsilon}\int T_q(y)\left(k^2 + \frac{\partial^2}{\partial y^2}\right) A_m(x,y)dy \tag{C.1}$$

which need the following properties relating the Fourier transform of functions, convolution between functions, with δ-functions or its derivatives.

$$f'(t) * g(t) = f(t) * g'(t) \tag{C.2}$$

$$f(t) * \delta(t) = f(t) \tag{C.3}$$

$$f(t) * \delta'(t) = f'(t) \tag{C.4}$$

where $f(t)$ and $g(t)$ are assumed to be continuous. Assuming $J_x(x)$ and $J_y(y)$ are triangular functions defined as

$$J_x(x) = \begin{cases} \left(\frac{x}{c} - 1\right) & 0 \le x \le c, \\ 0 & \text{else.} \end{cases} \tag{C.5}$$

$$J_y(y) = \begin{cases} \left(1 - \frac{y}{b}\right) & 0 \le y \le b, \\ 0 & \text{else.} \end{cases} \tag{C.6}$$

we have

$$J'_y(y) = -\frac{1}{b}[u(y) - u(y-b)] + \delta(y) \tag{C.7}$$

$$J''_y(y) = -\frac{1}{b}[\delta(y) - \delta(y-b)] + \delta'(y) \tag{C.8}$$

where $u(y)$ is the unit function. Further we have these integrals

$$\int J(y')\frac{\partial}{\partial y}e^{-\gamma_n|y-y'|}dy = J(y) * \frac{\partial}{\partial y}e^{-\gamma_n|y|} = J'(y) * e^{-\gamma_n|y|} \tag{C.9}$$

$$= -b\int_0^b e^{-\gamma_n|y-t|}dt + e^{-\gamma_n|y|} \tag{C.10}$$

$$J''(y) * e^{-\gamma_n|y|} = -\frac{1}{b}\left[e^{-\gamma_n|y|} - e^{-\gamma_n|y-b|}\right] + \frac{\partial}{\partial y}e^{-\gamma_n|y|} \tag{C.11}$$

$$\tag{C.12}$$

The Fourier transform of $J_x(x)$ and $J_y(y)$ are

$$\mathcal{J}_x(\omega) = \frac{e^{-j\omega c} - 1}{\omega^2 c} - \frac{1}{j\omega} \quad \text{and} \quad \mathcal{J}_y(\omega) = \frac{1 - e^{-j\omega b}}{\omega^2 b} + \frac{1}{j\omega} \tag{C.13}$$

Take the definition in (3.35) on page 33, the Fourier transform of the test function $T_0(x)$ and $T_0(y)$ are

$$\mathcal{T}_x(\omega) = \frac{1 - e^{-j\omega\frac{c}{2}}}{j\omega} \quad \text{and} \quad \mathcal{T}_y(\omega) = \frac{1 - e^{-j\omega\frac{b}{2}}}{j\omega}. \tag{C.14}$$

Some general properties relating to Fourier transforms are listed for quick reference

$$\int J_x(x')e^{j\omega_n(x-x')}dx' = J_x(x) * e^{j\omega_n x} = \mathcal{J}_x(\omega_n)e^{j\omega_n x} \tag{C.15}$$

$$\int J_x(x')\frac{\partial}{\partial x}e^{j\omega_n(x-x')}dx' = J'_x(x) * e^{j\omega_n x} = j\omega_n\mathcal{J}_x(\omega_n)e^{j\omega_n x} \tag{C.16}$$

$$\int T(x)e^{j\omega_n(x-x')}dx = \mathcal{T}(-\omega_n)e^{-j\omega_n x'} \tag{C.17}$$

$$\int T(x)\frac{\partial}{\partial x}e^{j\omega_n(x-x')}dx = j\omega_n\mathcal{T}(-\omega_n)e^{-j\omega_n x'} \tag{C.18}$$

$$\int T(y)\frac{\partial}{\partial y}e^{-\gamma_n|y|}dy = -T'(y) * e^{-\gamma_n|y|} \tag{C.19}$$

Appendix D

Scattering From Periodic Planar Arrays of Parallel Cylinders with Small Radius, TM polarization

Consider a periodic planar array of parallel cylinders with small radius, perfect conductivity and infinite length. Let all the cylinders have the same radius a which is much smaller than the wavelength. The axis of cylinder n is parallel with the z-axis and passes through the point $(x_n, y_n) = (0, ns)$ where s denotes the spacing between axes. With a z-polarized plane wave incident on the array as in Fig.D.1,

$$E_z^i(x, y) = E_0 e^{jk(x\cos\phi + y\sin\phi)} \tag{D.1}$$

Consider the surface current density J_s to be uniformly distributed around the surface of the cylinder. Then the field scattered from the cylinder n is given by

$$E_n^s = -I_n' J_0(ka_n) H_0^{(2)}(k\rho_n) \tag{D.2}$$

where

$$\begin{aligned} k^2 &= \omega^2 \mu\epsilon \\ \rho_n &= \sqrt{(x - x_n)^2 + (y - y_n)^2} \\ I_n' &= \frac{\omega\mu}{4} I_n \\ I_n &= 2\pi a_n J_s \end{aligned}$$

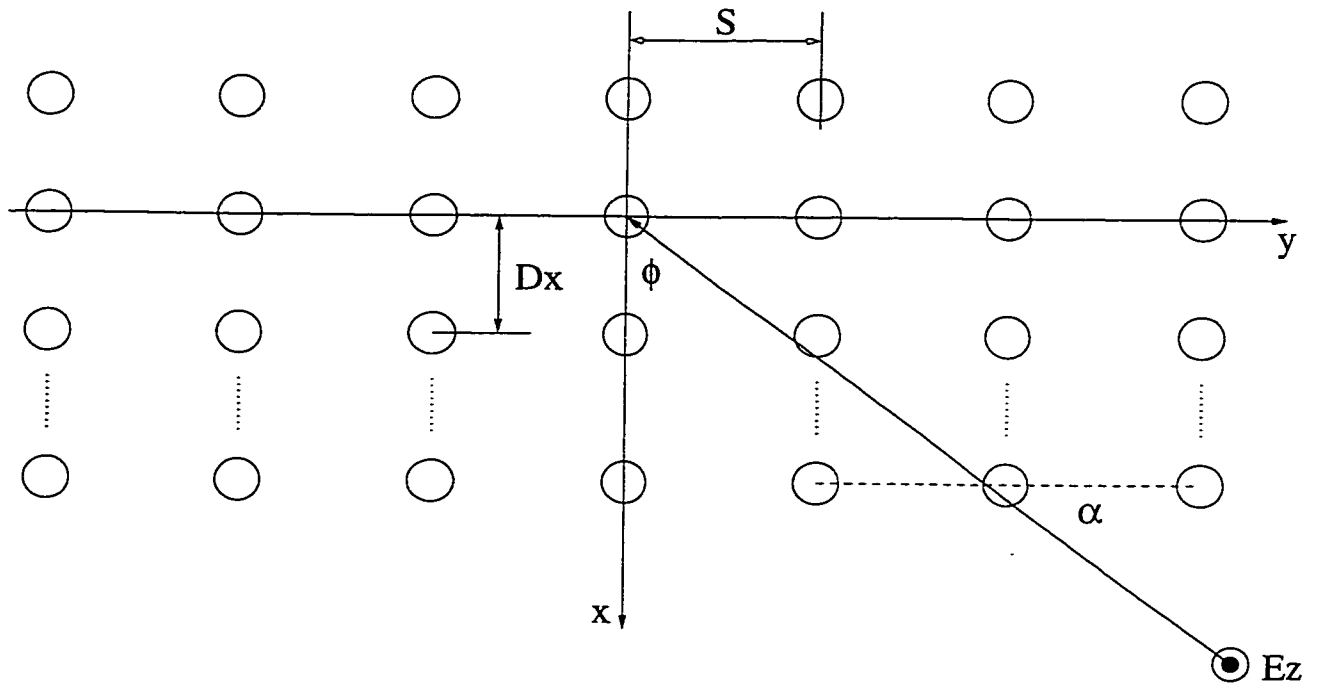

Figure D.1: Plane wave incident on periodic planar array.

where the superscript (2) is understood on the Hankel function $H_0(x)$ here after.

The electric field intensity has only a z component, so the subscript z is omitted in the above equations and the following. The field scattered by the array of cylinders is obtained from (D.2) simply by summing on n.

D.1 Boundary Conditions in General

The boundary condition requires that

$$E^s + E^i = 0, \text{ over all cylinder surfaces.} \tag{D.3}$$

Here E^s, and E^i represent the scattered and incident field, respectively. Using the equivalent principle, equivalent currents are assumed on cylinder surfaces, with the conducting cylinders removed, leaving an array of cylindrical current sheets radiating in free space. Assume the total number of cylinder is P, we may write the total scattered field as

$$E^s = \sum_{p=1}^{P} E_p \tag{D.4}$$

where E_p^s is the field radiated from surface current on p-th cylinder. Due to the geometrical feature, we further expand (D.3) as

$$E_m(x_m, y_m) + \sum_{p=1}^{P}{}' E_p = -E_m^i(x_m, y_m), \quad m = 1, 2, \cdots, P \tag{D.5}$$

where the $'$ means that the term $p = m$ is excluded in the summation. The above summation is over all the cylinders. The points (x_m, y_m) represent the relevant cylinder where the B. C. is to be ensured.

Strictly speaking, the boundary condition should be satisfied on surface of all the cylinders. While the radii of cylinders were assumed to be small, an approximation is made here to ensure B. C. only at the center of each cylinder. Hence (x_m, y_m) in (D.5) is referred to the center of cylinder m and terms relates to fields are considered as the averaged value around the circumference of the cylinder.

The first term in (D.5) is separated from the summation, since it represents the *self-term* which is the radiation from the current on the surface of the same cylinder. The field on surface of a cylinder radiated from the surface current on the same cylinder has a different expression from the field on surface of a cylinder radiated from the surface current on other cylinders.

D.2 Boundary Conditions for Periodic Arrays

Consider an array periodic in y direction and finite in the x direction. The number of rows in x direction is M. Since the geometry is periodic and the excitation is periodic along y-axis, a periodic solution is possible:

$$I'_{in} = I'_{i0} e^{jnks\sin\phi}, \; i = 1, 2, \cdots, M, \; n = -\infty, \; +\infty \tag{D.6}$$

where I'_{pn} is the current on p-th and n-th element in x and y-direction, respectively. I'_{p0} is the current on an element lying on x-axis in the same row. In view of (D.6), there is only one unknown current for each row of cylinders. I'_{p0} can be determined by applying B. C. on

elements lying on the x-axis. The scattered field on each cylinder at x-axis can be expressed as, for cylinder at $(x_p, 0)$

$$E_p(x_p, 0) = \sum_{i=1}^{M} E_{pi}(x_p, 0) \tag{D.7}$$

where indices p and i are counted along x-direction, $E_{pi}(x_p)$ represents field on cylinder p lying at $(x_p, 0)$ from all the contribution of cylinders lying in the ith row, i.e. summation over y-direction, which can be expressed as

$$E_{pi}(x_p, 0) = -I''_{i0} \begin{cases} \sum_{n=-\infty}^{+\infty} J_0(ka) H_0(k\rho_{inp}) e^{jnks\sin\phi}, & i \neq p \\ H_0(ka) + \sum_{n=1}^{+\infty} J_0(ka) H_0(nks) \cos(nks\sin\phi), & i = p \end{cases} \tag{D.8}$$

where

$$\begin{aligned} \rho_{inp} &= \sqrt{(x_p - x_i)^2 + (y_p - ns)^2} = \sqrt{(x_p - x_i)^2 + (ns)^2} \\ I''_{i0} &= I'_{i0} J_0(ka) = \frac{\omega\mu}{4} J_0(ka) I_{i0} \end{aligned}$$

I''_{i0} is related to the current on the ith element lying on x-axis, the subscript 0 is suppressed hereafter. The equation for B. C. can then be rewritten as

$$\sum_{i=1}^{M} Z_{pi} I''_i = E^i_p(x_p, 0), \quad p = 1, 2, \cdots, M \tag{D.9}$$

where Z_{pi} is given in (D.8) as

$$Z_{pi} = \begin{cases} \sum_{n=-\infty}^{+\infty} J_0(ka) H_0(k\rho_{inp}) e^{jnks\sin\phi}, & i \neq p \\ H_0(ka) + J_0(ka) \sum_{n=1}^{+\infty} H_0(nks) \cos nks\sin\phi, & i = p \end{cases} \tag{D.10}$$

and the incident field term on the right is defined by (D.23). The series contained above can be converted to a rapidly convergent series using the Poisson summation theorem, namely for $i \neq p$

$$\sum_{n=-\infty}^{+\infty} H_0(k\rho_{inp}) e^{jnks\sin\phi_i} = \frac{2j}{s} e^{jky_p\sin\phi_i} \sum_{n=-\infty}^{+\infty} \frac{e^{-\gamma_n|x_p - x_i|}}{\gamma_n} e^{j2n\pi y_p/s} \tag{D.11}$$

where

$$\gamma_n = \sqrt{\left(k\sin\phi_i + \frac{2n\pi}{s}\right)^2 - k^2},\ n = 0, \pm 1, \pm 2, \cdots, \pm\infty$$

Since $y_p = 0$ for Z_{pi}, we have for $i \neq p$

$$Z_{pi} = J_0(ka)\frac{2j}{s}\sum_{n=-\infty}^{+\infty}\frac{e^{-\gamma_n|x_p - x_i|}}{\gamma_n} \tag{D.12}$$

When $i = p$ the Poisson series is slowly convergent since the exponential term over $|x_p - x_i|$ vanishes. A summation formula is available in Gradshteyn and Ryzhik's table [22]. Further, we see from (D.12) that when the cylinders on x-axis is equally spaced. $[Z_{pi}]$ is a Toeplitz matrix.

D.3 Scattered Fields

Once the surface currents I_i' for the cylinders on x-axis, is solved from (D.9), the scattered field can then be evaluated

$$E^s(x,y) = -\sum_{i=1}^{M} I_{i0}''\sum_{n=-\infty}^{+\infty} H_0(k\rho_{in})e^{jnks\sin\phi} \tag{D.13}$$

where $\rho_{in} = \sqrt{(x - x_i)^2 + (y - ns)^2}$.

Again, the summation over n can be done via the Poisson summation formula, therefore the scattered field can be expressed as

$$E^s(x,y) = \sum_{i=1}^{M} -I_{i0}''\frac{2j}{s}e^{jky\sin\phi_i}\sum_{n=-\infty}^{+\infty}\frac{e^{-\gamma_n|x - x_i|}}{\gamma_n}e^{j2n\pi y/s} \tag{D.14}$$

D.4 Fields Radiated From Cylinders

First, we consider a line source carrying electrical current I located at (ρ', ϕ'). The field is

$$E_z(\rho, \rho') = -\frac{\omega\mu I}{4}H_0(k|\rho - \rho'|) \tag{D.15}$$

Er use the addition theorem for Hankel functions, and rewrite (D.15) as

$$E_z(\rho, \rho') = -\frac{\omega\mu I}{4}\sum_{-\infty}^{\infty}e^{jn(\phi - \phi')}\begin{cases} J_n(k\rho)H_n(k\rho'), & \rho < \rho' \\ H_n(k\rho)J_n(k\rho'), & \rho > \rho' \end{cases} \tag{D.16}$$

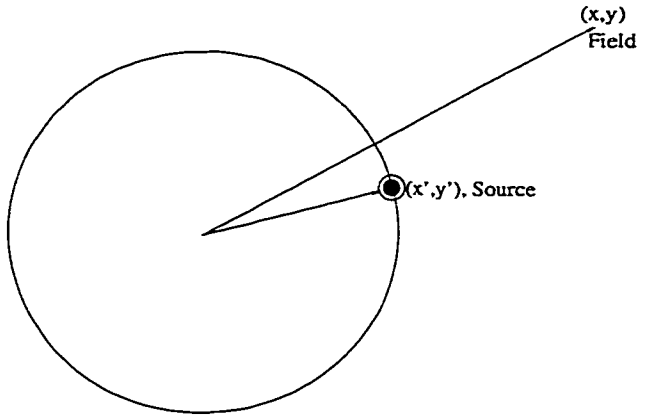

Figure D.2: Field from a uniformly distributed cylindrical current sheet.

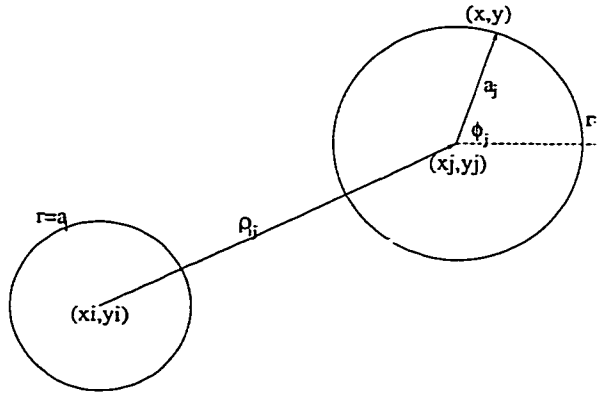

Figure D.3: The average field on surface of a cylinder.

Now consider a surface current J_s uniformly distributed on a cylindrical sheet with radius a, as shown in Fig.D.2. The segment current is $dI = J_s a d\phi$ where J_s is the surface current density. The electric field contributed from all the segments along the circumference is

$$E_z(\rho) = -\frac{\omega\mu a J_s}{4}\int_0^{2\pi} H_0(k|\rho - \mathbf{a}'|)d\phi \tag{D.17}$$

Performing the integral over ϕ', we have

$$E_z(\rho) = -\frac{\omega\mu I}{4}\begin{cases} J_0(k\rho)H_0(ka), & \rho < a \\ H_0(k\rho)J_0(ka), & \rho > a \end{cases} \tag{D.18}$$

D.5 Averaged Field on Surface of a Cylinder

Consider the average of the field on surface of cylinder j from a uniformly distributed cylindrical current sheet on surface of cylinder i, as shown in Fig.D.3. We have from (D.18)

$$\overline{E_{ji}}(\rho_j) = -\frac{I_i'}{2\pi a_j} J_0(ka_i) \int_C H_0(k|\rho_{ij} + \mathbf{a}_j|)dl \tag{D.19}$$

where

$$\begin{aligned} \rho_j &= \sqrt{x_j^2 + y_j^2} \\ \rho_{ij} &= \sqrt{(x_j - x_i)^2 + (y_j - y_i)^2} \end{aligned}$$

where a_i, a_j are radii of cylinder i and j, respectively, $\mathbf{a}_j$ is the vector from the center of cylinder j to the circumference, ρ_{ij} is the vector from the centers of cylinder i to the center of cylinder j. Expand $H_0(k|\rho_{ij} + \mathbf{a}_j|)$ as

$$H_0(k|\rho_{ij} + \mathbf{a}_j|) = \sum_{-\infty}^{\infty} (-)^n J_n(ka_j) H_n(k\rho_{ij}) e^{jn(\phi_{ij} + \phi_j)}, \ \rho_{ij} > a_j$$

where ϕ_j is in local coordinate on cylinder j. Performing the integral over ϕ_j, we have

$$\overline{E_{ji}}(\rho_j) = -I_i' J_0(ka_i) J_0(ka_j) H_0(k\rho_{ij}) \tag{D.20}$$

D.6 Averaged Incident Field on Surface of a Cylinder

Consider the following plane wave incident on surface of a cylinder with a small but finite radius a.

$$E^i(x, y) = E_0 e^{jk(x\cos\phi_i + y\sin\phi_i)} \tag{D.21}$$

where ϕ_i is the incident angle. Using a cylindrical wave expansion for plane waves [16], eq.(11-55b)

$$e^{jk\rho\cos(\phi - \phi')} = \sum_{-\infty}^{\infty} j^n J_n(k\rho) e^{jn(\phi - \phi')}$$

we have the average incident field on surface of a cylinder located on $(0, 0)$

$$\overline{E^i} = \frac{1}{2\pi a} \int_C E^i(\rho, \phi)dl = \frac{1}{2\pi} \int_0^{2\pi} E^i(a, \phi)d\phi = J_0(k\rho) \tag{D.22}$$

When the cylinder is located in (x_0, y_0) instead of $(0, 0)$, we may make a coordinate transform and rewrite the incident field as

$$\begin{aligned} E^i(x,y) &= E_0 e^{jk(x\cos\phi_i + y\sin\phi_i)} \\ &= E_0 e^{jk[(x_0+x')\cos\phi_i + (y_0+y')\sin\phi_i]} \\ &= E^i(x_0,y_0) e^{jk(x'\cos\phi_i + y'\sin\phi_i)} \end{aligned}$$

Performing the integral procedure similar to that in deriving (D.22) in coordinate $X'O'Y'$, we have the averaged incident field when the cylinder located away from origin written as

$$\overline{E^i}(x_0, y_0) = J_0(ka) E^i(x_0, y_0) \tag{D.23}$$

where $\overline{E^i}(x_0, y_0)$ denotes the averaged incident field on the cylinder under illumination centered at (x_0, y_0). $E^i(x_0, y_0)$ is defined in (D.21), and a is the radius of the cylinder.

D.7 A Summation Formula

A summation formula in [22] can be used to calculate the self-impedance term.

$$\sum_{k=1}^{\infty} J_0(kx)\cos kxt = -\frac{1}{2} + \frac{1}{x\sqrt{1-t^2}} + \sum_{l=1}^{m} \frac{1}{\sqrt{x^2 - (2\pi l + tx)^2}} + \sum_{l=1}^{n} \frac{1}{\sqrt{x^2 - (2\pi l - tx)^2}} \tag{D.24}$$

and

$$\begin{aligned} \sum_{k=1}^{\infty} N_0(kx)\cos kxt &= -\frac{1}{\pi}\left(C + \ln\frac{x}{4\pi}\right) + \frac{1}{2\pi}\left(\sum_{l=1}^{m}\frac{1}{l} + \sum_{l=1}^{n}\frac{1}{l}\right) \\ &- \sum_{l=m+1}^{\infty}\left(\frac{1}{\sqrt{(2\pi l + tx)^2 - x^2}} - \frac{1}{2\pi l}\right) \\ &- \sum_{l=n+1}^{\infty}\left(\frac{1}{\sqrt{(2\pi l - tx)^2 - x^2}} - \frac{1}{2\pi l}\right) \end{aligned} \tag{D.25}$$

where $x > 0$, $0 \le t < 1$, $C = 0.577,215,664,90\ldots$ is Euler's constant, and m, n satisfy the conditions

$$\begin{aligned} 2\pi m &< x(1-t) < 2\pi(m+1) \\ 2\pi n &< x(1+t) < 2\pi(n+1) \end{aligned} \tag{D.26}$$

In applying this to periodic wire arrays, we see that $x = ks$ and $t = \sin\phi$. Therefore

$$\begin{aligned} m &< \frac{s}{\lambda}(1 - \sin\phi) < m + 1 \\ n &< \frac{s}{\lambda}(1 + \sin\phi) < n + 1 \end{aligned} \tag{D.27}$$

Appendix E

Periodic Planar Array of Parallel Cylinders with Small Radius

Considering that the material referred to by J. H. Richmond [15] is not accessible to general public, we include his note here for reader's reference.

Periodic Planar Array of Parallel Cylinders with Small Radius

TM_z Polarization

Consider a periodic planar array of parallel cylinders with small radius, perfect conductivity and infinite length. Let all the cylinders have the same radius "a" which is much smaller than the wavelength. The axis of cylinder n is parallel with the z axis and passes through the point $(x_n, y_n) = (0, ns)$ where s denotes the spacing between axes. With a z-polarized plane wave incident on the array as in Figure 7,

20. $$E_z^i(x,y) = E_o e^{jk(x\cos\phi + y\sin\phi)}$$

and the excitation voltage is

21. $$V_m = E_z^i(x_m, y_m) = E_o e^{j\,mks\sin\phi}$$

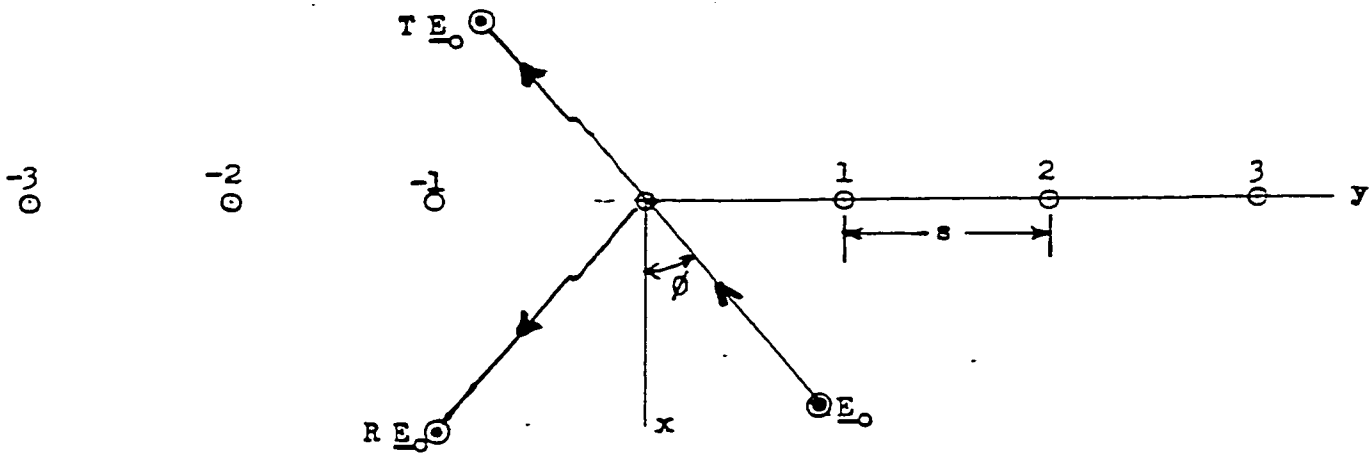

Fig. 7. Plane wave incident on periodic planar array.

Equation 16 represents an infinite system of simultaneous linear equations for the currents I_n'' induced on the cylinders. Since the environment is periodic and the excitation is periodic, a periodic solution is possible:

22. $$I_n'' = I_o'' \exp(j\,nks\sin\phi)$$

In view of eq. 22, there is only one unknown current: I_o'', and it can be determined by enforcing equation 16 with $m = 0$. With $m = 0$, we note that $\rho_{mn} = |n|\ s$. From eqs. 16 – 22 we obtain:

$$23. \quad I_o'' \left[\frac{H_o(ka)}{J_o(ka)} + 2 \sum_{n=1}^{\infty} H_o(nks) \cos(nks \sin\phi) \right] = E_o$$

Although the infinite series in eq. 23 converges slowly, summation formulas are available in:

I. S. Gradshteyn and I. M. Ryzhik, "Table of Integrals, Series and Products", Academic Press, New York, pages 976-977, Section 8.522.

From eq. 19 the field scattered by the array of cylinders is

$$24. \quad E_z^s = - I_o'' \sum_{-\infty}^{\infty} H_o(k \rho_n)\ e^{j\, nks \sin\phi}$$

where

$$25. \quad \rho_n = \sqrt{x^2 + (y - ns)^2}$$

A more convenient expression for the scattered field is

$$26. \quad E_z^s = \frac{-2j\ I_o''}{s}\ e^{jky \sin\phi} \sum_{-\infty}^{\infty} \frac{e^{-\gamma_n |x|}\ e^{j2n\pi y/s}}{\gamma_n}$$

where

$$27. \quad \gamma_n = \sqrt{(k \sin\phi + 2n\pi/s)^2 - k^2}$$

Most of the modes in eq. 26 have a positive real value for γ_n. These "evanescent modes" decay exponentially to negligible values when the observer moves far away from the array of cylinders. The zero-order mode, however, has $n = 0$ and

$$28. \quad \gamma_o = jk \cos\phi$$

This mode is just the reflected plane wave when x is positive. Thus, the reflection and transmission coefficients of the array of cylinders are

$$29. \quad R = \frac{-2\ I_o''}{E_o\ ks \cos\phi} \qquad \text{and} \qquad T = 1 + R$$

In eq.26 , the modes with n differing from zero are called "higher-order modes". If a higher-order mode has a pure imaginary value of γ_n, it is a propagating plane wave and is called a "grating mode". An evanescent mode makes the transition to a grating mode at the "cutoff condition" or "cuton condition" defined by $\gamma_n = 0$. For each grating mode, the direction of propagation is readily determined from eqs.26 and 27 .

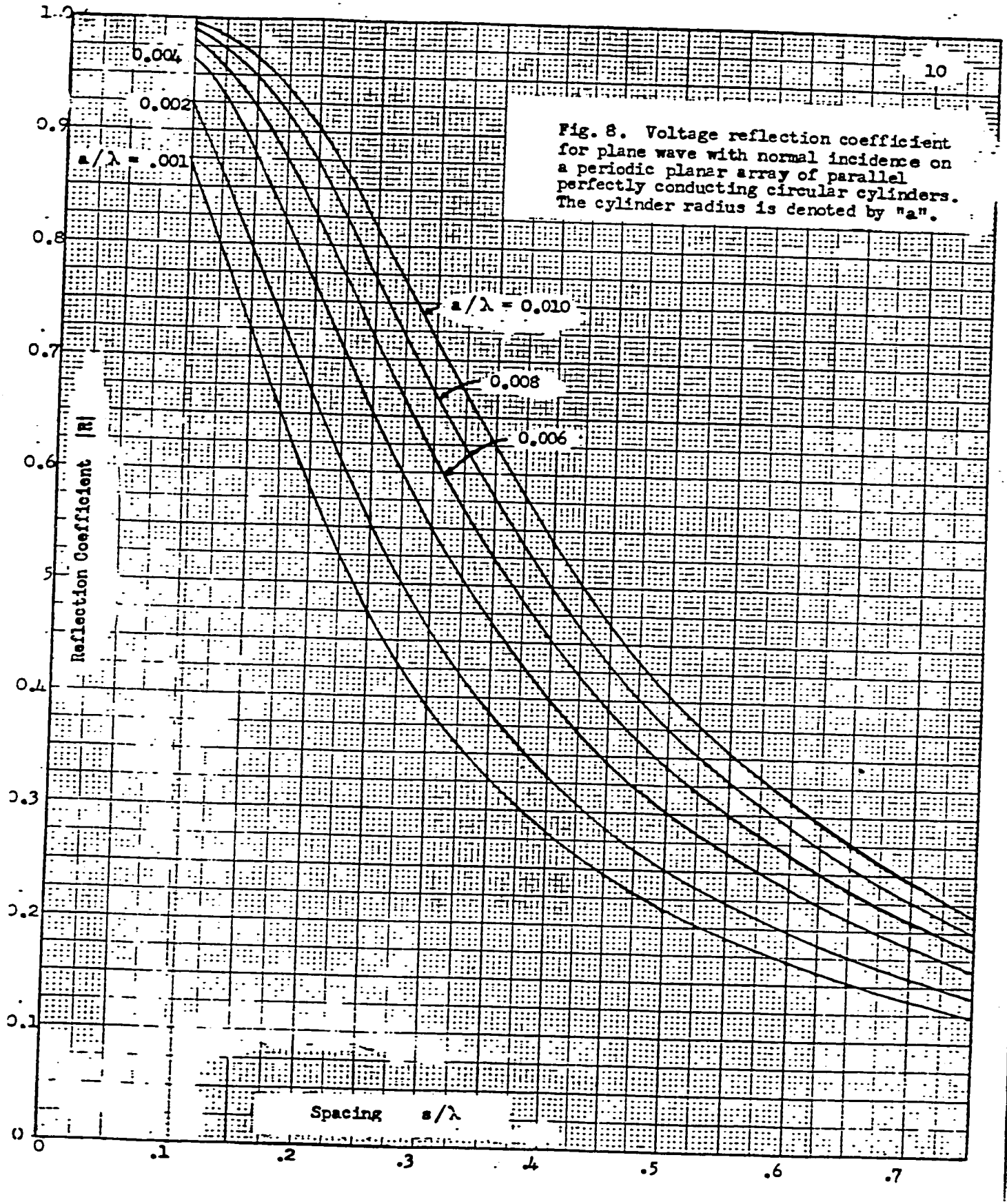

Fig. 8. Voltage reflection coefficient for plane wave with normal incidence on a periodic planar array of parallel perfectly conducting circular cylinders. The cylinder radius is denoted by "a".